

Interim Report

IR-10-005

Thermodynamics and Turbomachinery of the Oxyfuel Naki Cycles

Daniel Hoefftberger (daniel.hoefftberger@tugraz.at)

Approved by

Keywan Riahi
Acting Program Leader, Energy Program

June 2010

Interim Reports on work of the International Institute for Applied Systems Analysis receive only limited review. Views or opinions expressed herein do not necessarily represent those of the Institute, its National Member Organizations, or other organizations supporting the work.

Contents

1	Introduction	1
1.1	Greenhouse Effect - Global Warming	1
1.2	CO ₂ sequestration	2
1.3	Transport of CO ₂	3
1.4	Storage of CO ₂	4
1.5	Examples of oxyfuel cycles	4
1.5.1	Oxyfuel Steam Cycle	5
1.5.2	Semiclosed Oxyfuel Combustion - Combined Cycle	5
1.5.3	Graz Cycle	5
1.5.4	Matiant Cycle	6
1.5.5	Chemical Looping Combustion	6
1.6	History of the Naki Cycle, an oxy-fuel cycle originally proposed by Prof. Dr. Nebojsa Nakicenovic	7
1.7	Assignment of tasks	7
2	Thermodynamic Evaluation	8
2.1	Calculation in IPSEpro	8
2.1.1	Modules	8
2.1.2	Model of the cycles	8
2.1.3	Main modules of the library used for the Naki cycles	9
2.1.4	Thermophysical properties	9
2.2	Definition of cycle efficiencies	9
3	Main Assumptions, Efficiencies, and Pressure Losses	10
3.1	General assumptions	10
3.2	Fuel	10
3.3	General efficiencies	11
3.4	Isentropic efficiencies	11
3.5	Pressure losses	12
4	Thermodynamic Design of the Cycles	12
4.1	Naki I	13
4.1.1	Cycle description	13
4.1.2	Thermodynamic balance	13
4.1.3	IPSEpro schematic of Naki I	17
4.1.4	Turbomachinery arrangement	17
4.1.5	Influence of parameters	17
4.2	Naki II	19
4.2.1	Cycle description	21

4.2.2	Different turbomachinery configurations for Naki II	26
4.2.3	Comparison of the different turbomachinery configurations . .	28
4.2.4	Thermodynamic balance of the different turbomachinery configurations	30
4.2.5	Thermodynamic comparison between methane and syngas as fuel	31
4.2.6	IPSEpro schematic of the cycles	32
4.2.7	Influence of parameters	38
4.3	Naki III	43
4.3.1	Cycle description	43
4.3.2	Thermodynamic balance	47
4.3.3	IPSEpro schematic of Naki III	51
4.3.4	Turbomachinery arrangement and dimensions	51
5	Turbomachinery Dimensions	54
5.1	Layout of turbines	54
5.2	Layout of compressors	55
5.3	Calculation of Mach number	55
5.4	Main turbomachinery dimensions of Naki I	56
5.5	Main turbomachinery dimensions of Naki II	56
6	Turbomachinery Design Details	62
6.1	High-pressure turbine (HPT)	62
6.1.1	Rotor design	68
6.1.2	Burner details	68
6.1.3	Layout of stator blades	69
6.1.4	Rotor blades with ICS (Innovative Cooling System)	69
6.1.5	Velocity triangle of the HPT	71
6.1.6	Assembly of HPT	72
6.2	Low-pressure turbine (LPT)	73
6.2.1	Assembly of LPT	74
7	Economic Evaluation	76
7.1	Assumptions	76
7.1.1	Evaluation of the capital costs for a Naki I power plant	77
7.1.2	Evaluation of the capital costs for a Naki II and Naki III power plant	77
7.2	Basics of economic calculations	79
7.3	Results of the economic evaluation	82
7.4	Cost-sensitivity analysis	83
8	Conclusion and Outlook	88
Appendix A: Tables corresponding to diagrams of Chapter 4		91
	Naki I: For Chapter 4.1.5	91
	Naki II: For Chapter 4.2.7	92

Appendix B: Influence of thermodynamic parameters for Naki I	93
Basic values	93
Influence of cooling water temperature	93
Influence of TIT	96
Influence of TIP	99
Appendix C: Influence of thermodynamic parameters for Naki II	101
Basic values	101
Influence of cooling water temperature	102
Influence of TIT	106
Influence of TIP	110
Influence of LPT exit pressure	114
Appendix D: Cost Sensitivity Analysis	118
Cost sensitivity analysis for Naki I	118
Cost sensitivity analysis for Naki II	123
Cost sensitivity analysis for Naki III	128

Abstract

The increasing amount of carbon dioxide (CO_2) in the atmosphere causes continuing climate change. The Kyoto Protocol was agreed by a majority of governments around the world to address this challenge. Its aim is to reduce the emission of greenhouse gases by a substantial amount compared to the 1990 emissions. One promising way is to reduce the emissions of CO_2 using CCS (carbon dioxide capture and storage) in power generation and in some industrial plants which produce high quantities of this greenhouse gas. The capture of CO_2 can be accomplished by different methods like oxyfuel cycles, precombustion systems, and postcombustion systems.

To realize one alternative to capture CO_2 Prof. Nebojsa Nakicenovic of IIASA (International Institute for Applied Systems Analysis) proposed an oxyfuel cycle. This so-called Naki cycle which is, in principle, a closed cycle gas turbine with recuperative heat exchanger uses CO_2 as the working fluid. The pressure rise is accomplished in liquid state by a pump. Hence, the working fluid has to be condensed after being cooled down in the recuperative heat exchanger. To investigate the thermodynamic cycle efficiency and feasibility of turbomachinery this work was carried out.

In this work three different variants of the so-called Naki cycle (Naki I, Naki II, and Naki III) were studied. The cycles were modeled in the simulation software IPSEpro in which the thermodynamic investigation of these cycles was conducted. The thermodynamic evaluation of Naki I was performed using coal dust (pure carbon) as fuel. In the investigation of Naki II, two different fuels were compared. These are methane and syngas from coal gasification. The evaluation of Naki III was carried out using methane. With the thermodynamic data, a first dimensioning of the turbomachinery was possible. In the thermodynamic evaluation some parameters (for example turbine inlet temperature and pressure or mass flows) were chosen so that feasible turbomachinery dimensions could be expected.

For the most promising cycle, Naki II, a possible turbomachinery design was described in detail (especially the high-pressure turbine).

Lastly a rough economic evaluation of all three variants of the Naki cycle was carried out. The results of this evaluation give an overview of costs related to the capture of CO_2 . Each variant of the Naki cycle was compared with a reference plant without CO_2 capture. These comparisons lead to mitigation costs (i.e., the costs for one tonne CO_2 avoided by a Naki power plant in comparison to a reference plant).

Kurzfassung

Die steigende Konzentration von Kohlendioxid (CO_2) in der Atmosphäre führt zum Klimawandel, weshalb weltweit von einem Großteil der Länder das Kyoto Protokoll vereinbart wurde. Das Ziel dieses Protokolls ist eine deutliche Reduktion der Treibhausgasemissionen auf Basis der Emissionen von 1990. Unter Anderem bietet die Abtrennung und Speicherung von CO_2 bei fossil befeuerten Kraftwerken und Industrieanlagen, bei welchen in größerem Umfang CO_2 anfällt, eine vielversprechende Möglichkeit, um die CO_2 Emissionen zu senken. Die Abtrennung von CO_2 kann dabei durch verschiedene Systeme wie Sauerstoffverbrennung (Oxyfuel Prozesse), Abtrennung vor der Verbrennung (Precombustion Prozesse) oder Abtrennung nach der Verbrennung (Postcombustion Prozesse) erreicht werden.

Prof. Dr. Nebojsa Nakicenovic von der IIASA (International Institut for Applied Systems Analysis) schlug mit einem als Naki Cycle bezeichneten Oxyfuel Prozess eine Möglichkeit für die Abtrennung von CO_2 vor. Dabei handelt es sich im Prinzip um eine rekuperative Gasturbine mit halb-offenem Kreislauf und CO_2 als Arbeitsmedium. Die Druckerhöhung erfolgt in flüssiger Phase durch eine Pumpe anstelle einer Kompression im gasförmigen Zustand. Daher ist es erforderlich das Arbeitsmedium zu kondensieren, nachdem es im rekuperativen Wärmetauscher abgekühlt wurde. Um nun genauere Aussagen über den Prozesswirkungsgrad und die Verfügbarkeit von Turbomaschinen zu bekommen, wurde dieser Prozess untersucht.

Ziel dieser Arbeit war die thermodynamische Untersuchung von drei unterschiedlichen Varianten des Naki Cycles (Naki I, Naki II und Naki III) mit Hilfe des Softwarepaketes IPSEpro. Mit den aus dieser Simulation gewonnenen Daten war eine grobe Auslegung der Turbomaschinen möglich. Dazu wurden in der thermodynamischen Simulation die Werte für wesentliche Parameter wie z.B. Turbineneintrittstemperatur, Turbineneintrittsdruck oder Massenstrom des Arbeitsmediums in Bereichen gewählt, für welche baubare Turbomaschinen zu erwarten sind. Als Brennstoff für den Prozess Naki I wurde Kohlestaub (reiner Kohlenstoff) verwendet. Beim Prozess Naki II wurden Erdgas (Methan) und Synthesegas aus einer Kohlevergasung als Brennstoffe verwendet und miteinander verglichen. Die Untersuchung von Naki III wurde mit Methan durchgeführt.

Für den vielversprechendsten Prozess Naki II wurde eine detaillierte Konstruktion der Turbomaschinen (im speziellen der Hochdruckturbine) angefertigt.

Bei der weiters durchgeführten Kostenanalyse wurden alle drei Varianten des Naki Cycles mit einem entsprechenden Referenzkraftwerk ohne CO_2 Abtrennung verglichen. Diese Analyse führt zu den Vermeidungskosten (mitigation costs), die durch die vermiedene Emission einer Tonne CO_2 durch ein Naki Kraftwerk im Vergleich zu einem entsprechenden Referenzkraftwerk entstehen.

Foreword and Acknowledgments

Diploma Thesis of Daniel Höftberger, researched and written at the Institute for Thermal Turbomachinery and Machine Dynamics, Graz University of Technology

Head of the Institute:
Univ.-Prof. Dipl.-Ing. Dr.techn. Franz Heitmeir

Supervisors:
A.o.Univ.-Prof. Dipl.-Ing. Dr.techn. Wolfgang Sanz
Em.Univ.-Prof. Dipl.-Ing. Dr.techn. Herbert Jericha

I would like to express my gratitude to all those who helped me complete this diploma thesis.

I am deeply indebted to my supervisor a.o.Univ.-Prof. Dipl.-Ing. Dr.techn. Wolfgang Sanz for enabling this work and also for his great commitment and patient help during it. I thank him for looking closely at the final version of this work for English style and grammar and for correcting both.

I must also thank em.Univ.-Prof. Dipl.-Ing. Dr.techn. Herbert Jericha for his support during the layout and creation of the detail drawings of the turbomachinery with his wide knowledge. I am also grateful to Dipl.-Ing. Dr. techn. Emil Göttlich for his assistance in generating the detail drawings of the turbomachinery.

Thanks especially to Prof. Dr. Nebojsa Nakicenovic from IIASA for making this work possible and for sponsoring it.

I would also like to thank my brother Oliver for looking closely at the final version of this thesis for English style and grammar, and for correcting both.

Thanks also to my family for educating me and supporting me during my studies.

Höftberger Daniel

Graz, May 2009

About the Author

Daniel Höftberger works as a Scientific Assistant under the supervision of Prof. Jürgen Karl at the Institute of Thermal Engineering, Graz University of Technology. He has received his M.Sc. from Graz University of Technology in 2009. His study focused on Energy and Environmental Management Technology. In 2007 he received his Bachelor of Engineering SE in Mechanical Engineering from Graz University of Technology and the Diploma of International Welding Engineer from the Schweißtechnische Zentralanstalt SZA-Vienna, Austria.

Nomenclature

η	[-]	Net efficiency of a power plant
η_{net}	[-]	Net efficiency
η_m	[-]	Mechanical efficiency
η_{gen}	[-]	Generator efficiency
η_{tr}	[-]	Transformer efficiency
P_T	[MW]	Turbine power
P_C	[MW]	Power of compressors and feeding pumps
P_{aux}	[MW]	Auxiliary losses
P_{fuel}	[MW]	Power of fuel compression
P_{O_2}	[MW]	Power of oxygen generation and compression
P_{CO_2}	[MW]	Power of CO ₂ hand-over pump
P_{el}	[MW _{el}]	Electrical net power output of the power plant
Q_{in}	[MW _{th}]	Heat input
ξ_C	[%]	Combustion chamber heat-loss coefficient
t	[°C]	Temperature
TIT	[°C]	Turbine inlet temperature
TIP	[bar]	Turbine inlet pressure
Q	[MW _{th}]	Transferred heat in heat exchanger
Δt_{min}	[K]	Minimum temperature difference in heat exchangers
s	[kJ/kgK]	Entropy
f	[-], [hrs/yr]	Flow factor, yearly operating hours
ψ	[-]	Work coefficient
r	[-]	Degree of reaction
D_{mean}	[m]	Mean diameter of a turbomachinery stage
\dot{V}	[m ³ /s]	Volume flow
l	[m]	Blade length
n	[rpm]	Rotational speed
Δh	[kJ/kg]	Enthalpy drop of a turbine or compressor
Δh_{stage}	[kJ/kg]	Enthalpy drop of a turbine or compressor stage
Δh_{inlet}	[kJ/kg]	Enthalpy drop of the first stage of a turbine or compressor
Δh_{outlet}	[kJ/kg]	Enthalpy drop of the last stage of a turbine or compressor
z	[-]	Number of turbine or compressor stages

w_1	[m/s]	Relative velocity at stator blade row exit
$w_{1 \text{ Tip}}$	[m/s]	Relative velocity at the blade tip of the first compressor stage
w_2	[m/s]	Relative velocity at rotor blade row exit
c_1	[m/s]	Velocity at stator blade row exit
$c_{1 \text{ ax}}$	[m/s]	Axial velocity at stator blade row exit
c_2	[m/s]	Velocity at rotor blade row exit
$c_{2 \text{ ax}}$	[m/s]	Axial velocity at rotor blade row exit
c_{ax}	[m/s]	Axial velocity
u	[m/s]	Circumferential velocity
u_{Tip}	[m/s]	Circumferential velocity at the blade tip
a	[m/s]	Speed of sound
∂p	[Pa]	Differential pressure
$\partial \rho$	[kg/m ³]	Differential density
M	[-]	Mach number
α, α_1	[°]	Flow angle at stator blade row exit
α_2	[°]	Flow angle at rotor blade row exit
h_0	[m]	Width of the rotor disc at the center (R=0)
h	[m]	Width of the rotor disc at radius R
R	[m]	Radius
ρ	[kg/m ³]	Density
Ω	[rad/s]	Angular speed of the rotor
σ	[Pa]	Stress in the disc
a	[%/yr]	Capital charge rate
C_{fuel}	[€/GJ _{th}]	Fuel costs
b	[% of capital costs]	Cost rate due to operation and maintenance
C_{addit}	[€/kW _{el}]	Additional capital costs
C_{asu}	[€/(kg O ₂ /s)]	Additional costs for the air separation unit
C_{oth}	[€/(kg CO ₂ /s)]	Additional other costs (piping...)
C_{comp}	[€/(kg CO ₂ /s)]	Additional costs for CO ₂ -compression
\dot{m}_{O_2}	[kg/s]	Oxygen mass flow
\dot{m}_{CO_2}	[kg/s]	Carbon dioxide mass flow
C_C	[€/kW _{el}]	Specific plant capital costs
$\text{COE}_{C(R)}$	[ct/kWh _{el}]	Cost of electricity due to capital costs for a reference p
$\text{COE}_{C(N)}$	[ct/kWh _{el}]	Cost of electricity due to capital costs for a Naki plant
COE_{fuel}	[ct/kWh _{el}]	Cost of electricity due to fuel
$\text{COE}_{\text{O\&M}}$	[ct/kWh _{el}]	Cost of electricity due to operation and maintenance
$\text{COE}_{\text{total}}$	[ct/kWh _{el}]	Sum of all COEs of the considered power plant
COE_{diff}	[ct/kWh _{el}]	Difference of total COE of a Naki plant and the reference plant
MC	[€/t CO ₂ avoided]	Mitigation costs

Acronyms

C (C ₁ , C ₂ and C ₃)	Compressor (Compressor 1, 2 and 3)
CC	Combined cycle
CCS	Carbon dioxide capture and storage
CH ₄	Methane
CO	Carbon monoxide
CO ₂	Carbon dioxide
G	Generator
GU	Gear unit
GWP	Global warming potential
H ₂	Hydrogen
H ₂ O	Water
HPST	High-pressure steam turbine
HPT	High-pressure turbine
HRSG	Heat recovery steam generator
HTEX	Heat exchanger
ICS	Innovative cooling system
IIASA	International Institute for Applied Systems Analysis
IPST	Intermediate pressure steam turbine
IPT	Intermediate pressure turbine
LPST	Low-pressure steam turbine
LPT	Low-pressure turbine
N ₂ O	Nitrous oxide
O ₂	Oxygen
O&M	Operation and maintenance
SCOC-CC	Semi Closed Oxyfuel Combustion - Combined Cycle

List of Tables

1	General assumptions	10
2	Fuel assumptions	11
3	General efficiencies	11
4	Isentropic efficiencies	12
5	Pressure losses	12
6	Power balance of Naki I	15
7	Mass flows of Naki I	15
8	Power balance for variants	30
9	Mass flows for variants	31
10	Power balance for methane and syngas as fuel	33
11	Mass flows for methane and syngas as fuel	33
12	Power balance of Naki III	51
13	Mass flows of Naki III	53
14	Dimensions of the uncooled turbine of Naki I	56
15	Main turbomachinery dimensions of variant 1a	58
16	Main turbomachinery dimensions of variant 1b	59
17	Main turbomachinery dimensions of variant 2	60
18	Main turbomachinery dimensions of variant 3	61
19	General economic assumptions	76
20	Additional costs [28]	77
21	Comparison of equipment size for a Naki I plant of 270 MW net power output	78
22	Comparison of equipment size for a Naki II and Naki III plant of 270 MW net power output	79
23	Estimated costs for a Naki II, Naki III, and conv. CC plant of 270 MW net power output	80
24	Investment costs of the different power plants	80
25	Mass flows of the Naki plants with a net power output of 270 MW	80
26	Economic comparison for a 270 MW Naki I plant	82
27	Economic comparison for a 270 MW Naki I, Naki II, and Naki III plant	83
28	Influence of TIT and pressure after feeding pump on net efficiency for Naki I	91
29	Influence of cooling water temperature on net efficiency for Naki I	91
30	Influence of TIT and pressure after feeding pump on net efficiency for Naki II	92
31	Influence of expansion pressure on net efficiency for Naki II	92
32	Influence of cooling water temperature on net efficiency for Naki II	92
33	Basic values for the variation of parameters for Naki I	93
34	Influence of cooling water temperature on efficiency for Naki I	93

35	Influence of cooling water temperature on thermal power (Naki I) . . .	94
36	Influence of cooling water temperature on power (Naki I)	95
37	Influence of TIT on efficiency (Naki I)	96
38	Influence of TIT on thermal power (Naki I)	97
39	Influence of TIT on power (Naki I)	98
40	Influence of TIP on efficiency (Naki I)	99
41	Influence of TIP on thermal power (Naki I)	100
42	Influence of TIP on power (Naki I)	100
43	Basic values for the variation of parameters for Naki II	101
44	Influence of cooling water temperature on efficiency for Naki II	102
45	Influence of cooling water temperature on thermal power (Naki II) . .	103
46	Influence of cooling water temperature on power, part 1 (Naki II) . .	104
47	Influence of cooling water temperature on power, part 2 (Naki II) . .	105
48	Influence of TIT on efficiency (Naki II)	106
49	Influence of TIT on thermal power (Naki II)	107
50	Influence of TIT on power, part 1 (Naki II)	108
51	Influence of TIT on power, part 2 (Naki II)	109
52	Influence of TIP on efficiency (Naki II)	110
53	Influence of TIP on thermal power (Naki II)	111
54	Influence of TIP on power, part 1 (Naki II)	112
55	Influence of TIP on power, part 2 (Naki II)	113
56	Influence of the LPT exit pressure on efficiency (Naki II)	114
57	Influence of the LPT exit pressure on thermal power (Naki II)	115
58	Influence of the LPT exit pressure on power, part 1 (Naki II)	116
59	Influence of the LPT exit pressure on power, part 2 (Naki II)	117
60	Influence of fuel costs on mitigation costs for Naki I	118
61	Influence of capital costs on mitigation costs for Naki I	119
62	Influence of capital charge rate on mitigation costs for Naki I	120
63	Influence of net efficiency of reference plant on mitigation costs for Naki I	121
64	Influence of net efficiency of Naki I plant on mitigation costs	122
65	Influence of fuel costs on mitigation costs for Naki II	123
66	Influence of capital costs on mitigation costs for Naki II	124
67	Influence of capital charge rate on mitigation costs for Naki II	125
68	Influence of net efficiency of reference plant on mitigation costs for Naki II	126
69	Influence of net efficiency of Naki II plant on mitigation costs	127
70	Influence of fuel costs on mitigation costs for Naki III	128
71	Influence of capital costs on mitigation costs for Naki III	129
72	Influence of capital charge rate on mitigation costs for Naki III	130
73	Influence of net efficiency of reference plant on mitigation costs for Naki III	131
74	Influence of net efficiency of Naki III plant on mitigation costs	132

List of Figures

1	Contribution of different greenhouse gases to climate change [1] . . .	2
2	Global carbon emissions from fossil fuel use [2]	3
3	Simplified cycle schematic of Naki I	14
4	Detailed IPSEpro schematic of Naki I	14
5	Q-t-diagram of the recuperative heat exchanger	15
6	Principle T-s-diagram of Naki I	16
7	IPSEpro schematic of Naki I with calculation data	18
8	Turbomachinery arrangement of Naki I	19
9	Influence of TIT and pressure after feeding pump on net efficiency (Naki I)	20
10	Influence of cooling water temperature on net efficiency (Naki I) . . .	20
11	Simplified cycle schematic of Naki II	21
12	Detailed IPSEpro schematic of Naki II	23
13	Principle T-s-diagram of Naki II	24
14	Q-t-diagram of recuperative heat exchanger 3	25
15	Q-t-diagram of recuperative heat exchanger 2	25
16	Turbomachinery arrangement variant 1a	26
17	Turbomachinery arrangement variant 1b	27
18	Turbomachinery arrangement variant 2	28
19	Turbomachinery arrangement variant 3	29
20	IPSEpro schematic of variant 1 with calculation data (methane) . . .	34
21	IPSEpro schematic of variant 2 with calculation data (methane) . . .	35
22	IPSEpro schematic of variant 3 with calculation data (methane) . . .	36
23	IPSEpro schematic of variant 1 (syngas)	37
24	Influence of TIT and pressure (after feeding pump) on net efficiency .	38
25	Q-t-diagram of recuperative heat exchangers 2 and 3 for the optimum TIT and a lower TIT	39
26	Q-t-diagram of recuperative heat exchangers 2 and 3 for a higher TIT than the optimum TIT	40
27	Influence of TIT on net efficiency (detail)	41
28	Influence of expansion pressure on net efficiency	42
29	Influence of cooling water temperature on net efficiency	42
30	Simplified cycle schematic of Naki III	44
31	Detailed IPSEpro schematic of Naki III	46
32	Principle T-s-diagram of the CO ₂ cycle of Naki III	48
33	Principle T-s-diagram of the double pressure steam cycle of Naki III .	49
34	Q-t-diagram of recuperative heat exchanger 3	50
35	Q-t-diagram of recuperative heat exchanger 2	50
36	IPSEpro schematic of Naki III with calculation data	52

37	Turbomachinery arrangement of the CO ₂ cycle of Naki III	53
38	High-pressure turbine (HPT) - overview	63
39	HPT exterior view	64
40	HPT section A-A	65
41	Detail combustion chamber	66
42	Rotor design of the HPT	69
43	Burner	70
44	Burner cone	70
45	Guide vanes	71
46	Rotor blade with ICS (innovative cooling system)	71
47	Velocity triangle of the HPT	72
48	Assembly of HPT	73
49	Low-pressure turbine (LPT) - overview	75
50	Influence of capital costs on mitigation costs for Naki I	84
51	Influence of capital charge rate on mitigation costs for Naki I	86
52	Influence of fuel costs on mitigation costs for Naki I	86
53	Influence of net efficiency of the reference plant on mitigation costs (Naki I)	87
54	Influence of net efficiency of the Naki I plant on mitigation costs	87
55	Influence of cooling water temperature on efficiency for Naki I	93
56	Influence of cooling water temperature on thermal power (Naki I)	94
57	Influence of cooling water temperature on power (Naki I)	95
58	Influence of TIT on efficiency (Naki I)	96
59	Influence of TIT on thermal power (Naki I)	97
60	Influence of TIT on power (Naki I)	98
61	Influence of TIP on efficiency (Naki I)	99
62	Influence of TIP on thermal power (Naki I)	100
63	Influence of TIP on power (Naki I)	101
64	Influence of cooling water temperature on efficiency for Naki II	102
65	Influence of cooling water temperature on thermal power (Naki II)	103
66	Influence of cooling water temperature on power, part 1 (Naki II)	104
67	Influence of cooling water temperature on power, part 2 (Naki II)	105
68	Influence of TIT on efficiency (Naki II)	106
69	Influence of TIT on thermal power (Naki II)	107
70	Influence of TIT on power, part 1 (Naki II)	108
71	Influence of TIT on power, part 2 (Naki II)	109
72	Influence of TIP on efficiency (Naki II)	110
73	Influence of TIP on thermal power (Naki II)	111
74	Influence of TIP on power, part 1 (Naki II)	112
75	Influence of TIP on power, part 2 (Naki II)	113
76	Influence of the LPT exit pressure on efficiency (Naki II)	114
77	Influence of the LPT exit pressure on thermal power (Naki II)	115
78	Influence of the LPT exit pressure on power, part 1 (Naki II)	116
79	Influence of the LPT exit pressure on power, part 2 (Naki II)	117
80	Influence of fuel costs on mitigation costs for Naki I	118
81	Influence of capital costs on mitigation costs for Naki I	119

82	Influence of capital charge rate on mitigation costs for Naki I	120
83	Influence of net efficiency of reference plant on mitigation costs for Naki I	121
84	Influence of net efficiency of Naki I plant on mitigation costs	122
85	Influence of fuel costs on mitigation costs for Naki II	123
86	Influence of capital costs on mitigation costs for Naki II	124
87	Influence of capital charge rate on mitigation costs for Naki II	125
88	Influence of net efficiency of reference plant on mitigation costs for Naki II	126
89	Influence of net efficiency of Naki II plant on mitigation costs	127
90	Influence of fuel costs on mitigation costs for Naki III	128
91	Influence of capital costs on mitigation costs for Naki III	129
92	Influence of capital charge rate on mitigation costs for Naki III	130
93	Influence of net efficiency of reference plant on mitigation costs for Naki III	131
94	Influence of net efficiency of Naki III plant on mitigation costs	132

Thermodynamics and Turbomachinery of the Oxyfuel Naki Cycles

Daniel Hoeflberger (daniel.hoeflberger@tugraz.at)

1 Introduction

1.1 Greenhouse Effect - Global Warming

The greenhouse effect is a natural phenomenon that keeps the temperature of the atmosphere 33 °C higher than without it [1]. The surface of the earth is heated up by the sun and radiates the heat back into space in form of infrared radiation. The infrared radiation is partially absorbed by gases like carbon dioxide (CO₂), methane (CH₄), nitrous oxide (N₂O), and others. Although the global warming potential (GWP) of CH₄ (GWP=4) and N₂O (GWP=310) is much higher than that of CO₂ (GWP=1) for a time horizon of 100 years, the contribution of CO₂ to global warming is with a value of 65 % higher than that of other gases, as shown in *Figure 1* from [1]. CH₄ has a 19 % share and N₂O a 6 % share. The rest of 10 % is shared by other gases. Through the anthropogenic emission of these greenhouse gases the greenhouse effect is boosted, which leads to global warming. The worldwide growth in emissions of greenhouse gases has been recognized since 1988. In *Figure 2* – from [2] – the global carbon emissions in GtC (gigatons of carbon) from 1850 to 1990 due to the use of fossil fuels are shown. For 1990-2100 different scenarios of carbon emission are depicted. Case A and B are without environmental taxes and CO₂ emission constraints. Case C has these conditions.

Because of the rising emissions of greenhouse gases in the past and hence global warming and atmospheric change, the Kyoto Protocol [3] was agreed in 1997 and is accepted by the majority of governments around the world. The goal of the Kyoto Protocol is to reduce emissions of greenhouse gases by a substantial amount compared to the 1990 emissions. There are different ways to reduce anthropogenic CO₂ emissions [4]:

- **Increase in efficiency**

Through increased efficiencies in power generation and power use, the consumption of fossil fuels can be reduced. This is already accepted, and technical improvements will make it possible in the future.

- **Use of fossil fuels with lower carbon content**

A change from carbon rich fuels like coal to fuels with lower carbon and higher hydrogen content like natural gas can help reduce the emissions of CO₂. For example, in power plants it is possible to save around 420 kg CO₂/MWh by using natural gas instead of coal.

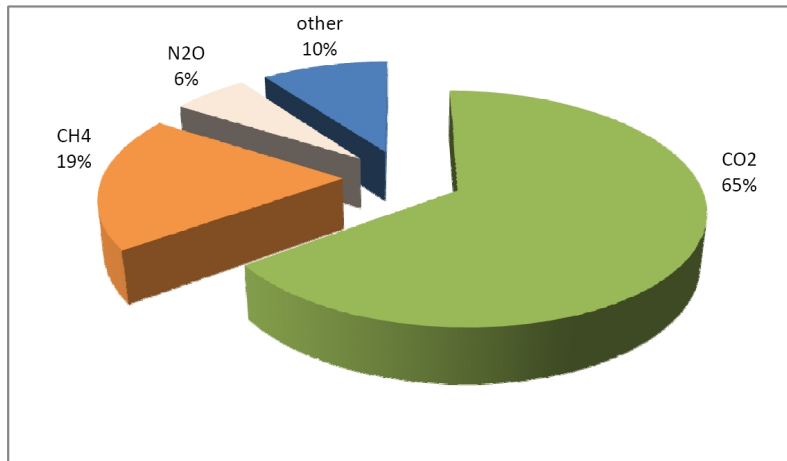


Figure 1: Contribution of different greenhouse gases to climate change [1]

- **Decrease in atmospheric CO₂ concentration due to natural sinks**
Natural CO₂ sinks have a wide influence on the carbon cycle. Specific arrangements in agriculture such as afforestation have made it possible to lower the increasing CO₂ concentration in the atmosphere.
- **Intensified use of nuclear energy and renewable energy**
With the use of nuclear energy and renewable energy like wind power, geothermal energy, and biomass, the emissions can be reduced significantly.
- **Carbon dioxide capture and storage (CCS)**
The combustion-generated CO₂ is separated and transported to underground deposits. CCS is especially applicable in power generation and in industrial plants that produce high quantities of CO₂.

1.2 CO₂ sequestration

There are different methods of sequestering CO₂ in power generation. The sequestration rate of CO₂ depends on its concentration. For example the exhaust gas of fossil fuel burned with air is diluted with nitrogen. Hence the CO₂ concentration is very low and the sequestration is inefficient. To avoid dilution with other gases some so-called oxyfuel systems and precombustion sequestration systems have been developed.

- **Oxyfuel cycles**
In oxyfuel cycles pure oxygen is used to burn fossil fuels. This leads to working fluids containing only CO₂ and H₂O. The H₂O can be removed by proper condensation. Then the combustion-generated CO₂ can easily be retained and either used for other technical applications or stored.
- **Postcombustion capture of CO₂**
Postcombustion systems separate the CO₂ from the exhaust gas. As the com-

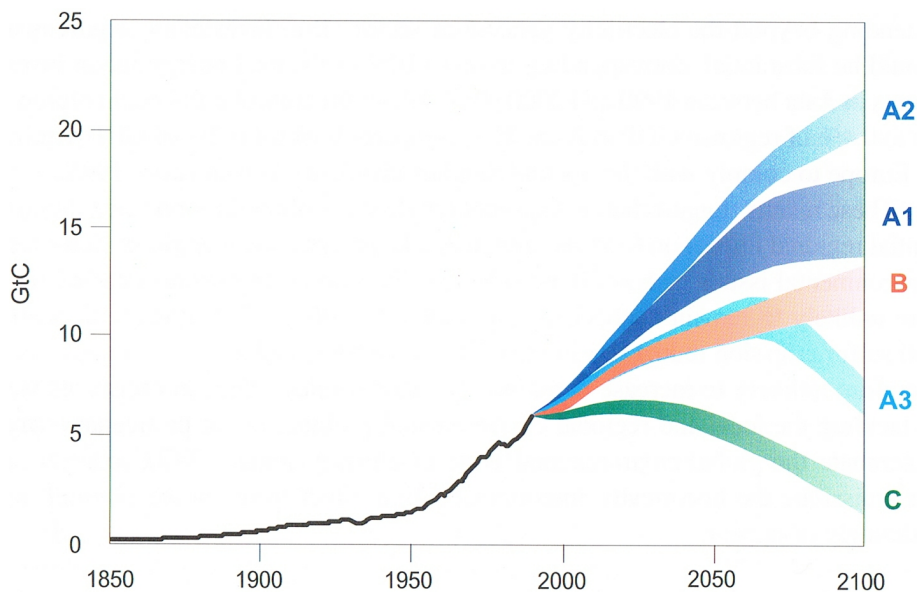


Figure 2: Global carbon emissions from fossil fuel use [2]

bustion of fuel with air the exhaust gas is diluted with nitrogen, the concentration of CO_2 is very low. Thus the separation system is ineffective. The high volume flows lead to very large separation systems. The efficiency of the power plant is also lowered remarkably because of the separation process which is mainly gas scrubbing. Gas scrubbing systems work with solvents to absorb the CO_2 from the exhaust gas. The solvent is then heated up, and the CO_2 is desorbed. The energy demand of this desorbing process is very high, which results in lowered efficiency of the power plant. After regeneration of the solvent, it is used again.

- **Precombustion capture of CO_2**

In precombustion systems the CO_2 is removed from the fuel before it is burned with air. For this purpose fuels like natural gas or syngas from coal gasification are transformed into a mixture of CO_2 and H_2 . This mixture has a high CO_2 concentration and low volume flow. Thus the separation is much easier and more effective than in postcombustion processes. The separation is effected by gas scrubbing or by membranes. After the removal of CO_2 the remaining H_2 is fed to the heat engine or gas turbine and burned with air.

1.3 Transport of CO_2

Because of the high specific volume of CO_2 at low pressures, the transport of CO_2 is easier to handle when it is compressed or liquefied. The pressure level at which CO_2 is transported is usually 100 bar. The liquefaction of CO_2 is accomplished by intercooled compression or cryogenic processes. The corrosive properties of wet CO_2 make it necessary to reduce the water content to 60 % of the saturation state at ambient temperature. The dehumidification is accomplished by the condensation of water during intercooled compression and additional desiccants. Because of the high

quantities of combustion-generated CO₂ in power generation, transport by pipeline or tanker ships is a rational solution [4].

- **Tanker ships**

The transport of liquefied CO₂ is similar to that of liquefied gas. It should therefore be possible to transport CO₂ over long distances to potential storage facilities like oil and gas fields via tanker ships.

- **Pipelines**

Via pipelines it is possible to transport high quantities of CO₂ over long distances. CO₂ pipelines have been used successfully since the 1980s in North America to deliver CO₂ to oil fields for enhanced oil recovery. About 50 Mt CO₂ are transported each year in these pipelines which have a total length of more than 2 500 km.

1.4 Storage of CO₂

To remove the CO₂ from the carbon cycle it has to be placed long-term depository. Such depositories may be [1]:

- **Oceans**

There are different ways to store CO₂ in oceans. It can be scattered in a depth of 1 000 to 2 000 m in a very dilute form. Another option is to discharge it at a deep of 3 000 m. In this case the liquid CO₂ will form a lake on the seabed. A third way is to release solid CO₂ at depth.

- **Aquifers**

An aquifer is a deep, porous rock formation which contains underground water. As it is enclosed by tight rock formations, there is no water interexchange with other underground water flows. These properties allow CO₂ to be stored long-term in these aquifers.

- **Oil and gas fields**

Oil and gas fields have held liquids and gases for millions of years. Depleted fields are thus very suitable for CO₂ storage. Another option is to use the CO₂ for enhanced oil or gas recovery. In this case CO₂ is pumped into the fields to get more oil or gas out of it.

- **Coal seams**

Coal seams contain methane in pores. If it is not profitable to mine the coal from the coal seam and if it has never been disturbed, it is possible to pump CO₂ into it. The CO₂ then displaces the methane, which can be recovered. This process is known as CO₂-enhanced coal bed methane production.

1.5 Examples of oxyfuel cycles

Below some examples of oxyfuel cycles are described. Other oxyfuel cycles (e.g., the Lorentzen-Petterson cycle or the van Steenderen project) are reproduced in [6]. The COOPERATE demo power cycle, which is similar to the Naki cycle, is presented in [7]. Reviews of different oxyfuel cycles are given in [8].

1.5.1 Oxyfuel Steam Cycle

Fossil fuel like coal is burned with pure oxygen in a boiler. Recirculated exhaust gas is delivered to the combustion area to decrease the temperature. Hence, the hot gas consists only of CO_2 and H_2O . The hot gas is cooled down in the boiler generating steam for a steam cycle. After leaving the steam generator, the combustion-generated CO_2 and H_2O are separated. The remaining mass flow is fed back to the combustion area. The H_2O of the removed mass flow is separated by an intercooled compression with water separation. The remaining combustion-generated CO_2 can then be liquefied and is ready for transport and storage. [5]

1.5.2 Semiclosed Oxyfuel Combustion - Combined Cycle

The Semiclosed Oxyfuel Combustion - Combined Cycle (SCOC-CC) [13] consists of a high-temperature Brayton cycle (high-temperature turbine, combustion chamber, compressor, and HRSG) with CO_2 as working fluid and a conventional bottoming double-pressure steam cycle (high-pressure turbine, low-pressure turbine, condenser, and feeding pumps).

Recycled CO_2 is supplied to the combustion chamber and is heated up to 1 400 °C by burning fuel. Fuel and a nearly stoichiometric mass flow of oxygen are fed to the combustion chamber, which is operated at a pressure level of 40 bar. The exit gas of the combustion chamber which consists of CO_2 and H_2O drives a high-temperature turbine. After this it passes through a HRSG to generate steam for a conventional double-pressure steam cycle. In a condenser the H_2O condenses and can easily be separated. The remaining CO_2 stream is compressed by a compressor and fed to the combustion chamber again, after the combustion-generated CO_2 has been removed.

The SCOC-CC provides an efficiency of nearly 50 % [13].

1.5.3 Graz Cycle

The Graz Cycle [13, 16, 26, 27] consists of a high-temperature cycle and a low-temperature cycle. Fossil fuel, together with a nearly stoichiometric mass flow of oxygen, is fed to the combustion chamber, which is operated at a pressure level of 40 bar. The high flame temperature is reduced by circulating working fluid and steam from a high-pressure steam turbine. Hence the exit mass flow of the combustion chamber (working fluid) consists only of H_2O and CO_2 . After the combustion chamber the working fluid has a temperature of 1 400 °C and drives the high-temperature turbine. Then it passes through the HRSG that produces the steam for the high-pressure turbine. After the HRSG about 55 % of the working fluid is compressed and fed back to the combustion chamber. The remaining mass flow which contains the combustion-generated CO_2 and H_2O is fed to a condensation process in which the water is removed. The condensed water is fed to the HRSG in which it is vaporized and superheated. It then drives the high-pressure turbine and afterwards is fed to the combustion chamber. The condensation heat is used in a

low-pressure steam cycle for further power generation. At the end of the condensation process the captured CO_2 is ready for further use or storage.

The Graz Cycle provides an efficiency of about 53 % [13].

1.5.4 Matiant Cycle

The Matiant Cycle [10] is a power cycle with internal combustion, reheating (also internal combustion), and CO_2 as working fluid. CO_2 is heated up in a combustion chamber by burning natural gas with a stoichiometric mass flow of oxygen. With a temperature of 1 300 °C and a pressure of about 40 bar the working fluid drives a turbine and afterwards it is reheated to 1 300 °C. The reheating is also done with natural gas and a stoichiometric mass flow of oxygen. After driving a second turbine the working fluid is fed to a recuperative heat exchanger where it is cooled down. In a staged compression with intercooling and water separation the H_2O is removed, and finally the CO_2 is condensed at a pressure level of 70 bar. The liquid CO_2 is pumped to a pressure level of 300 bar and fed to the recuperative heat exchanger. But before the recuperative heat exchanger, the combustion-generated CO_2 is removed. The supercritical CO_2 is heated up to about 600 °C and then it drives a further turbine. This turbine expands the working fluid to 40 bar. The exit mass flow of this turbine is fed back to the recuperative heat exchanger and heated up, before it is fed to the combustion chamber again.

The Matiant Cycle reaches an efficiency of about 45 % [10].

1.5.5 Chemical Looping Combustion

The Chemical Looping Combustion Cycle [9] gets the oxygen that is needed for the combustion of fossil fuels from a chemical process and therefore no air separation unit is needed. There are two alternatives:

- **Chemical Looping Combustion - Combined Cycle [9]**

Compressed air is piped into an oxidation reactor where the oxygen of the air reacts with a metal to form a metal oxide. As this reaction is exothermic, the air is heated up. The exhaust air of the oxidation reactor which has a reduced oxygen content drives an air turbine and afterwards passes through an HRSG to generate steam for a multipressure steam cycle, before it leaves via the stack. The metal oxide produced flows to the reduction reactor, where it is reduced to metal by fossil fuel which is also fed into the reduction reactor. In other words, the fuel is burned with the oxygen that was chemically bound to the metal. As a result of this oxygen transport, there is no nitrogen in the area where the fuel is burned just the combustion-generated gases CO_2 and H_2O . Next, the metal is transported back to the oxidation reactor. The combustion-generated gases drive a so-called CO_2 turbine, and are then used to preheat the fuel. The H_2O of the exhaust gas is removed through a two-stage intercooled compression with water separation. The nearly pure CO_2 is then compressed to 80 bar and further cooled down to 30 °C. At this pressure and temperature level it is liquid and can be pumped to 100 bar by a pump.

It is then ready for transport and storage.

The Chemical Looping Combustion - Combined Cycle provides an efficiency of about 50 %.

- **Chemical Looping Combustion - Steam Cycle [9]**

In the Chemical Looping Combustion alternative the oxygen reactor is built as a steam generator. The reactors work at atmospheric conditions (pressure). The exhaust gas generated in the reduction reactor is used only to preheat the fuel, before the H₂O is removed and the CO₂ is liquefied.

This alternative has an efficiency of about 40%.

1.6 History of the Naki Cycle, an oxy-fuel cycle originally proposed by Prof. Dr. Nebojsa Nakicenovic

In 1998 Prof. Dr. Nebojsa Nakicenovic, Dr. Cesare Marchetti, and Prof. Dipl.-Ing. Dr.techn. Jericha Herbert discussed an oxyfuel cycle as recommended by Prof. Dr. Nakicenovic that uses pure CO₂ as the working fluid. The fuel of this supercritical cycle with internal combustion should be coal dust (pure carbon). In principle it works like a closed cycle gas turbine with a recuperative heat exchanger but with internal combustion. The main feature due to the working fluid is the pressure rise in liquid state accomplished by a pump instead of the pressure rise in gaseous stage by a compressor. Therefore the CO₂ working fluid has to be condensed. The pressure levels discussed for this cycle were 400 bar for the turbine inlet pressure and 70 bar for the pressure in the condenser. The result of this discussion was that the realization of this cycle is difficult but possible with a lower turbine inlet pressure level. At the "Energiewende - 10. Symposium für Energieinnovation" of the Graz University of Technology in Graz in February 2008 Nakicenovic and Jericha talked about the cycle again. Nakicenovic then commissioned the Institute for Thermal Turbomachinery and Machine Dynamics of Graz University of Technology to perform a feasibility study in form of this diploma thesis supported by IIASA (The International Institute for Applied Systems Analysis), Laxenburg, Austria. The present work is thus a continuation of this discussion in which the thermodynamics of the Naki cycle as well as the feasibility of thermal turbomachinery are investigated.

1.7 Assignment of tasks

In the present work three variants of the Naki cycle are investigated. These variants are called Naki I, Naki II, and Naki III. All cycles are supercritical oxyfuel cycles with internal combustion and use CO₂ as working fluid. Fuel can be coal dust (pure carbon) for Naki I and natural gas (methane) or syngas from coal gasification for Naki II and Naki III. The combustion-generated water is removed from the working fluid after driving the turbine and being cooled down. The pure CO₂ can be condensed. After the condenser the combustion-generated CO₂ is removed and can be stored. Hence there is no CO₂ emitted by Naki cycle power plants.

There are three main tasks:

- **Thermodynamic simulation of the cycles with IPSEpro**
The variants of the Naki cycles have to be modeled and analyzed using the commercial software IPSEpro by SIMTECH Simulation Technology.
- **Turbomachinery layout**
A rough layout of the main turbomachinery dimensions for the different variants has to be performed.
- **Economic evaluation**
A rough economic evaluation for the different variants of the Naki cycle has to be carried out. The COE (cost of electricity) of the different variants has to be compared with those of a conventional power plant, leading to the CO₂ mitigation costs.

2 Thermodynamic Evaluation

All thermodynamic evaluations were performed with the commercial software IPSEpro by SIMTECH Simulation Technology [11]. This flexible software allows the modeling and analysis of thermodynamic cycles. In the software a cycle is defined by modules that are connected with streams. Modules from a standard library or self made modules are used.

2.1 Calculation in IPSEpro

2.1.1 Modules

In the Model Development Kit (MDK) libraries of self-made modules can be created. The modules are defined through equations. In the present work some modules that were designed for the simulation of the Graz Cycle in [12] are used. The Graz Cycle also works with fluids of high CO₂ content. Therefore its modules are suitable for the cycles investigated in this study.

2.1.2 Model of the cycles

Modules from a library are placed in a graphical environment and connected through streams that are represented by lines. This model defines the cycle. Because of this flexible modeling it is possible to define a large variety of different cycles and thermodynamic processes. As IPSEpro uses stable iteration algorithms, it does not need much time for the calculation. Therefore it is possible to analyze the characteristics of different modules, parts of processes, and whole processes very efficiently. Some results can be depicted directly in the model.

2.1.3 Main modules of the library used for the Naki cycles

- **Combustion chamber:**
The combustion chamber was designed for the Graz Cycle and modified in [12] for working fluids consisting of water and CO₂. Its design makes the use of different fuels possible. For example, pure carbon, methane, and syngas as used in the present work.
- **Cooled Turbine:**
This module includes the model for film-cooled blades. It was designed for the Graz Cycle in [12].
- **Turbine:**
The module turbine is used as a conventional uncooled turbine for polytropic expansion of CO₂ containing working fluids.
- **Compressor:**
As the compressor includes the equation for polytropic compression of different fluids, it can also be used as pump for liquid fluids in the calculation.
- **Heat exchanger (HTEX):**
The heat exchangers are designed as counter-flow heat exchangers.

2.1.4 Thermophysical properties

For the thermophysical properties of the fluids the same library as for the Graz Cycle in [14] with real gas properties of CO₂ and H₂O is used. All other fluids are modeled as ideal gas. Because of the limited pressure range for oxygen in the library, the results for oxygen compression are modeled with [15]. The thermophysical properties for H₂ and CO (components of syngas) are also taken from [15].

2.2 Definition of cycle efficiencies

The definition of cycle efficiencies used in this work is the same as in [16]. *Equation 1* defines the net efficiency.

$$\eta_{net} = \frac{(P_T - P_C) * \eta_m * \eta_{gen} * \eta_{tr} - P_{aux} - P_{fuel} - P_{O_2} - P_{CO_2}}{Q_{in} * (1 + \xi_C)} \quad (1)$$

P_T : Power of all turbines

P_C : Power of pumps and compressors of the cycle

η_m , η_{gen} , and η_{tr} : mechanical, generator, and transformer efficiency

P_{aux} : Auxiliary losses

P_{fuel} : Power of fuel compression

P_{O_2} : Power of oxygen generation and compression

P_{CO_2} : Power of CO_2 hand-over pump

Q_{in} : Heat input

ξ_C : Combustion chamber heat-loss coefficient

3 Main Assumptions, Efficiencies, and Pressure Losses

3.1 General assumptions

Table 1 shows some of the main assumptions used in the investigation. The calculation is done with a cooling water temperature of 5 °C. The combustion chamber heat-loss coefficient considers the heat that is lost through the insulation of the combustion chamber. The energy that is needed by auxiliary systems is included through the auxiliary losses. The air separation unit is also considered with the efforts for oxygen production. The combustion-generated CO_2 is given off in liquid state and at a pressure level of 100bar. The turbine and combustion chamber cooling is done with working fluid (CO_2) with a temperature of 300 °C. The combustion chamber cooling mass flow is assumed with 3 % of the combustion chamber main mass flow. For the cooled turbine the cooling mass flow is calculated in the model cooled turbine.

Table 1: General assumptions

Cooling water temperature	5	°C
Combustion chamber heat-loss coefficient ξ_c	0.25	% of heat input
Auxiliary losses P_{aux}	0.35	% of heat input
Oxygen production	0.25	kWh/kg
Exit pressure CO_2	100	bar
Coolant temperature	300	°C
Combustion chamber cooling mass flow	3	% of main mass flow

3.2 Fuel

Table 2 gives an overview of the calorific values of carbon, methane, and syngas from coal gasification. In the case of syngas the calorific values of the components H_2 and CO are also shown. The composition of syngas in weight% is shown. The supply pressure of methane and syngas means the pressure at which fuel arrives at the power plant.

Table 2: Fuel assumptions

Calorific value carbon (coal dust)	33 914	kJ/kg
Calorific value methane	50 015	kJ/kg
Calorific value H ₂ in syngas	119 989	kJ/kg
Calorific value CO in syngas	10 103	kJ/kg
Calorific value syngas	14 126	kJ/kg
H ₂ in syngas	6.1	wt%
CO in syngas	67.4	wt%
CO ₂ in syngas	26.5	wt%
Supply pressure methane	50	bar
Supply pressure syngas	1	bar

3.3 General efficiencies

General efficiencies are shown in *Table 3*. The mechanical efficiency of 99 % is without gear units. It is reduced to consider gear unit losses. This reduction corresponds to the ratio of gear unit power to turbine power and is about 1.7 % points (97.3 % mechanical efficiency), if the whole turbine power is transferred via gear units.

Table 3: General efficiencies

Mechanical efficiency η_m	99 ¹	% of generator power
Generator efficiency η_{gen}	98.5	% of generator power
Transformer efficiency η_{tr}	99.65	% of generator power

3.4 Isentropic efficiencies

The isentropic efficiency of small compressors is assumed to be lower than the efficiency of larger ones, as shown in *Table 4*. There is also a difference in efficiency between the cooled and the uncooled turbine. This is because of the cooling mass flow, which is mixed into the main flow, thereby disturbing the main flow through the turbine.

¹Efficiency without gear units

Table 4: Isentropic efficiencies

Pump	85	%
Small compressor (O ₂ and fuel comp.)	85	%
Large compressor (CO ₂ comp.)	88	%
Turbine cooled	91	%
Turbine uncooled	92	%

3.5 Pressure losses

In *Table 5* the pressure losses of the main components are shown.

Table 5: Pressure losses

Combustion chamber	4	% of pressure
Heat exchanger	3	% of pressure
Condenser	0	% of pressure
Pipes	0	% of pressure

4 Thermodynamic Design of the Cycles

The Naki oxyfuel cycles with internal combustion for CO₂ capture are in principle closed cycle gas turbines with recuperative heat exchangers. The working fluid in the supercritical cycles is CO₂. In the different variants called Naki I, Naki II, and Naki III fuel is burned with pure oxygen. Therefore an air separation unit is needed. The oxygen/fuel ratio is assumed to have a value of 1. While in Naki I only pure carbon (coal dust) can be burned, Naki II and Naki III are able to be fired with hydrogenous fuels like natural gas (methane) or syngas from coal gasification.

As mentioned, the cycles are in principle recuperative gas turbines that use CO₂ as working fluid. The main difference from conventional gas turbines is the pressure rise in liquid state by a feeding pump instead in gaseous state by a compressor. Therefore it is necessary to condense the working fluid after the recuperative heat exchanger. The condensation is done at a pressure level of 45 bar and a corresponding condensation temperature of 9.98 °C.

CO₂ has the property that it needs a higher pressure ratio of the turbine than other gases (e.g., air) to reach the same turbine outlet temperature for a given turbine inlet temperature. Hence the turbine inlet pressures for a cycle with CO₂ have to be higher. Therefore a pressure of 200 bar (after the feeding pump) is chosen in the present work.

4.1 Naki I

The first variant called Naki I is designed to burn pure carbon (coal dust). Coal dust is mixed with liquid CO₂. The resulting pulp is pumped into the combustion chamber by a piston pump. With an oxygen/fuel ratio of 1 there is only CO₂ in the working fluid after the combustion chamber. Therefore it can be easily condensed after the recuperative heat exchanger. The combustion produced CO₂ is removed after the condenser and pumped to a pressure level of 100 bar where it is provided for transport and storage.

4.1.1 Cycle description

In *Figure 3* a simplified cycle schematic of Naki I is shown and *Figure 4* depicts the detailed schematic sketch of the cycle.

The feeding pump (1) pumps 280 kg/s liquid CO₂ from the condenser (5) into the recuperative heat exchanger (2). The pressure after the feeding pump is 200 bar. In the recuperative heat exchanger the working fluid is heated up as high as possible. The temperature is limited by a minimum temperature difference of 10 K in this heat exchanger. Its principle Q-t-diagram is shown in *Figure 5*. Then the supercritical working fluid enters the combustion chamber (3), where it is heated up to a temperature of 850 °C. Oxygen is delivered by the oxygen supply (7) (air separation unit). Through a 4-stage intercooled compression it is brought into the combustion chamber. The coal dust is delivered by the fuel supply (6). Because of pressure losses in the heat exchanger and the combustion chamber, the turbine inlet pressure (TIP) is about 189.1 bar. After the expansion of the working fluid in the turbine (4) it is cooled down in the recuperative heat exchanger (2). It then flows to the condenser (5), where it is condensed at a pressure level of 45 bar. The combustion-generated liquid CO₂ is separated and pumped to a pressure of 100 bar by the hand-over pump (8). It is ready then for transport and storage.

The process is depicted in the principle T-s-diagram shown in *Figure 6*.

4.1.2 Thermodynamic balance

The IPSEpro schematic with calculation data is depicted in *Figure 7*. *Table 6* gives an overview of the power balance. The main mass flows of the cycle are shown in *Table 7*. The working fluid mass flow of 280 kg/s is chosen to achieve an electrical output of 50 MW. The pressure after the feeding pump of 200 bar and the pressure losses in heat exchanger and combustion chamber result in a TIP of 189.1 bar. With this TIP, a condenser pressure of 45 bar and a TIT of 850 °C, Naki I reaches a thermal cycle efficiency of 50.7 %. The net efficiency considering auxiliary losses, O₂ supply, and CO₂ compression is about 37.3 %. The cycle needs 4 kg/s coal dust and 10.6 kg/s oxygen in this configuration, and it produces about 14.6 kg/s CO₂ as shown in *Table 7*.

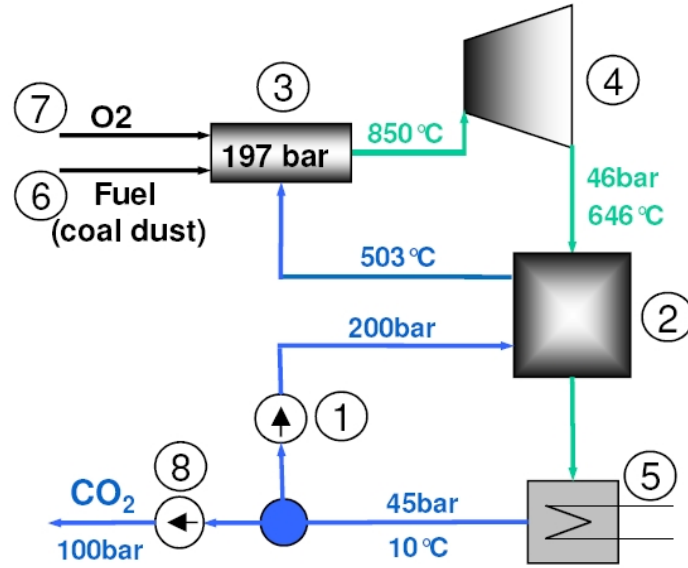


Figure 3: **Simplified cycle schematic of Naki I:** ① Feeding pump; ② Recuperative heat exchanger; ③ Combustion chamber; ④ Turbine (uncooled); ⑤ Condenser; ⑥ Fuel supply; ⑦ Oxygen supply; ⑧ CO₂ hand-over pump

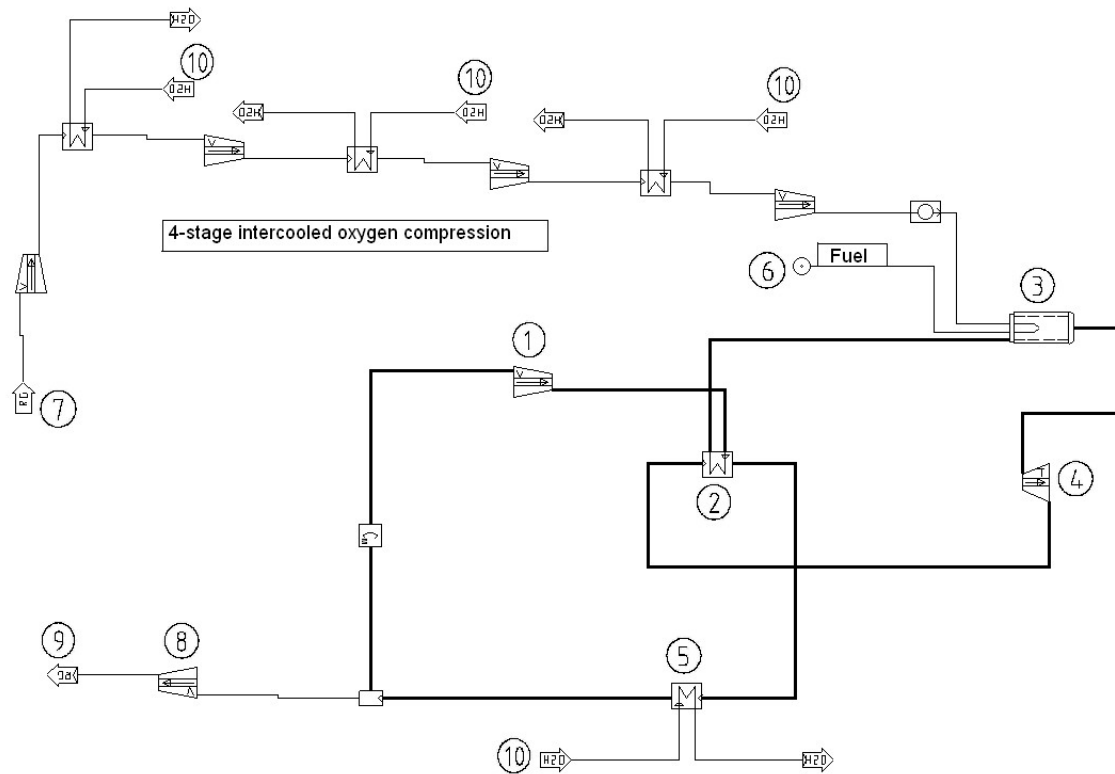


Figure 4: **Detailed IPSEpro schematic of Naki I:** ① Feeding pump; ② Recuperative heat exchanger; ③ Combustion chamber; ④ Turbine (uncooled); ⑤ Condenser; ⑥ Fuel supply; ⑦ Oxygen supply; ⑧ CO₂ hand-over pump; ⑨ CO₂ sink; ⑩ Cooling water supply

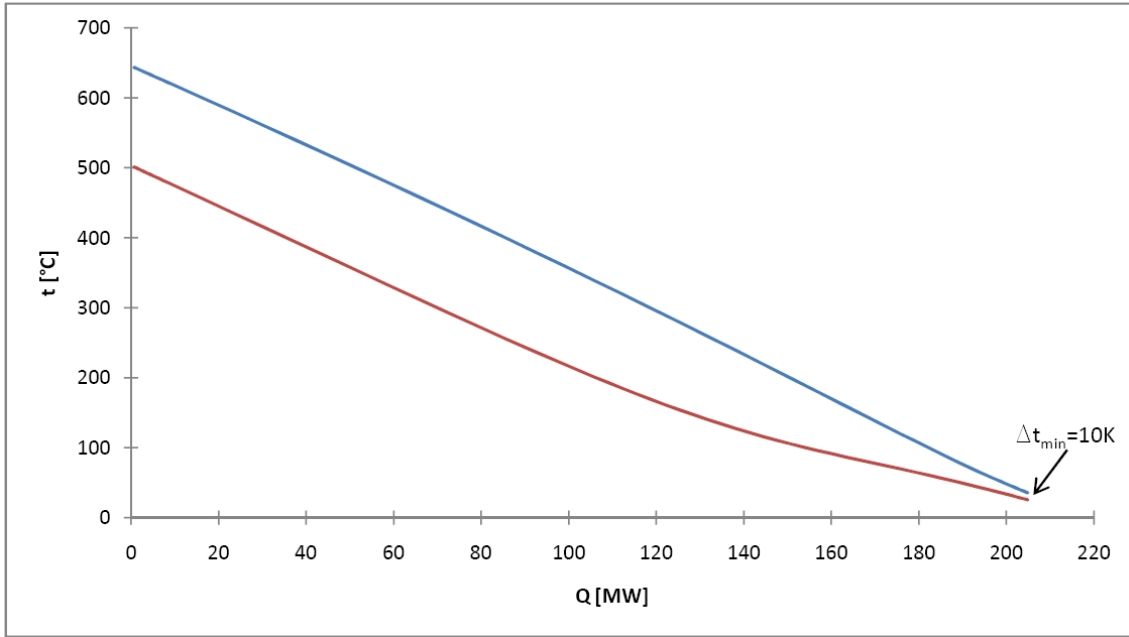


Figure 5: Q-t-diagram of the recuperative heat exchanger

Table 6: Power balance of Naki I

Heat input	135.1	MW
Turbine	74.2	MW
Feeding pump	5.7	MW
Thermal cycle efficiency	50.7	%
Auxiliary losses	0.47	MW
Net electrical efficiency	48.1	%
O ₂ generation	9.5	MW
O ₂ compression	4.9	MW
Efficiency considering O₂ supply	37.4	%
CO ₂ compression	0.11	MW
Net efficiency	37.3	%
Net electrical power	50.4	MW

Table 7: Mass flows of Naki I

Working fluid (CO ₂)	280.0	kg/s
Fuel (coal dust)	4.0	kg/s
Oxygen	10.6	kg/s
Captured CO ₂	14.6	kg/s

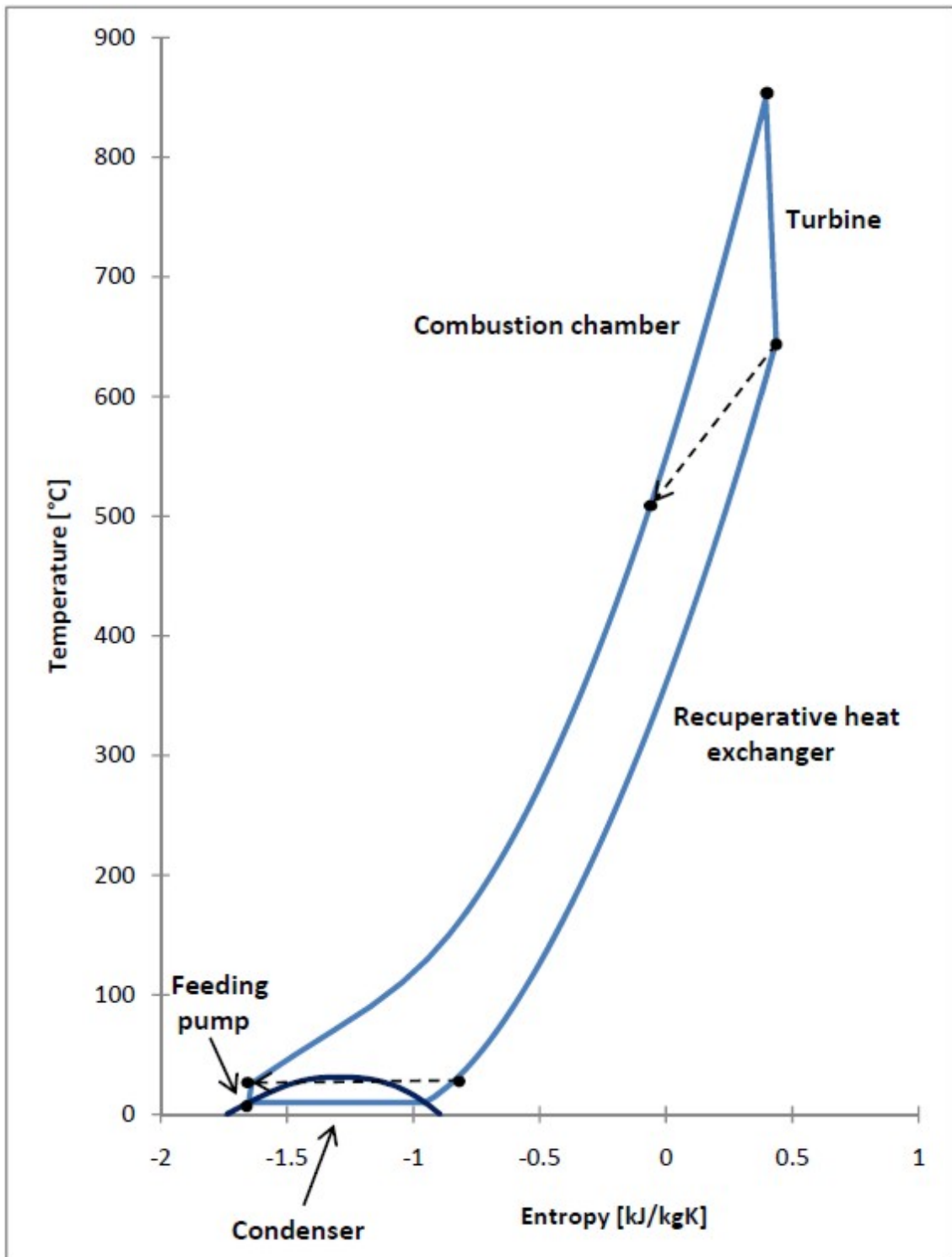


Figure 6: Principle T-s-diagram of Naki I

4.1.3 IPSEpro schematic of Naki I

The IPSEpro schematic shown in *Figure 7* gives all thermodynamic data (pressure, enthalpy, temperature, and mass flow) of the calculation.

4.1.4 Turbomachinery arrangement

The cycle Naki I, with its small pressure ratio of about 4.1, is designed with one high-speed turbine with a speed of 20 000 rpm. This uncooled turbine has only three stages. It drives the generator with a speed of 3 000 rpm over a gear unit as shown in *Figure 8*. The feeding pump is on the same shaft and coupled to the generator.

4.1.5 Influence of parameters

The influence of TIT and pressure after the feeding pump on net efficiency is depicted in *Figure 9*. In *Appendix A, Table 28*, the corresponding values are shown. The minimum temperature difference in the recuperative heat exchanger is fixed at 10 K (see *Figure 5*) and the condenser pressure of 45 bar is also kept constant. The TIT is limited to 900 °C, because of the usage of uncooled turbine blades. It is possible to use uncooled turbine blades up to 900 °C (but with short life cycles).

The net efficiency increases with rising TIT for a given pressure level as a result of the higher temperature level of heat input and expansion, while the temperature of the hot heat exchanger drain stream has a constant outlet temperature. A higher TIT leads to a higher turbine exit temperature and therefore allows higher preheating of the cold flow. This also raises the temperature level of heat input (Carnot). The hot drain stream of the heat exchanger passes to the condenser, where its condensation heat is cooled away.

The net efficiency increases with higher pressures because of the higher turbine power in ratio to heat input. The increase in net efficiency with rising pressures at a given TIT becomes lower for higher pressure levels. One point is the increasing temperature of the hot heat exchanger drain stream (it goes into the condenser). This means that more heat has to be cooled away. The temperature of this hot heat exchanger drain stream is the result of the exit temperature of the feeding pump and the minimum temperature difference of 10 K in the heat exchanger. With rising pressures, the exit temperature of the feeding pump increases, which results in a temperature rise of the hot heat exchanger drain stream. Moreover, the ratio of feeding pump power to turbine power increases with rising pressures.

Figure 10 shows the influence of cooling water temperature and therefore rising condenser pressure on net efficiency. Corresponding values are given in *Appendix A Table 29*. The net efficiency decreases with rising cooling water temperature. This is because of the increasing power demand of the feeding pump because of rising working fluid temperatures, despite the decreasing pressure ratio. The ratio of turbine power to heat input also decreases, and the increasing power demand of oxygen compression with higher intercooling temperatures of the oxygen also negatively influences net efficiency.

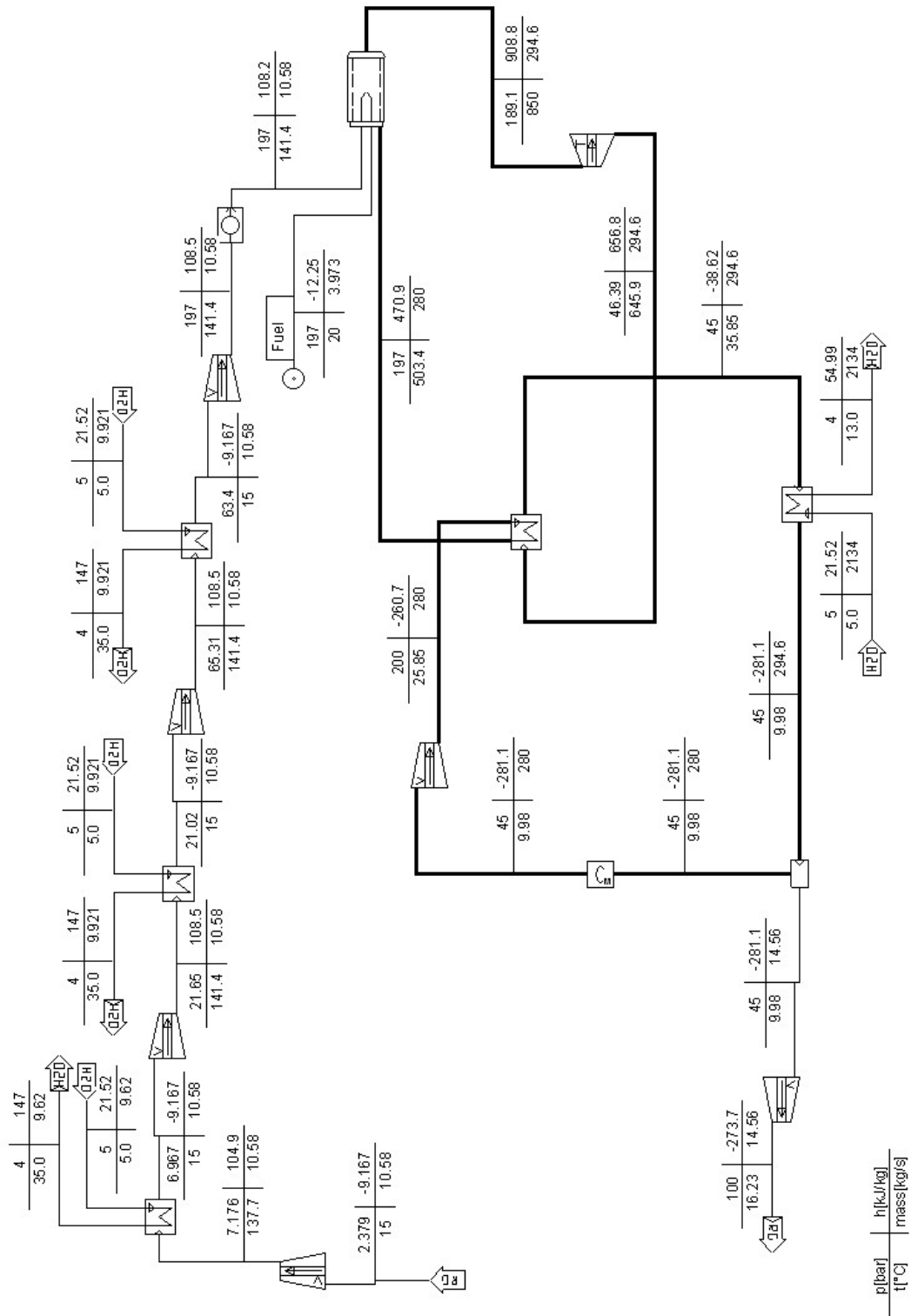


Figure 7: IPSEpro schematic of Naki I with calculation data

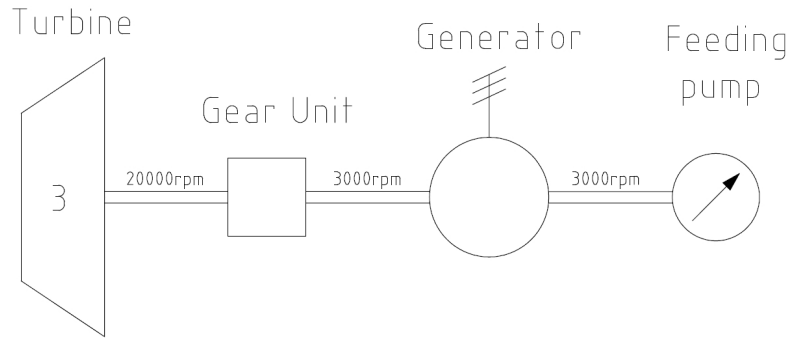


Figure 8: Turbomachinery arrangement of Naki I

In *Appendix B* there are additional data about the influence of the parameters mentioned previously on the efficiency of the cycle and on the power of different components of the cycle.

4.2 Naki II

Naki II is the second variant of an oxyfuel cycle with internal combustion and based on CO_2 as the working fluid. This process can be fired with fuels containing carbon and hydrogen like natural gas, which is investigated, or syngas from coal gasification. Because of the combustion of hydrogenous fuels, there is also H_2O in the working fluid. To enable the condensation of CO_2 it is necessary to remove the H_2O before it reaches the condenser. This is accomplished by a three-stage intercooled compression of the H_2O -containing working fluid. In this way most of the water is condensed in the intercoolers and separated.

The turbine inlet temperature (TIT) in this calculation is about $1\,400\text{ °C}$ and the pressure after the feeding pump is 200 bar. Because of pressure losses in the recuperative heat exchangers and the combustion chamber, the turbine inlet pressure (TIP) is about 186.3 bar. The exit pressure of the low-pressure turbine and hence the inlet pressure of the first compressor is about 4 bar to enable the three-stage intercooled compression to 45 bar.

The expansion of the working fluid from a temperature of $1\,400\text{ °C}$ to 750 °C is done in cooled turbines. In these turbines the required cooling mass flow influences the efficiency in a negative way. Thus the cooled turbine should work with as few stages as possible to reach high cycle efficiencies. However the less favorable properties of CO_2 like the high density and therefore low volume flow make the dimensioning of the turbine difficult and cause a high number of turbine stages. A reduction in the number of stages can be achieved by a high rotational speed of the turbine or larger dimensions due to a high mass flow. A high-speed turbine necessitates gear units with high transmission ratios. Thus the speed of the turbine is limited. Hence the maximum speed in the present work is about 20000 rpm. To achieve feasible turbine dimensions at this speed, a mass flow of 400 kg/s is chosen. With these assumptions the number of cooled turbine stages can be kept low.

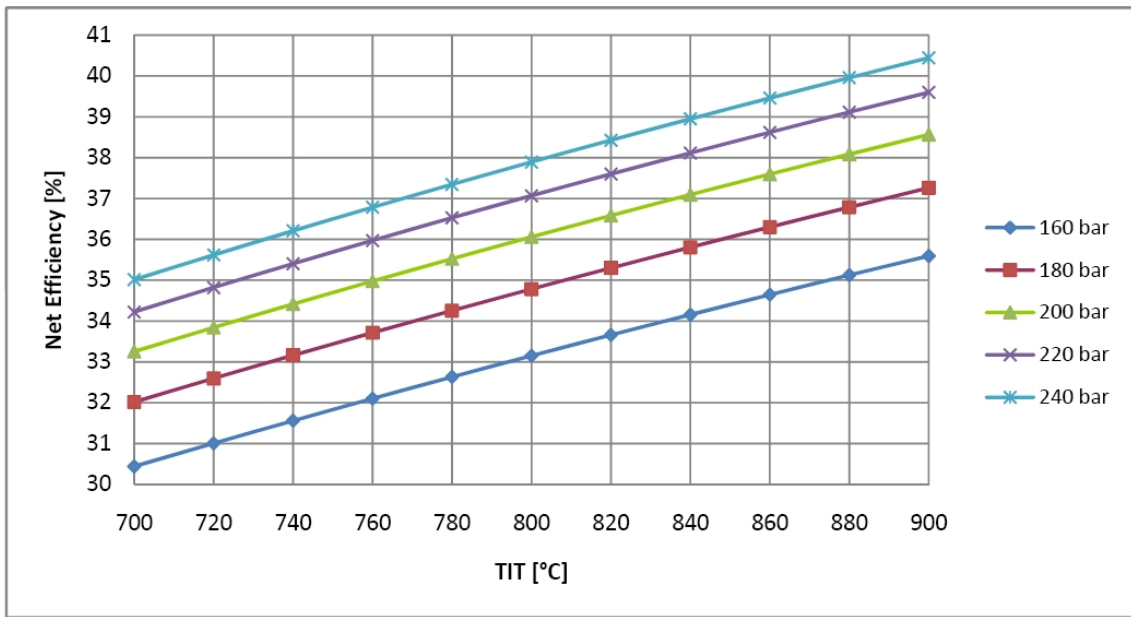


Figure 9: Influence of TIT and pressure after feeding pump on net efficiency (Naki I)

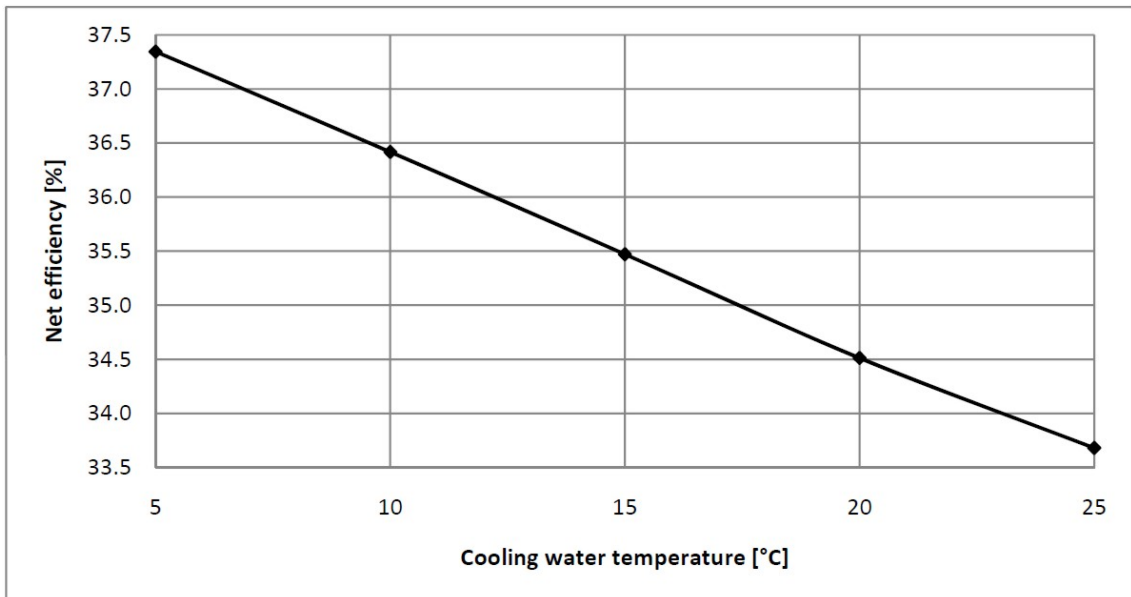


Figure 10: Influence of cooling water temperature on net efficiency (Naki I)

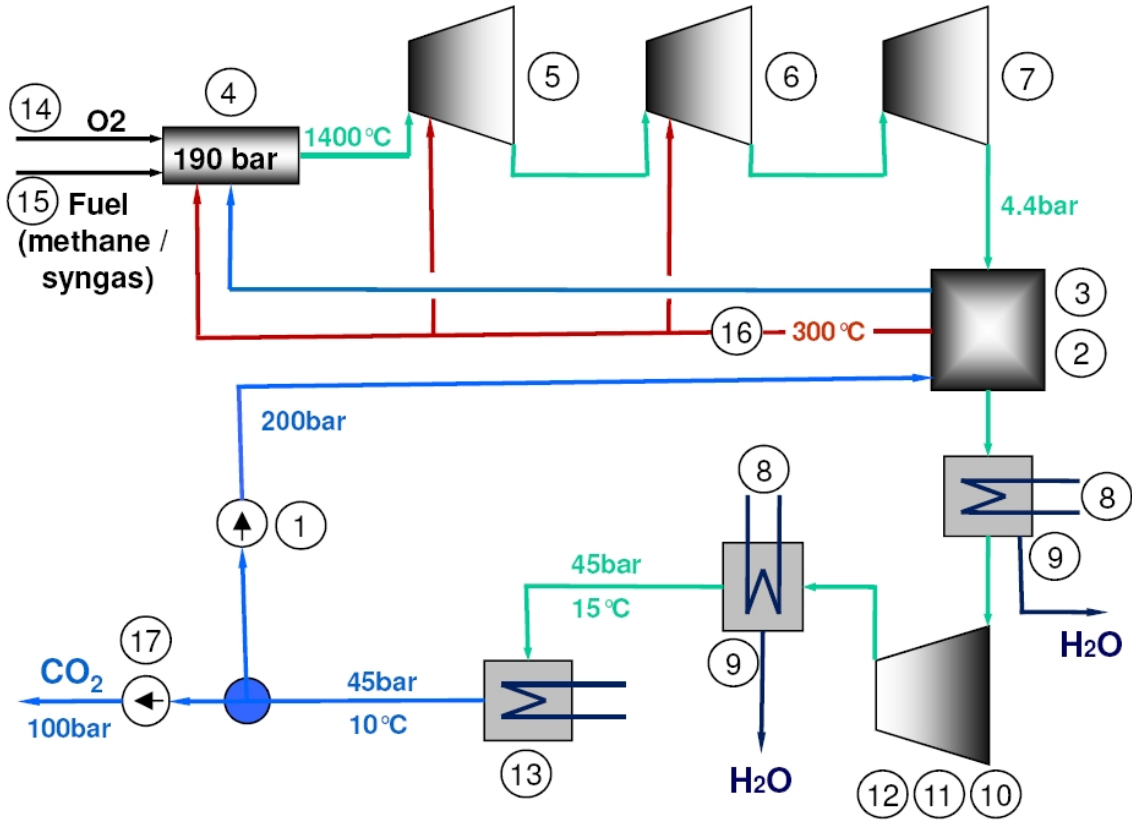


Figure 11: **Simplified cycle schematic of Naki II:** ① Feeding pump; ②, ③ Recuperative heat exchanger; ④ Combustion chamber; ⑤ High-pressure turbine (HPT); ⑥ Intermediate pressure turbine (IPT); ⑦ Low-pressure turbine (LPT); ⑧ Heat exchanger (cooler); ⑨ Water separator; ⑩ Compressor C1; ⑪ Compressor C2; ⑫ Compressor C3; ⑬ Condenser; ⑭ Oxygen supply; ⑮ Fuel supply (methane or syngas); ⑯ CO₂ cooling stream (combustion chamber and turbine cooling); ⑰ CO₂ hand-over pump

4.2.1 Cycle description

Figure 11 depicts a simplified flow scheme of the Naki II cycle. A detailed schematic of this cycle is shown in Figure 12.

The split-up into a HPT, an IPT, and a LPT is performed for the thermodynamic calculation to distribute the turbine power between compressors and generator and to obtain data for the turbomachinery layout. In different turbomachinery arrangements the HPT, IPT, and LPT can also be on the same shaft or in the same casing.

Liquid CO₂ from the condenser (13) is pumped to a pressure of 200 bar by the feeding pump (1). In the first recuperative heat exchanger (2) it is heated up to 300 °C. Then the stream is split up into the combustion chamber feed stream and the cooling stream (16). The combustion chamber feed stream flows into the second recuperative heat exchanger (3), where it is heated to as high a temperature

as possible. The limit gives a minimum temperature difference of 10 K in heat exchanger 3, or 5 K in heat exchanger 2. Heat exchanger 2 has an explicit pinch point. Therefore its minimum temperature difference is lower than in heat exchanger 3. Principle Q-t-diagrams of these heat exchangers are shown in *Figure 14* and *15*. At the kink in the hot stream of heat exchanger 2 (pinch point) the temperature falls below the saturation temperature of water. Thus water begins to condense and the gradient of the line decreases.

A partial stream of the cooling stream (16) with a temperature of 300 °C is used for combustion chamber cooling. Its mass flow equals 3 % of combustion chamber feed mass flow. In the combustion chamber (4) all feed streams are heated up to 1 400 °C by burning fuel. This can be methane (natural gas) or syngas from coal gasification. The pressure rise for methane from 50 bar to the combustion chamber pressure is accomplished by a two-stage intercooled compression. Syngas with an initial pressure of 1 bar is transported into the combustion chamber through a 4-stage intercooled compression. The compression of the fuel is calculated by hand with thermophysical properties from [15] and not with IPSEpro. The necessary oxygen is produced in an air separation unit and compressed through a 4-stage intercooled compression.

The exit stream of the combustion chamber with a temperature of 1 400 °C and a pressure of 186.3 bar flows into the HPT (5) and afterwards into the IPT (6). Both turbines are cooled with CO₂ at a temperature level of 300 °C (stream 16). In these turbines the cooling mass flow is mixed into the main stream, resulting in the outlet mass flow of each turbine being higher than the inlet mass flow. The outlet temperature of IPT is 750 °C. Therefore the LPT (7) needs no cooled turbine blades. The LPT expands the working fluid to a pressure level of 4 bar. After the LPT the working fluid (about 96 % CO₂ and 4 % H₂O) with the combustion products is used to preheat the feeding stream in the recuperative heat exchangers 3 and 2. Then it is cooled down to 15 °C in a cooler (8). At this temperature level a fraction of water condenses and is separated by a water separator (9). The next step is a three-stage intercooled compression from 4 bar to 45 bar to separate the water resulting from burning fuel containing hydrogen. This is done by the compressors C1 to C3, coolers (8), and water separators (9). Then the nearly pure CO₂ can be condensed in the condenser (13) at a pressure level of 45 bar and a corresponding condensation temperature of 9.98 °C.

After the condenser the major part of CO₂ is used again as working fluid and transferred to the feeding pump. The rest (the combustion-generated CO₂) is separated and pumped to 100 bar by the hand-over pump (17). Then the separated CO₂ is ready for transport and storage.

Figure 13 depicts the principle T-s-diagram for the working fluid of the cycle. The marked kink is the start point of condensation of combustion-generated water. After the three-stage intercooled compression of the working fluid, all the combustion-generated water is condensed and separated. The working fluid thus consists of nearly pure CO₂ before it enters the condenser.

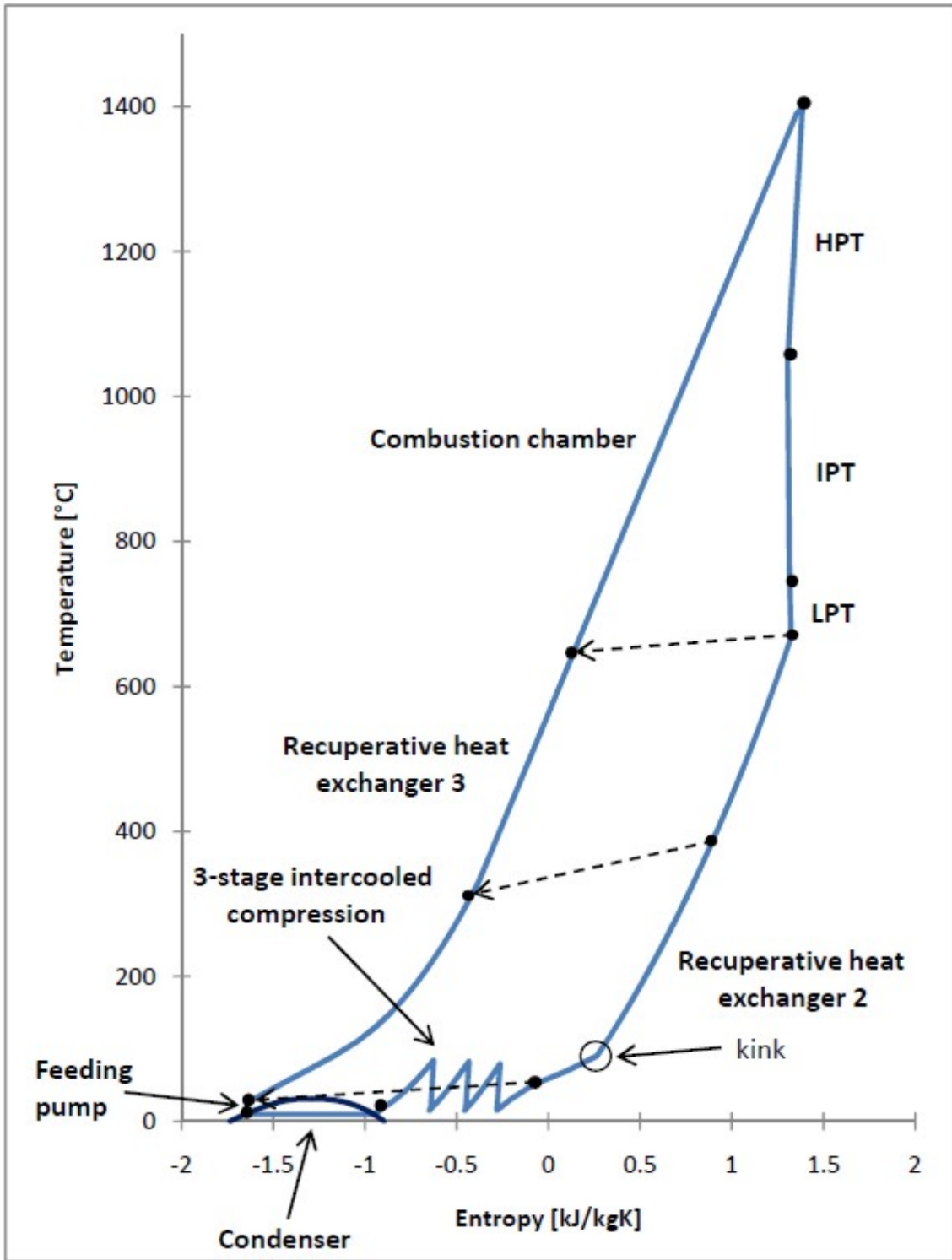


Figure 13: Principle T-s-diagram of Naki II

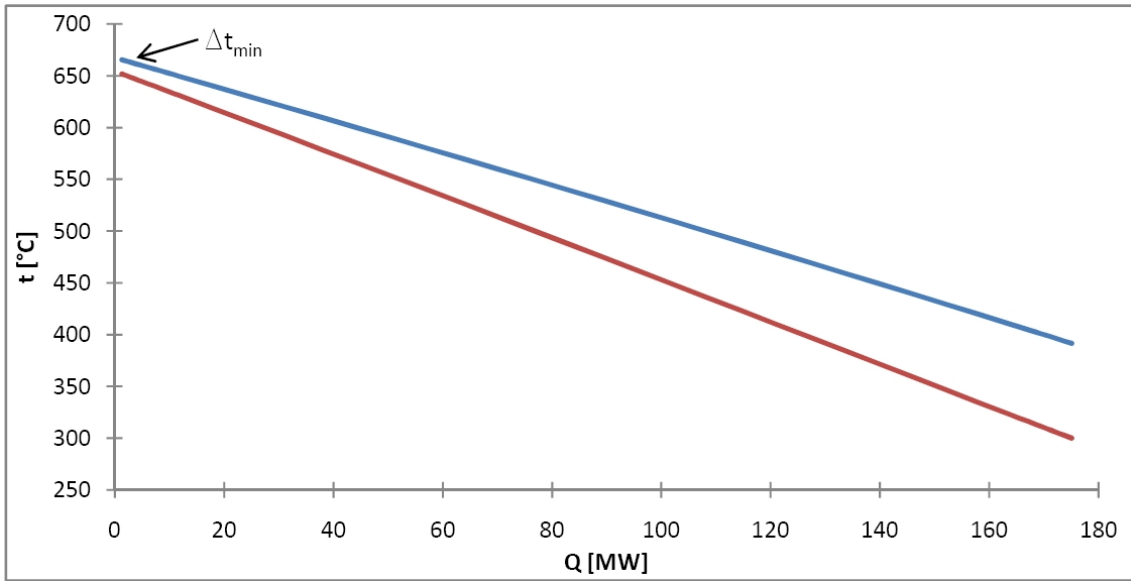


Figure 14: Q-t-diagram of recuperative heat exchanger 3

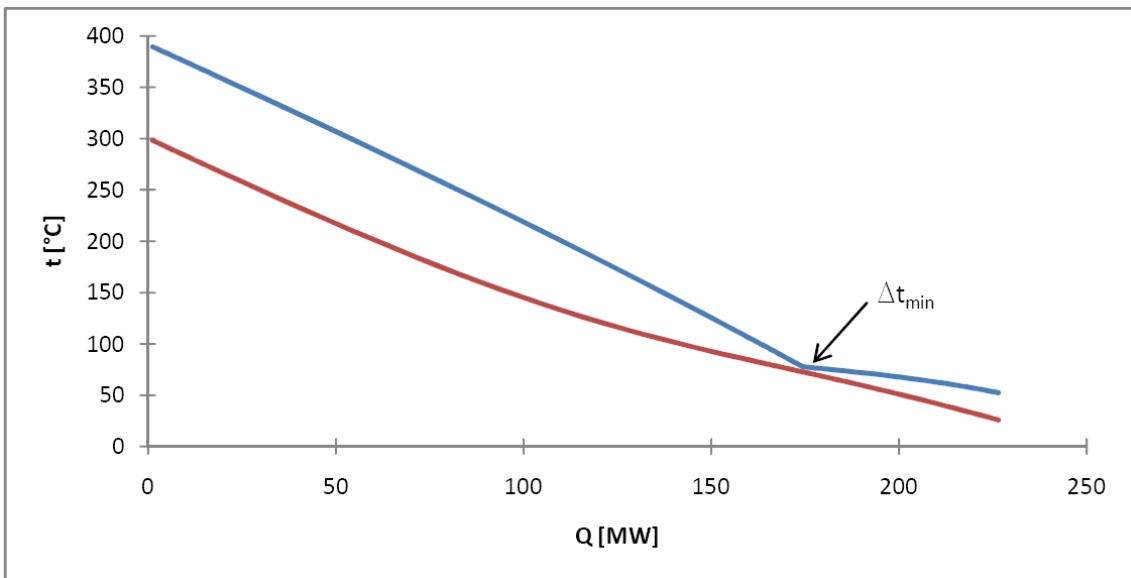


Figure 15: Q-t-diagram of recuperative heat exchanger 2

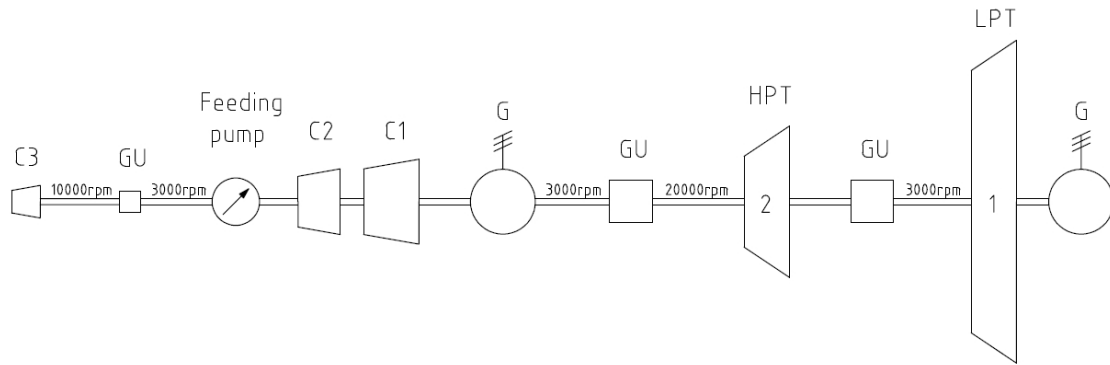


Figure 16: **Turbomachinery arrangement variant 1a:** HPT ... High-pressure turbine; LPT ... Low-pressure turbine; GU ... Gear unit; G ... Generator; C1, C2, C3 ... Compressors 1, 2, and 3

4.2.2 Different turbomachinery configurations for Naki II

In the present work three different variants of turbomachinery design and arrangement are investigated. Variants 1a and 1b are based on the same thermodynamic layout, but differ in terms of the turbomachinery arrangement.

Variant 1a: Low number of cooled turbine stages

Figure 16 depicts the turbomachinery arrangement of this variant. The HPT has two stages. In the thermodynamic calculation and in Table 15 the first stage is called HPT and the second stage IPT. Both stages are on the same shaft and in the same casing. Thus they are physically one turbine with a speed of 20 000 rpm. There is a gear unit on every side of this turbine, each transferring half of the turbine power. The left gear unit drives a generator, the compressors C1, C2, and C3, and the feeding pump. The compressors and the feeding pump are on the left side of the generator because their shaft diameter is too small to transmit the generator power. Compressors C1 and C2 and the feeding pump are coupled to the generator. Hence they have a speed of 3 000 rpm. Compressor C3 has a speed of 10 000 rpm in order to achieve a low number of stages. An additional small gear unit with a power of 26 MW is thus needed. The LPT is on the right side of the shaft next to the right gear unit. It has a speed of 3 000 rpm and is directly coupled to the second generator.

This variant has the advantage of only having two cooled turbine stages with only two high-power gear units and one smaller gear unit for the compressor C3. However, the power of each high-power gear unit is about 190 MW. Such gear units are not in use yet and require additional development work.

Variant 1b: Low number of cooled turbine stages with limited gear unit power

This variant shown in Figure 17 is an alternative to variant 1a. The power of all gear units in this arrangement is lower than 100 MW. Such gear units are already in successful operation in standard gas turbine units. The HPT and IPT are in

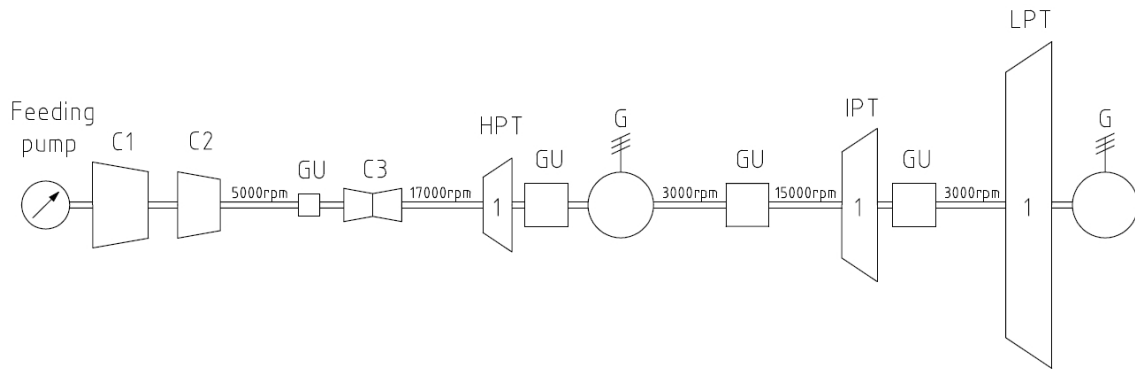


Figure 17: **Turbomachinery arrangement variant 1b:** HPT ... High-pressure turbine; IPT ... Intermediate pressure turbine; LPT ... Low-pressure turbine; GU ... Gear unit; G ... Generator; C1, C2, C3 ... Compressors 1, 2, and 3

different casings so that the power can be distributed to a larger number of gear units and the lower gear unit power can be achieved. Because of the different casings and the gear units between the HPT and the IPT, each of these turbines can have its own speed. The HPT has a speed of 17 000 rpm and the IPT of 15 000 rpm.

On the left side of the HPT are the compressors and the feeding pump. The double-flow Compressor C3 is directly coupled to the HPT with a speed of 17 000 rpm. Compressor C1 and C2 and the feeding pump have a speed of 5 000 rpm. A gear unit with a power of about 64 MW is thus necessary. The power gear unit on the right side of the HPT with a power of 98 MW drives a generator. The IPT with its speed of 15 000 rpm drives both generators via two power gear units (each of which has a power of 98 MW). The LPT is directly coupled to the right generator with a speed of 3 000 rpm.

Variant 2: Arrangement with a free-running compression shaft and without a gear unit for the power shaft

The main advantage of the design shown in *Figure 18* is that the generator is directly driven by power turbines. IPT and LPT are physically one turbine with a speed of 3 000 rpm. The only difference is that the stages of the IPT are cooled and the stages of the LPT are uncooled. The high-speed HPT with a speed of 14 500 rpm drives the compressors and the feeding pump. Compressor C3 is designed as double-flow compressor and thus it allows a speed of 14 500 rpm (Mach number limitation, see *Chapter 5.2*). It can thus be directly coupled to the HPT. Compressors C1 and C2 and the feeding pump have a speed of 5 000 rpm, a gear unit with a power of about 80 MW is thus necessary.

Variant 3: Limit of turbomachinery layout

The turbomachinery arrangement of variant 3 as shown in *Figure 19* uses turbines that are located at the edges of turbomachinery layout. The HPT with one cooled stage has a speed of 16 167 rpm. It drives the compressors and the feeding pump

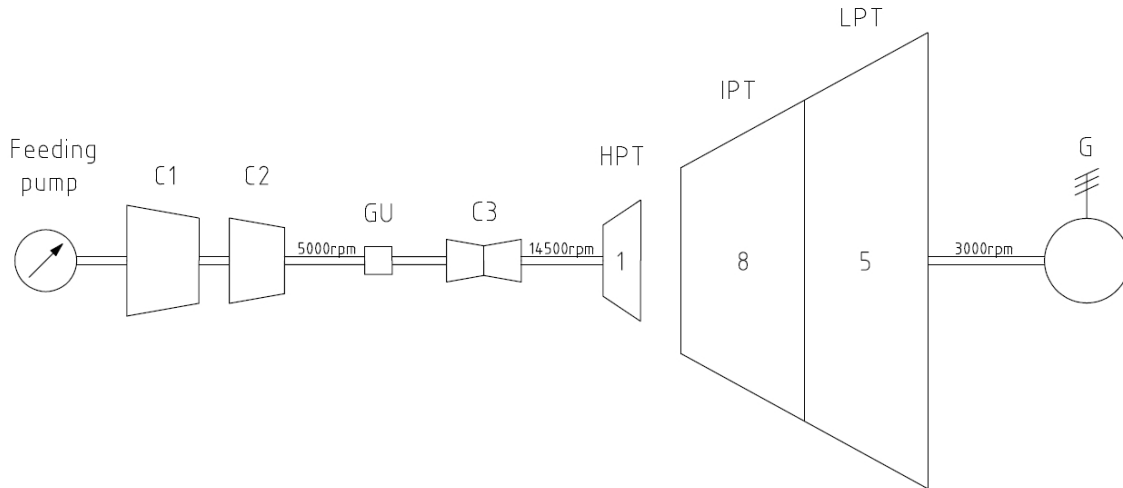


Figure 18: **Turbomachinery arrangement variant 2:** HPT ... High-pressure turbine; IPT ... Intermediate pressure turbine; LPT ... Low-pressure turbine; GU ... Gear unit; G ... Generator; C1, C2, C3 ... Compressors 1, 2, and 3

via the left shaft end. Compressor C3 is designed as double-flow compressor and can thus reach a speed of 16 167 rpm and can be directly coupled to the HPT. Compressors C1 and C2 and the feeding pump have a speed of 5 000 rpm. A gear unit with a power of 64 MW is thus necessary. The right shaft end of the HPT drives the generator via a power gear unit with a power of about 190 MW. This power gear unit reduces the speed to 3 000 rpm and is coupled to the LPT. The LPT with its speed of 3 000 rpm is directly coupled to the generator. The LPT has two stages. The first stage has film-cooled blades and the second stage has cooled blade roots. In the thermodynamic calculation the first stage is called IPT and the second stage LPT. The advantage of this variant is that it has a simple turbomachinery arrangement with one power gear unit and one generator. Furthermore, it has only two film-cooled turbine stages. However, the power gear unit with its power of about 190 MW is not yet in use and requires additional development work as mentioned before in variant 1a.

4.2.3 Comparison of the different turbomachinery configurations

The turbomachinery arrangement in variant 1a with a two-stage HPT has the advantage that there is a single casing that has to withstand high pressures at high temperature levels. The HPT exit stream has a temperature of 750 °C and a pressure of 7.8 bar. Because of this low temperature and pressure level it can be transported easily through a transition line to the LPT. A disadvantage of this variant is that power gear units with a power of 190 MW are not yet in use and require additional development work. Another disadvantage is that the turbomachinery arrangement with its 3 gear units (2 power gear units and one smaller gear unit) and 2 generators is difficult to operate.

Variant 1b was designed to reduce the power of the power gear units to values

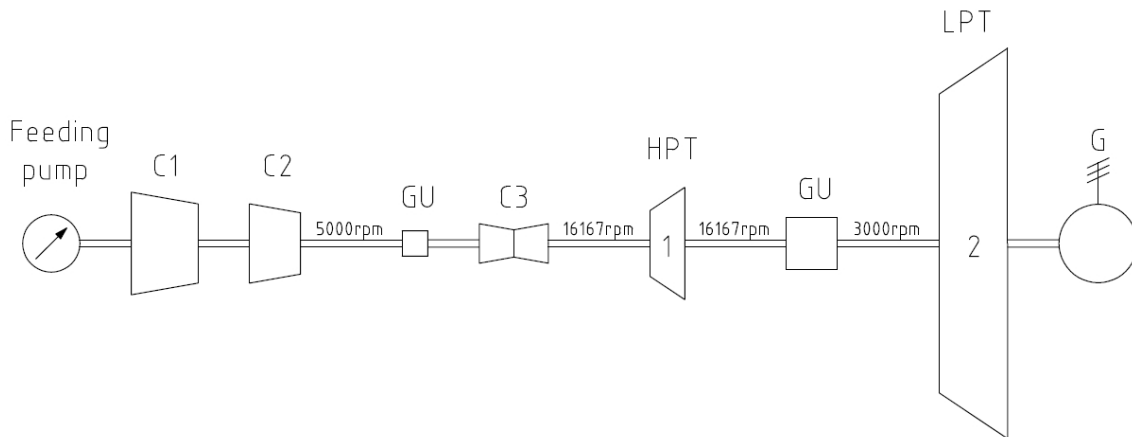


Figure 19: **Turbomachinery arrangement variant 3:** HPT ... High-pressure turbine; LPT ... Low-pressure turbine; GU ... Gear unit; G ... Generator; C1, C2, C3 ... Compressors 1, 2, and 3

lower than 100 MW. Such gear units are already in successful operation in standard gas turbine units. The two-stage HPT of variant 1a is split into two turbines for variant 1b. Each turbine has its own casing and its own speed. Between these two casings there are a generator and two gear units. Thus, the hot exit working fluid of the first turbine (HPT) with a temperature of 1050 °C and a pressure of 46.5 bar has to be transported through a long transition line to the second turbine (IPT). This transport is a complex operation to carry out successfully at this temperature and pressure level. Another disadvantage of this variant is that there are three turbine casings. Two of them have to withstand high pressures at high temperature levels. Also the complicate turbomachinery arrangement with 3 turbines, 4 gear units (3 power gear units and 1 smaller gear unit), and therefore the longer shaft is intricate to handle.

Variant 2 has the advantage that the generator is directly driven by a power turbine. The double-flow compressor C3 is directly driven by the HPT. Only the compressors C1 and C2 and the feeding pump are driven via a gear unit. All turbines can be physically in the same casing but there have to be bearings between the HPT and the other turbine. The exit mass flow of the HPT with a temperature of 1146 °C and a pressure of 83.4 bar has to be transported to the next turbine over this distance. The disadvantage of this variant is the high number of cooled stages and therefore the lower net efficiency.

Variant 3 has the advantage that it has only two cooled turbine stages and that compressor C3 is directly driven by the HPT. However, this variant needs one power gear unit with a power of about 190 MW that is not yet in use. The exit mass flow of the HPT with a temperature of about 910 °C and a pressure of 21 bar has to be transferred to the LPT via transition lines, because there is a gear unit between the two turbines.

In summary the turbomachinery arrangement in variant 3 has to be preferred because of the simplified turbomachinery arrangement in comparison to variant 1a

Table 8: Power balance for variants

		Variant 1	Variant 2	Variant 3
Heat input	MW	528.2	578.0	526.6
High-pressure turbine	MW	186.5	110.9	276.0
Intermediate pressure turbine	MW	194.6	183.9	78.6
Low-pressure turbine	MW	54.9	165.0	79.7
Feeding pump	MW	9.6	12.0	9.6
Working fluid compressor	MW	79.6	98.9	79.8
Thermal cycle efficiency	%	65.7	60.4	65.5
Auxiliary losses	MW	1.8	2.0	1.8
Net electrical efficiency	%	62.5	58.1	62.6
Methane compression	MW	2.4	2.7	2.4
O ₂ generation	MW	37.8	41.4	37.7
O ₂ compression	MW	19.3	21.1	19.2
Efficiency considering O₂ and fuel supply	%	51.2	46.8	51.4
CO ₂ compression to 100bar	MW	0.2	0.2	0.2
Net efficiency	%	51.2	46.8	51.3
Net electrical power	MW	270.3	270.3	270.3

and 1b. The temperature and pressure in the transition line in variant 3 are higher than in variant 1a, but there are techniques to handle them. The higher net efficiency of about 4.5 % points of variant 3 in comparison to variant 2 (see *Table 8*) also leads to this preference. Thus, the detailed turbomachinery layout (see *Chapter 6*) is only performed for variant 3. Also the economic evaluation is performed only for variant 3.

4.2.4 Thermodynamic balance of the different turbomachinery configurations

Figure 20, *Figure 21*, and *Figure 22* depict the IPSEpro schematics with thermodynamic data of variant 1, 2, and 3. Variant 1a and 1b have the same IPSEpro schematic. They differ only in the turbomachinery arrangement. They are thus called variant 1 in the thermodynamic power balance.

Table 8 gives a comparison of the power balance between variant 1, variant 2, and variant 3. A TIT of 1 400 °C and a feeding pump pressure of 200 bar (because of pressure losses in the heat exchangers and the combustion chamber, the resulting TIP is 186.3 bar) are used in all three calculations. Moreover, the exit pressure of the LPT of about 4 bar is the same in all investigations. In variant 1 a combustion chamber feed stream (in *Table 9* it is called working fluid) of 400 kg/s was chosen to obtain larger turbomachinery dimensions and thus a low number of turbine stages. In variant 2 the combustion chamber feed stream is 382.3 kg/s for the same electrical output of the power plant. It is 399.2 kg/s in variant 3 because of the same reason.

In variant 2 the IPT has eight stages and in variant 1 and 3 only one. Thus the cooling mass flow of the second variant, with 43 % of the turbine inlet mass flow, is

Table 9: Mass flows for variants

		Variant 1	Variant 2	Variant 3
Working fluid (CO ₂)	kg/s	400.0	382.3	399.2
Combustion chamber cooling	kg/s	12.0	11.5	12.0
Turbine cooling	kg/s	57.9	194.0	60.0
Turbine inlet mass flow	kg/s	464.6	451.3	463.6
Ratio of turbine cooling to inlet mass flow	%	12.5	43.0	12.9
Fuel	kg/s	10.5	11.5	10.5
Oxygen	kg/s	42.0	46.0	41.9
Captured CO ₂	kg/s	29.0	31.8	28.9
Separated H ₂ O	kg/s	23.6	25.8	23.5

much higher than for the first which is 12.5 %. Between variant 1 and 3 the cooling mass flow is only slightly different. Because of the lower temperature of the LPT exit flow caused by the high cooling mass flow, it is not possible to preheat the feed stream of the combustion chamber in variant 2 to such a high temperature as in the other variants. A higher heat input is thus necessary to reach the same TIT. The higher heat input in variant 2 leads to a higher fuel and oxygen demand, as shown in *Table 9*. The high cooling mass demand also increases the need for feeding pump and working fluid compressor power. This leads to a 5.3 % points lower thermal cycle efficiency in comparison to variant 1. The difference in power demand for fuel compression, oxygen generation, and oxygen compression are proportional to the respective mass flows shown in *Table 9*.

The TIT of the LPT in variant 1 and variant 2 is 750 °C. As this temperature is fixed in the calculation, only the pressure can vary. Because of the higher cooling mass flow of the IPT in variant 2, the temperature of 750 °C is reached at a higher pressure level (see *Figure 20* and *21*). The higher mass flow of the LPT in the second variant is also caused by the higher cooling mass flow. These two parameters lead to higher LPT power in the second variant. Variant 3 is in this respect different from the first two variants. The TIT of the LPT in variant 3 is about 786 °C and higher than in the other variants. The power of the LPT in variant 3 is thus higher than in variant 1.

Variants 1 and 3 have nearly the same net efficiency. The differences in net efficiency between variant 1 and 2 of 4.4 % points and between variant 2 and 3 of 4.5 % points are only caused by a different number of cooled turbine stages (variant 1 has two cooled stages, variant 2 has nine, and the variant 3 also has two cooled stages).

4.2.5 Thermodynamic comparison between methane and syngas as fuel

This comparison is done for variant 1 with a turbomachinery arrangement, as shown in *Figure 16* and *17*, respectively. Both arrangements have the same thermodynamic results. *Figure 20* and *Figure 23* depict the IPSEpro schematic of the cycle with calculation data for methane firing and syngas firing, respectively. The process of

coal gasification is not considered in this investigation.

The power balance for methane and syngas as fuel is shown in *Table 10*. The pressure after the feeding pump is 200 bar (the resulting TIP is 186.3 bar), the expansion pressure 4 bar and the TIT is 1 400 °C in both cycles. In the syngas-fired cycle, the working fluid mass flow is 399.2 kg/s for the same electrical power output instead of 400 kg/s as in the methane-fired cycle.

The fuel mass flow of the syngas-fired cycle is higher (see *Table 11*) because of the lower calorific value of syngas (see *Table 2*). This leads to a higher exit mass flow of the combustion chamber (in *Table 11* it is called turbine inlet mass flow). It includes the working fluid mass flow, the cooling mass flow of the combustion chamber, and the mass flow of combustion-generated products like CO₂ and steam. To reach the same TIT with the higher exit mass flow of the combustion chamber, a higher heat input is necessary. This means that a higher mass flow has to be heated up to 1 400 °C. The turbines also have more power because of the higher mass flow. Therefore, there is only a slight difference in the thermal cycle efficiency.

The efficiency in terms of the oxygen and fuel supply of the syngas-fired cycle is about 1.3 % points lower. The reason is that the fuel compression of syngas takes much more power because of the assumption on fuel delivery pressure. Methane is supplied with 50 bar and syngas with 1 bar. A second point is the higher fuel mass flow of the cycle with syngas firing as mentioned before. On the other hand, the lower oxygen mass flow and thus the lower power demand for oxygen production and compression has a positive effect on efficiency.

Finally, the net efficiency for syngas firing is about 1.4 % points lower than the value for methane firing, with the most significant differences occurring in the fuel supply.

Table 11 shows the main mass flows of the cycles. The working fluid mass flow refers to the feed stream of the combustion chamber. The reason for the higher turbine cooling mass flow of the syngas-fired cycle is the higher turbine inlet mass flow. The turbine cooling mass flow is 12.5 % of turbine inlet mass flow for the methane-fired cycle and 12.4 % for syngas.

4.2.6 IPSEpro schematic of the cycles

The IPSEpro schematic includes the thermodynamic data (pressure, enthalpy, temperature, and mass flow) of the calculation. *Figure 20* depicts the IPSEpro schematic of variant 1 fired with methane. *Figure 23* shows the same variant but with syngas from coal gasification as fuel. The second variant fired with methane is pictured in *Figure 21*. In the IPSEpro schematic of variant 2 there are three turbines. The IPT (the middle turbine in this schematic) has 8 stages, but the module cooled turbine is designed for a lower number of stages. Therefore the simulation in IPSEpro was performed with 8 one-stage turbines instead of the one depicted IPT with 8 stages. For a clearly arranged schematic, only this one turbine (IPT) is depicted. *Figure 22* shows the IPSEpro schematic of variant 3.

Table 10: Power balance for methane and syngas as fuel

		Methane	Syngas
Heat input	MW	528.2	542.4
High-pressure turbine	MW	186.5	193.1
Intermediate pressure turbine	MW	194.6	200.4
Low-pressure turbine	MW	54.9	55.5
Feeding pump	MW	9.6	9.6
Working fluid compressor	MW	79.6	83.3
Thermal cycle efficiency	%	65.7	65.6
Auxiliary losses	MW	1.8	1.9
Net electrical efficiency	%	62.5	62.5
Fuel compression	MW	2.4	22.8
O ₂ generation	MW	37.8	30.0
O ₂ compression	MW	19.3	15.5
Efficiency considering O₂ and fuel supply	%	51.2	49.9
CO ₂ compression to 100bar	MW	0.2	0.4
Net efficiency	%	51.2	49.8
Net electrical power	MW	270.3	270.3

Table 11: Mass flows for methane and syngas as fuel

		Methane	Syngas
Working fluid (CO ₂)	kg/s	400.0	399.2
Combustion chamber cooling	kg/s	12.0	12.0
Turbine cooling	kg/s	57.9	59.7
Turbine inlet mass flow	kg/s	464.6	482.8
Ratio of turbine cooling to inlet mass flow	%	12.5	12.4
Fuel	kg/s	10.5	38.3
Oxygen	kg/s	42.0	33.3
Captured CO ₂	kg/s	29.0	50.8
Separated H ₂ O	kg/s	23.6	20.8

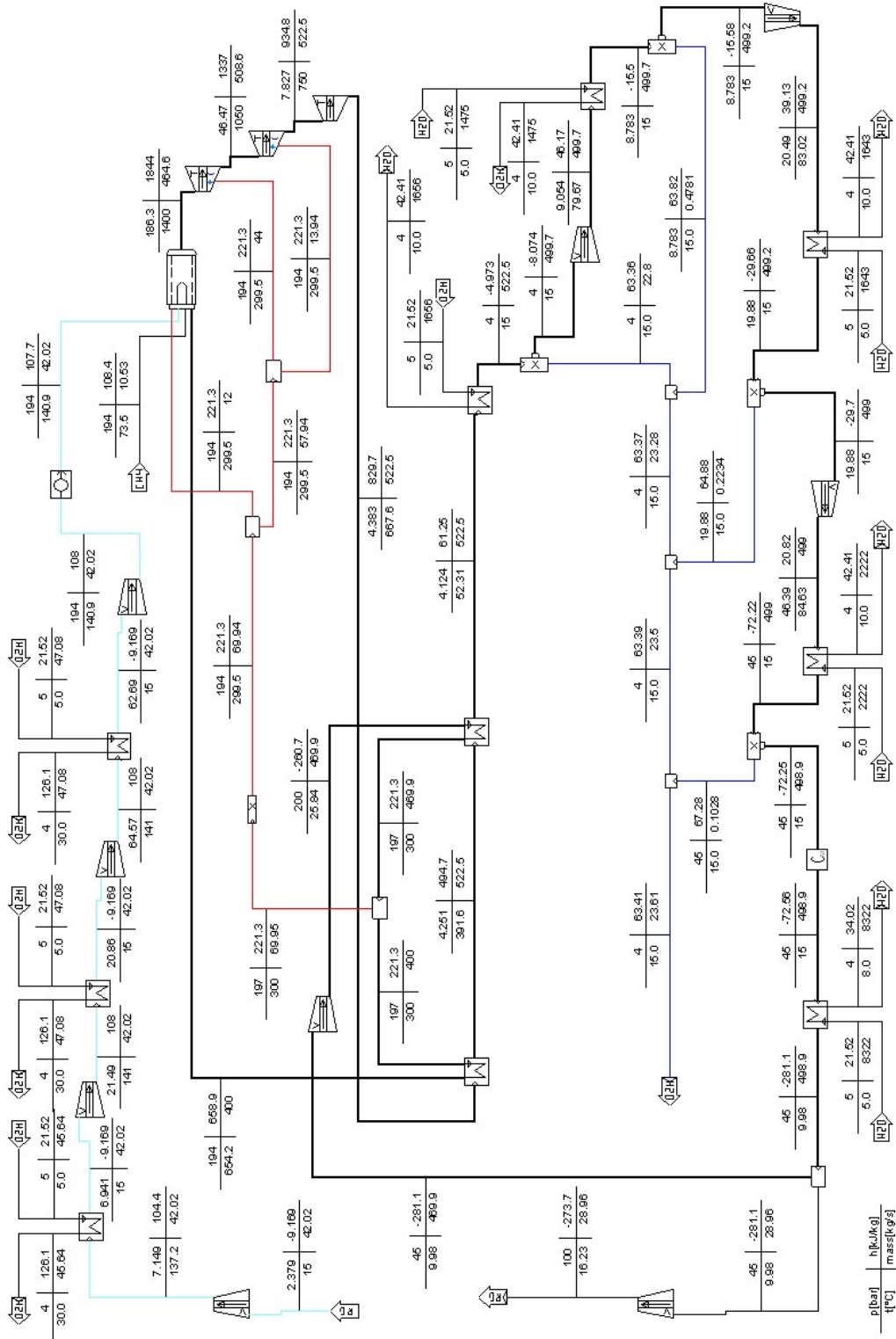
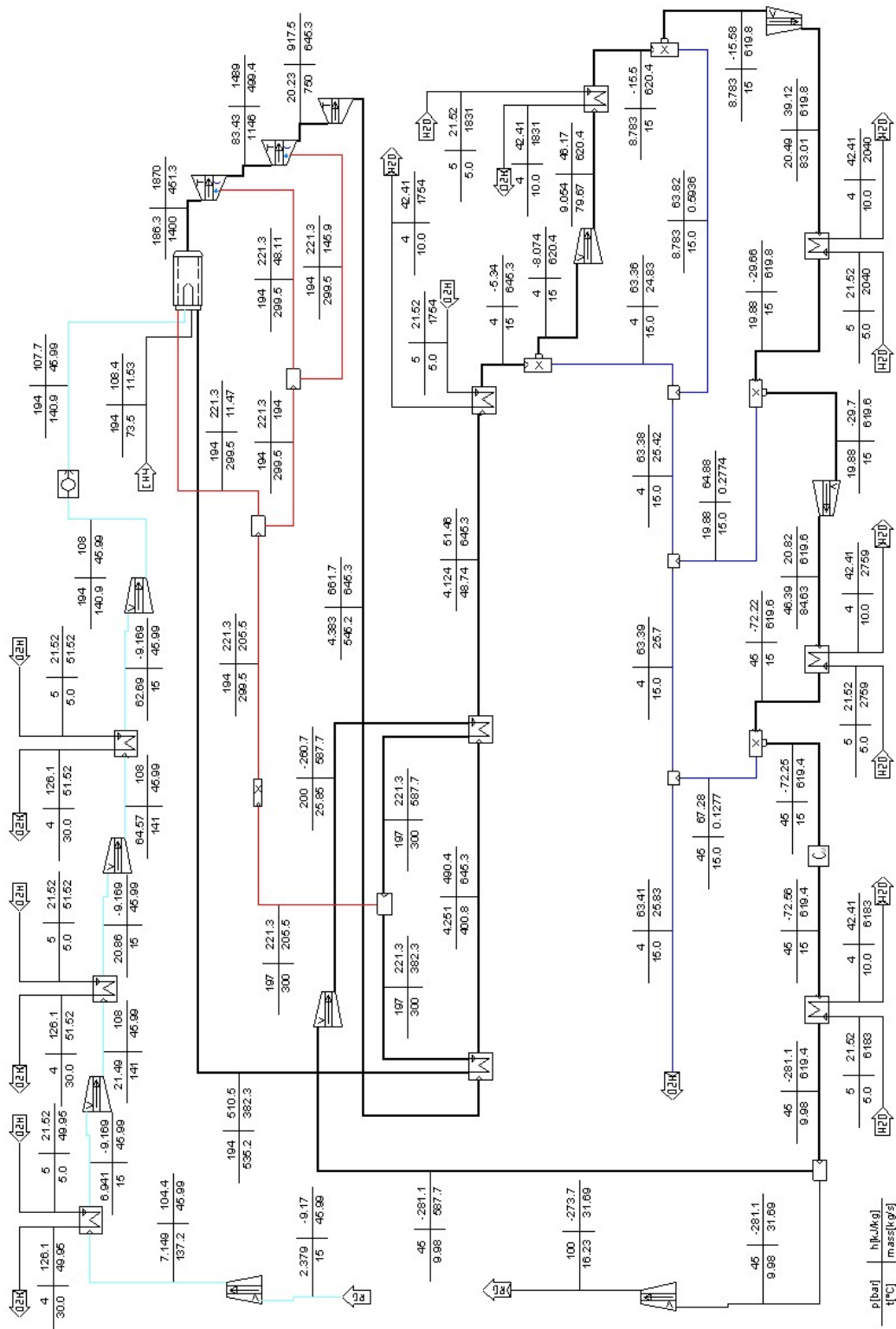


Figure 20: IPSEpro schematic of variant 1 with calculation data (methane)



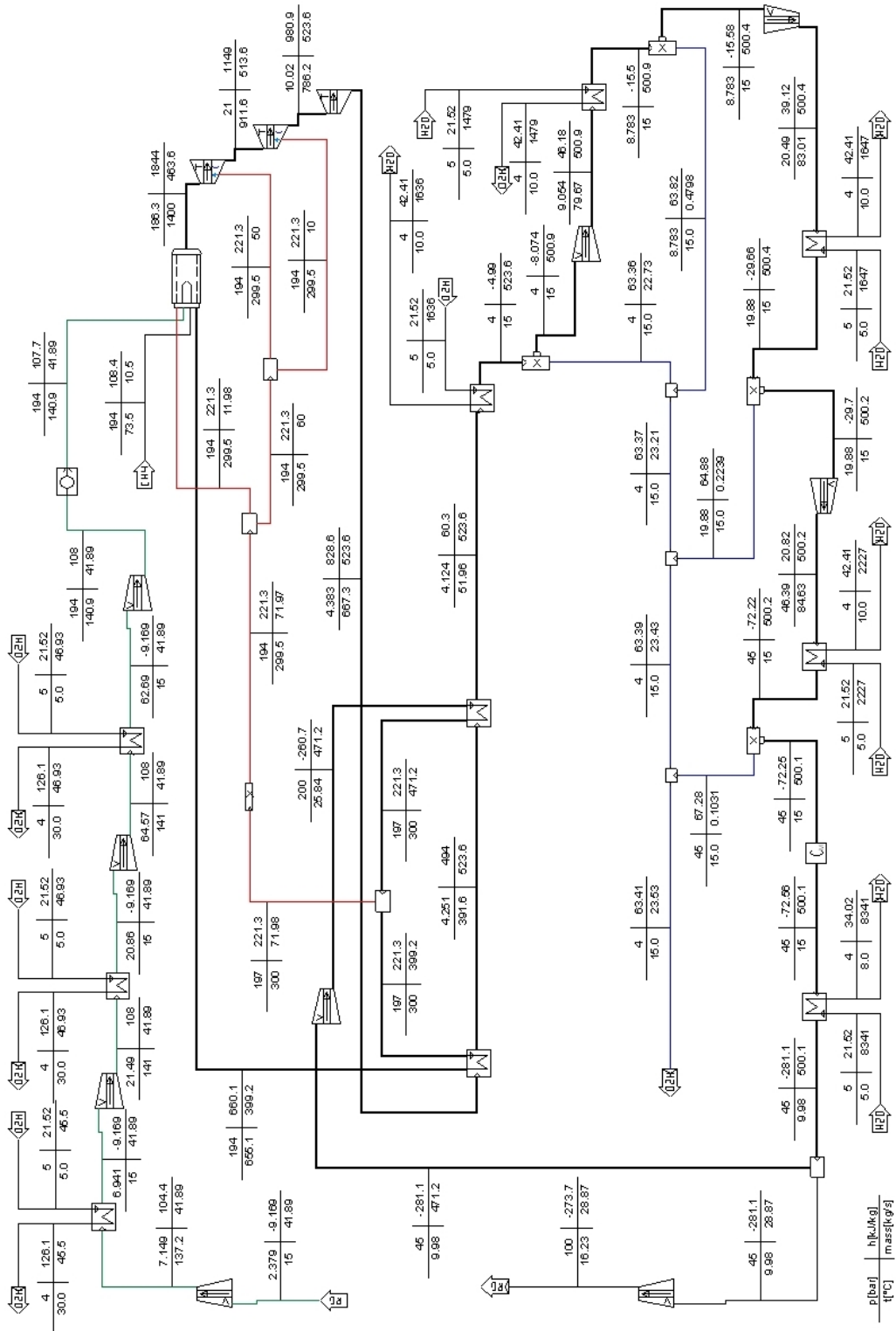


Figure 22: IPSEpro schematic of variant 3 with calculation data (methane)

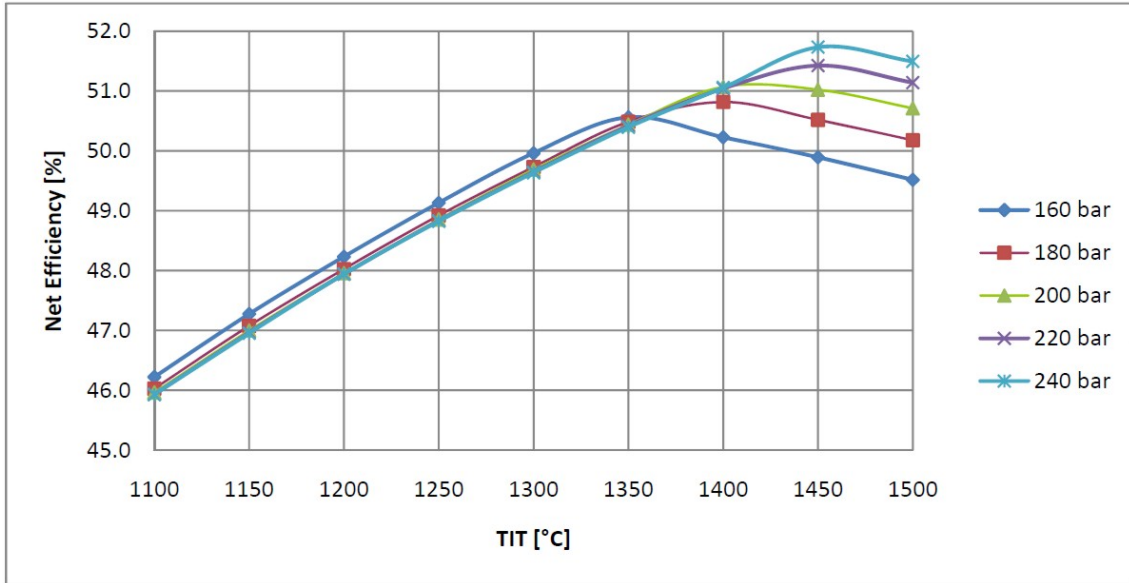


Figure 24: Influence of TIT and pressure (after feeding pump) on net efficiency

4.2.7 Influence of parameters

All calculations for a parameter study were performed for variant 1 and methane as fuel.

Figure 24 depicts the influence of different TIT on net efficiency at different pressure levels. Corresponding values are shown in Table 30 in Appendix A. The LPT exit pressure is about 4 bar and held constant. There is an optimum TIT for each pressure level. The turbine exit temperature (LPT) in the optimum of each pressure level is about 670 °C. At this temperature level the minimum temperature difference in heat exchanger 2 (HTEX 2) is near to its limit of 5 K and also in HTEX 3 it is near to its limit of 10 K. The principal Q-t-diagrams are shown in Figures 14 and 15. Therefore the temperature differences between the hot and the cold stream in both recuperative heat exchangers have the lowest values. This means that each HTEX has its best point at this temperature level. A principle Q-t-diagram of both heat exchangers for the optimum TIT is shown in Figure 25.

The pressure ratio of the turbines rises with higher turbine inlet pressures because of the constant turbine exit pressure. To obtain the same turbine exit temperature at different pressure ratios the TIT has to vary. The highest net efficiency of raising pressures is therefore reached at higher TITs. The highest value of net efficiency for each pressure level also rises with higher pressures. This is because of the higher TIT and therefore the higher mean temperature of heat input, whereas the exit temperature of the hot stream of HTEX 2 is nearly constant. This exit stream of HTEX 2 goes into a cooler and its heat is cooled away. The exit temperature of the hot stream of HTEX 2 depends on the inlet temperature of the cold stream of HTEX 2 (= exit temperature of the feeding pump) and the minimum temperature difference in HTEX 2. There is only a slight increase in the exit temperature of

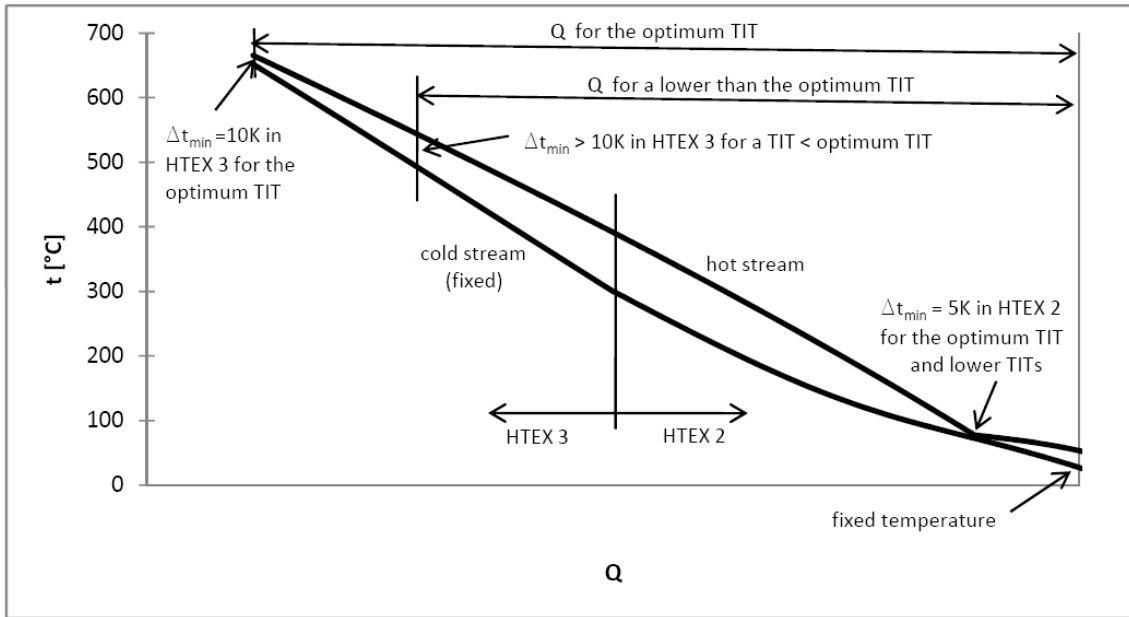


Figure 25: Q - t -diagram of recuperative heat exchangers 2 and 3 for the optimum TIT and a lower TIT

the feeding pump with rising pressures because of the constant feeding pump inlet temperature of $9.98\text{ }^{\circ}\text{C}$ and the compression of working fluid in liquid state.

For TITs lower than the optimum TIT at given pressure levels, the exit temperature of the turbine is lower than $670\text{ }^{\circ}\text{C}$. In *Figure 25* a principle Q - t -diagram of both heat exchangers (2 and 3) for TITs lower than the optimum TIT is shown. The inlet temperature of the cold stream is fixed because of the constant exit temperature of the feeding pump. Hence the temperature increase of the cold stream in the heat exchangers is fixed. The temperature of the hot stream is fixed due to the minimum temperature difference of 5 K in HTEX 2. This means that HTEX 2 limits the temperature of the combustion chamber feed stream. Because of the lower turbine exit temperature, the heat transferred in both heat exchangers is lower than for optimum TIT with a higher turbine exit temperature. In *Figure 25* this effect is depicted by the displaced start point of the Q - t -diagram for lower TITs. The minimum temperature difference of HTEX 3 at the displaced start point is higher than 10 K . Thus HTEX 3 is not operated at its best point. The temperature difference between the hot and the cold stream in ratio to the transferred heat is higher than in case of an optimum TIT. These aspects lead to the decrease of net efficiency at TITs below the optimum TIT.

For TITs higher than the optimum TIT at given pressure levels the turbine exit temperature is higher than $670\text{ }^{\circ}\text{C}$. The principle Q - t -diagram of both heat exchangers for TITs higher than the optimum TIT is shown in *Figure 26*. The inlet temperature of the cold stream and therefore the temperature of the cold stream through both heat exchangers are fixed by the exit temperature of the feeding pump. Because of the higher turbine exit temperature, the transferred heat in both heat exchangers is higher than for optimum TIT. Therefore the start point in *Figure 26*

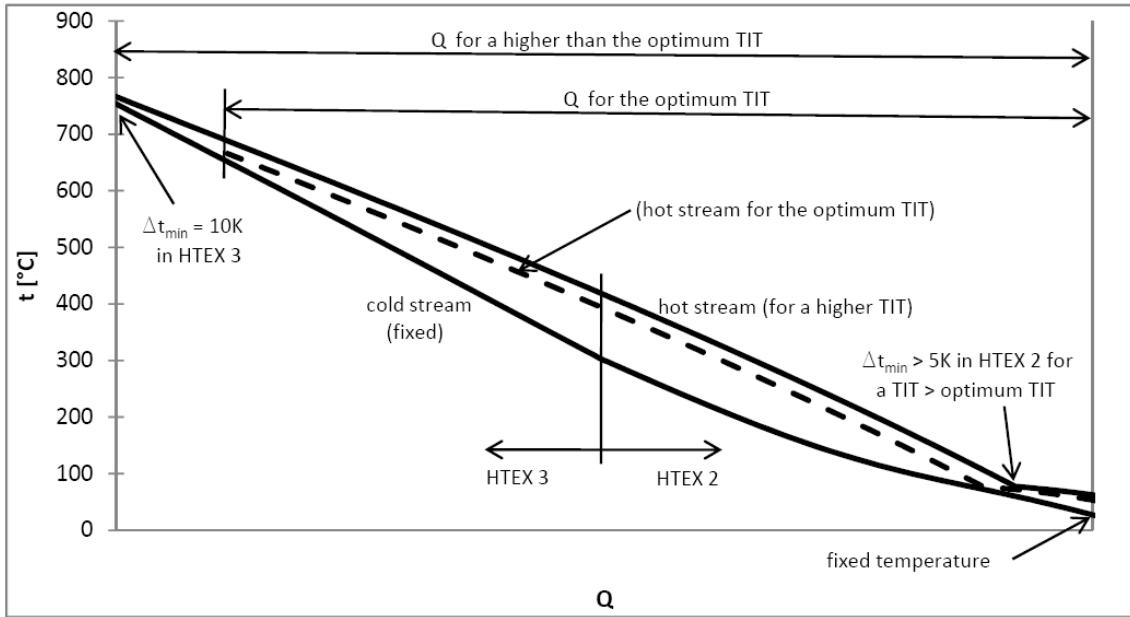


Figure 26: Q - t -diagram of recuperative heat exchangers 2 and 3 for a higher TIT than the optimum TIT

is displaced to the left side. As, in this case the minimum temperature difference in HTEX 3 would be lower than 10 K, the hot stream has to be moved to the right. This means that HTEX 3 limits the temperature of the combustion chamber feed stream. Because of the displacement of the hot stream, the minimum temperature difference in HTEX 2 becomes higher than 5 K. The temperature difference between the hot and the cold steam increases, resulting in a decrease in the efficiency of the heat exchangers. The increased minimum temperature difference in HTEX 2 leads to a higher exit temperature of the hot stream of HTEX 2. As, this stream goes to a cooler, its heat is cooled away. These effects lead to a decrease in net efficiency, with rising TIT after the optimum TIT.

Figure 27 shows the net efficiency at TITs lower than the optimum TIT. The net efficiency for a given TIT decreases with increasing pressure. This is because fuel (methane) and oxygen compression need more power for higher pressures. The temperature of the hot exit stream of HTEX 2 (it goes to a cooler) also increases with rising pressures.

The influence of expansion pressure on net efficiency is shown in *Figure 28*. Corresponding values are given in *Table 31* in *Appendix A*. The expansion pressure is the pressure after the LPT and also the inlet pressure of compressor C1 (see *Figure 12*). The TIT is 1 400 °C and the pressure after the feeding pump is 200 bar (the TIP is 186.3 bar). The highest net efficiency is reached between 4 bar and 5 bar. At this pressure range the outlet temperature of the low-pressure turbine is about 670 °C. Therefore, both heat exchangers (2 and 3) are at their optimal point as mentioned. At lower pressures the turbine outlet temperature is lower than 670

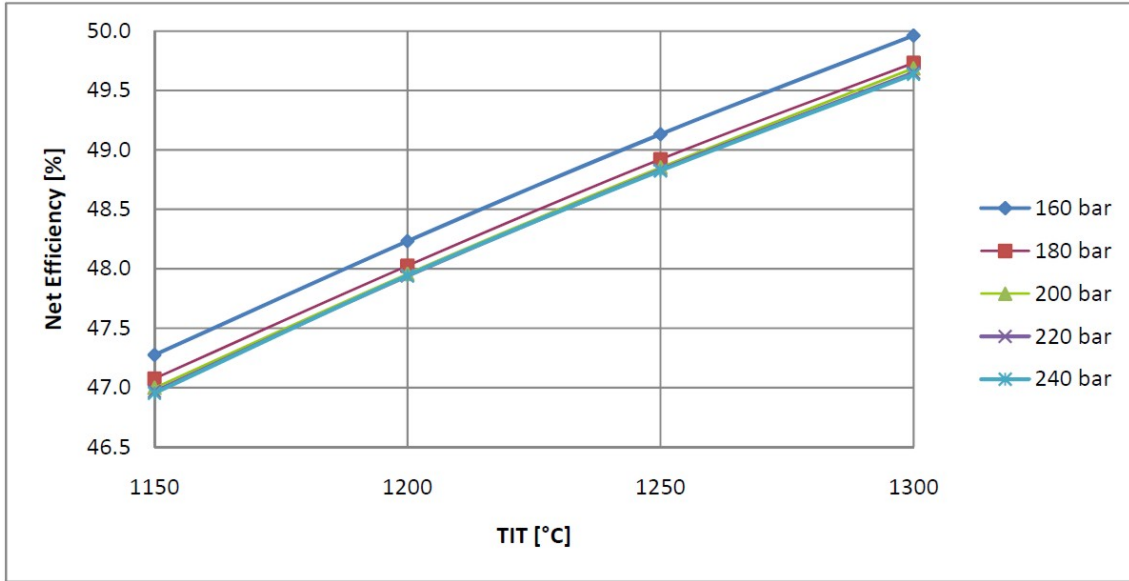


Figure 27: Influence of TIT on net efficiency (detail)

°C and therefore HTEX 2 limits the temperature of the combustion chamber feed stream, while the minimum temperature difference in HTEX 3 is higher than 10 K. At higher pressures the turbine outlet temperature is higher than 670 °C and therefore HTEX 3 provides the limit, while HTEX 2 has a higher temperature difference.

The heat exchangers have a big influence on net efficiency. Therefore it is important to handle all parameters in such a way that the heat exchangers reach their optimal point. This is, as mentioned before, at an LPT exit temperature of about 670 °C. However, this value is only valid for variant 1 (see *Chapter 4.2.2*) with methane.

Figure 29 depicts the influence of cooling water temperature on net efficiency. *Table 32* in *Appendix A* shows the corresponding data. With rising values of cooling water temperature the condenser pressure also increases. Thus the power demand of the compressors C1, C2, and C3 increases. The feeding pump power demand also increases with rising inlet temperatures of working fluid despite the decrease in pressure ratio. The higher compressor inlet temperature of fluids (fuel, oxygen, and working fluid) also increases the power demand for compression (if there is a cooler before the compressor).

In *Appendix C* there are some additional data about the influence of the parameters mentioned previously on the efficiency of the cycle and on the power of different components of the cycle.

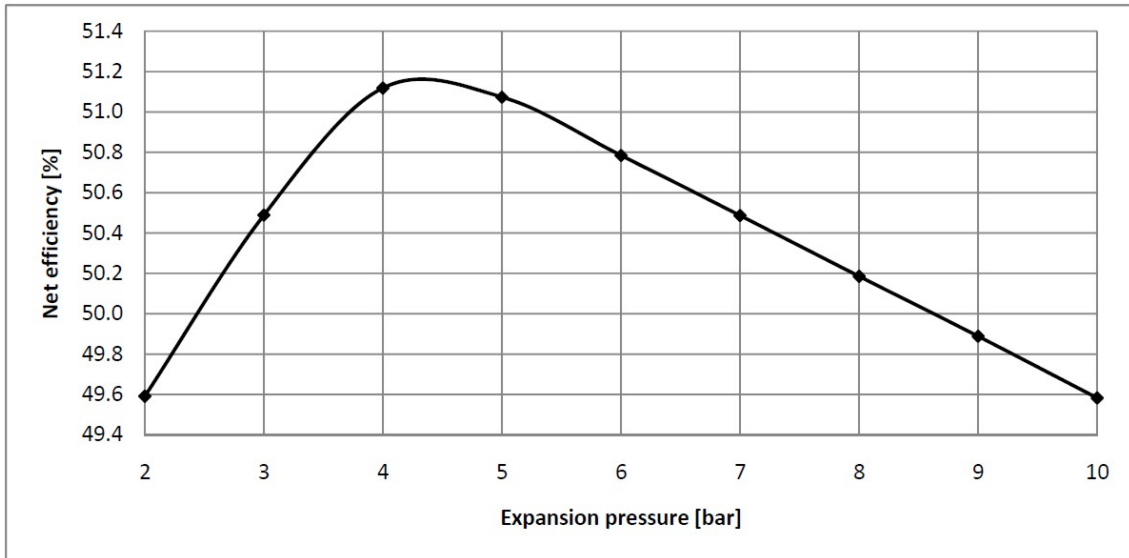


Figure 28: Influence of expansion pressure on net efficiency

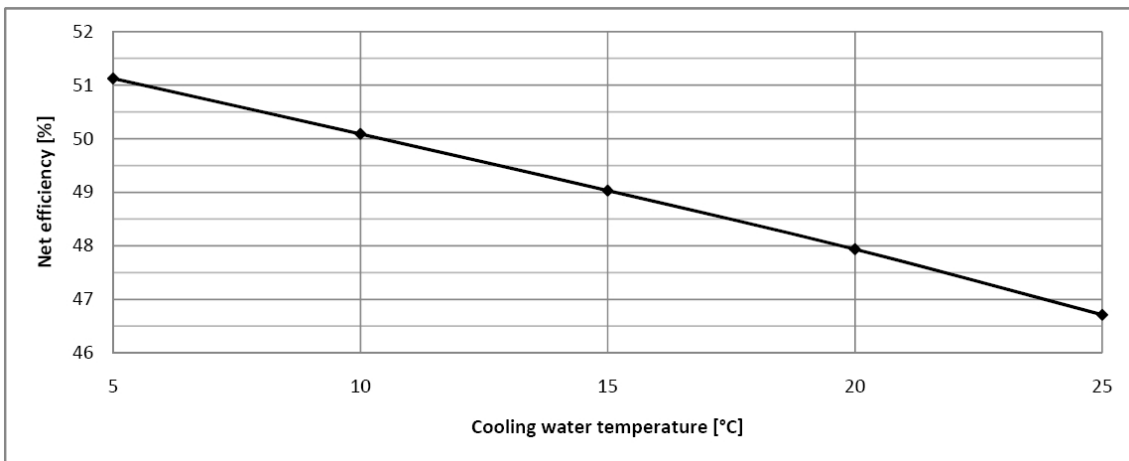


Figure 29: Influence of cooling water temperature on net efficiency

4.3 Naki III

The third variant of an oxyfuel cycle with internal combustion is Naki III. It is also based on CO₂ as the working fluid. The cycle can be fired with carbon and hydrogen containing fuels like methane which is investigated, or syngas from coal gasification. The main difference between Naki III and Naki II is the conventional bottoming steam cycle in Naki III (see simplified flow scheme in *Figure 30*). This double pressure reheat steam cycle is the same as that used in [13]. The pressure losses on the water/steam side of the heat recovery steam generator (preheaters, steam generators, and superheaters), and the temperature differences in these heat exchangers are the same as in [13]. On the hot side of the heat exchangers the pressure losses are 3 % of the pressure of the working fluid (CO₂ and combustion-generated water). The data of the steam turbines are very conventional, and such turbines are in operation in combined cycle plants.

The pressure after the feeding pump of the CO₂ cycle is 200 bar. Because of pressure losses in recuperative heat exchangers and the combustion chamber, the TIP is about 186.2 bar. The expansion from a TIT of 1 400 °C to a temperature of 750 °C is done in cooled turbines. The exit working fluid of the LPT with a pressure of 4 bar and a temperature of 652 °C is transferred to the heat recovery steam generator as shown in the simplified cycle scheme in *Figure 30*. There the heat of the working fluid is used to produce steam for the double pressure steam cycle. The high-pressure live steam of this cycle has a pressure of 120 bar and a temperature of 560 °C. After the high-pressure steam turbine, the steam is reheated to a temperature of 560 °C at a pressure level of 30 bar. The intermediate pressure steam turbine expands the steam to a pressure level of 4 bar. At this pressure level the exit steam with a temperature of 280 °C is mixed with low-pressure steam (260 °C) and fed to the low-pressure steam turbine. The high volume flow at the exit of the low-pressure steam turbine demands a four-flow design at 3 000 rpm.

The exit working fluid of the heat recovery steam generator has to be compressed to 45 bar. At this temperature level the CO₂ can be condensed at a temperature level of 9.98 °C. The combustion-generated water is condensed in coolers and removed by two water separators before it reaches the CO₂ condenser. The heat of the exit stream of the compressor is used to preheat the working fluid before it enters the combustion chamber. To enable high preheating temperatures the compression from about 4 bar to 45 bar is done with one compressor and without intercooling.

The combustion chamber and the turbines of the CO₂ cycle are the same as those used in Naki II, variant 1a. The HPT and IPT are on the same shaft and in the same casing. Physically, therefore, they are one turbine, with the HPT as first stage and the IPT as second stage. The IPT with a speed of 3 000 rpm has its own shaft and casing.

4.3.1 Cycle description

A simplified flow scheme of Naki III is depicted in *Figure 30*. *Figure 31* shows the detailed schematic of Naki III. Components (8) to (13) are parts of the heat recovery steam generator (HRSG).

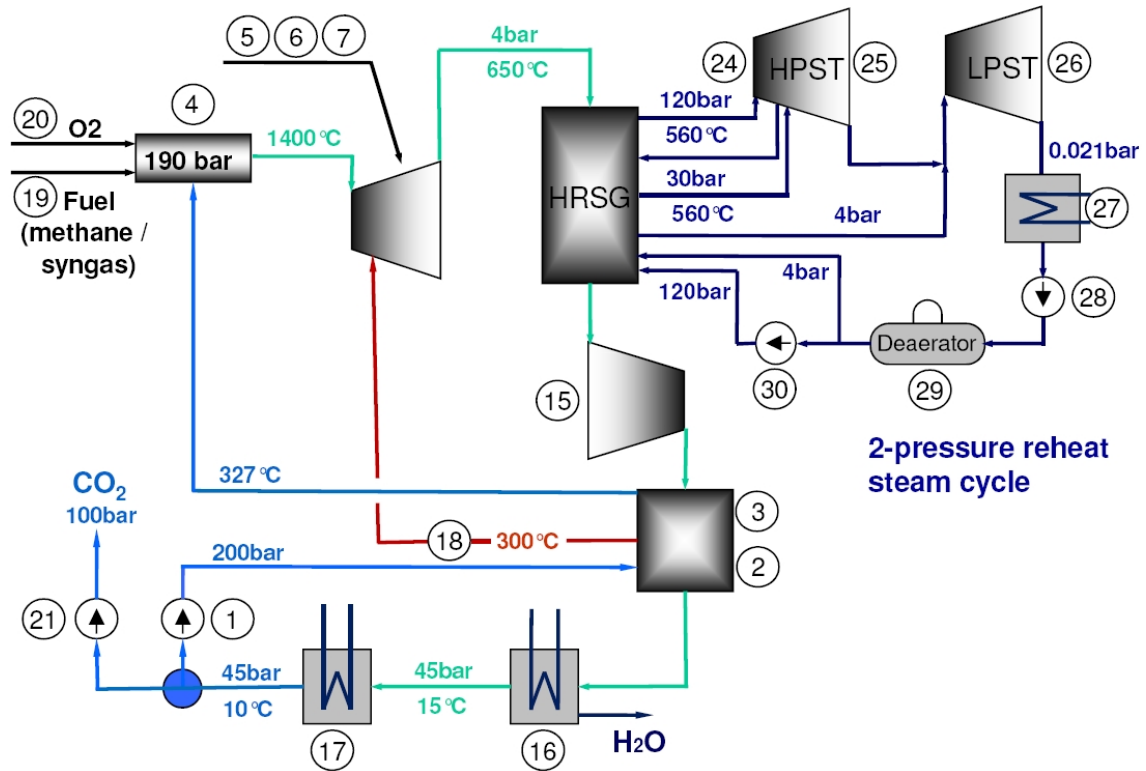


Figure 30: **Simplified cycle schematic of Naki III:** ① Feeding pump; ②,③ Recuperative heat exchanger; ④ Combustion chamber; ⑤ High-pressure turbine (HPT); ⑥ Intermediate pressure turbine (IPT); ⑦ Low-pressure turbine (LPT); ⑮ Working fluid compressor; ⑯ Heat exchanger (cooler); ⑰ CO₂ condenser; ⑱ Turbine cooling stream; ⑲ Fuel supply (methane or syngas); ⑳ Oxygen supply (generation and compression); ㉑ CO₂ hand-over pump; ㉔ High-pressure steam turbine (HPST); ㉕ Intermediate pressure steam turbine (IPST); ㉖ Low-pressure steam turbine (LPST); ㉗ Condenser of steam cycle; ㉘ Condensate pump; ㉙ Deaerator; ㉚ Feeding water pump

The description of the cycle starts at the feeding pump of the CO₂ cycle. 400 kg/s liquid CO₂ from the condenser with a pressure of 45 bar are pumped to a pressure level of 200 bar by the feeding pump (1). In the recuperative heat exchanger (2) (=HTEX 2) the working fluid is heated up to a temperature of 300 °C. The exit stream of this heat exchanger is split up into the combustion chamber feed stream and the turbine cooling stream (18). In the recuperative heat exchanger (3) (=HTEX 3) the combustion chamber feed stream is heated as high a temperature as possible. A minimum temperature difference of 10 K in HTEX 3 limits the temperature of this combustion chamber feed stream to about 327 °C. The minimum temperature difference in HTEX 2 is about 6 K. It can be lower than 10 K because of the explicit pinch point. Principle Q-t-diagrams of HTEX 2 and HTEX 3 are shown in *Figure 34* and *35*. The pinch point of HTEX 2 is at the kink of the hot stream in the Q-t-diagram. At this point the temperature of the hot stream falls below the saturation temperature of water and thus water begins to condensate. Because of the heat of condensation, the temperature gradient of this hot stream decreases. The cooling of the combustion chamber is done with the working fluid because its temperature is only 327 °C. The turbine cooling stream (18) has a temperature of 300 °C, as mentioned above.

In the combustion chamber (4) the working fluid is heated up to 1 400 °C by burning fuel. In this investigation methane is used as fuel. The pressure rise of methane with an initial pressure of 50 bar is achieved by a two-stage intercooled compression (20). The stoichiometric oxygen mass flow is delivered by an air separation unit and fed to the combustion chamber after a four-stage intercooled compression (19). Because of pressure losses in the recuperative heat exchangers and in the combustion chamber the TIP is about 186.2 bar. The HPT (5) and the IPT (6) are cooled turbines. Therefore the turbine cooling stream (18) with a temperature of 300 °C is used. The exit temperature of the IPT is 750 °C at a pressure level of 8 bar. The uncooled LPT (7) expands the working fluid (about 94 % CO₂ and 6 % H₂O) to a pressure of 4 bar. The exit temperature of the LPT is 652 °C. With this temperature the working fluid is fed to the heat recovery steam generator (HRSG) which consists of parts (8) to (13). In the HRSG the working fluid is cooled down to a temperature of 79 °C. A small amount of the combustion-generated water of the working fluid is condensed in the heat recovery steam generator. This liquid water is separated by the water separator (14). The working fluid which has a pressure of 3.9 bar and a temperature of 79 °C is then compressed to 47.8 bar by the working fluid compressor (15). The exit temperature of this compressor is about 337 °C. The working fluid is then transferred at this temperature to the recuperative heat exchangers (3 and 2) and used to preheat the combustion chamber feed stream. Afterwards the working fluid is cooled down to 15 °C in the cooler (16). At this temperature level the rest of the combustion-generated water becomes liquid and can be separated by the water separator (14). Thus the working fluid consists of nearly pure CO₂. It is then fed to the condenser and condensed at a pressure level of 45 bar and a corresponding condensation temperature of 9.98 °C. About 400 kg/s of the liquid CO₂ is piped to the feeding pump (1) and used for the process again. The rest, the combustion-generated CO₂, is separated and pumped to a pressure of 100 bar by the hand-over pump (21). The separated CO₂ is then ready for transport and storage.

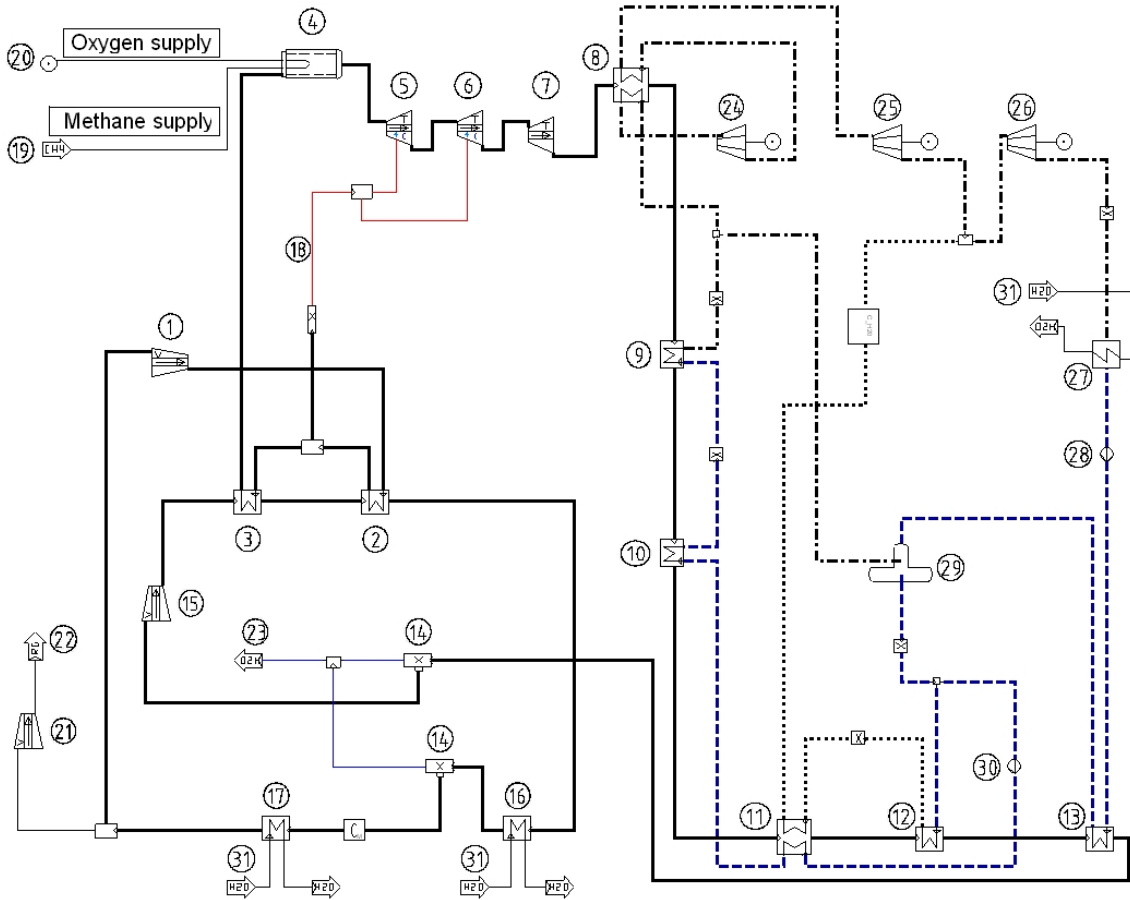


Figure 31: **Detailed IPSEpro schematic of Naki III:** ① Feeding pump; ②,③ Recuperative heat exchanger; ④ Combustion chamber; ⑤ High-pressure turbine (HPT); ⑥ Intermediate pressure turbine (IPT); ⑦ Low-pressure turbine (LPT); ⑧ Superheater for high-pressure live steam and reheater; ⑨ High-pressure steam generator; ⑩ High-pressure preheater; ⑪ High-pressure preheater and low-pressure superheater; ⑫ Low-pressure steam generator; ⑬ Condensate preheater; ⑭ Water separator; ⑮ Working fluid compressor; ⑯ Heat exchanger (cooler); ⑰ CO₂ condenser; ⑱ Turbine cooling stream; ⑲ Fuel supply (methane or syngas); ⑳ Oxygen supply (generation and compression); ㉑ CO₂ hand-over pump; ㉒ CO₂ sink; ㉓ Water sink; ㉔ High-pressure steam turbine (HPST); ㉕ Intermediate pressure steam turbine (IPST); ㉖ Low-pressure steam turbine (LPST); ㉗ Condenser of steam cycle; ㉘ Condensate pump; ㉙ Deaerator; ㉚ Feeding water pump; ㉛ Cooling water supply

The description of the double pressure reheat steam cycle starts at the deaerator (29). The pressure in the deaerator is 6 bar and the corresponding boiling temperature is about 159 °C. The exit stream is split up into a high-pressure and a low-pressure stream. The high-pressure stream with a mass flow of 83.6 kg/s goes to the feeding water pump (30) and is pumped to a pressure level of 140 bar. It is then preheated in the preheaters (11) and (10). Afterwards the water is vaporised in the steam generator (9). In the superheater the steam is heated to a temperature of 560 °C. The TIP is 120 bar because of pressure losses in the heat exchangers. The high-pressure steam turbine (24) expands the steam to a pressure of 33.1 bar. With an exit temperature of 362 °C (from the high-pressure turbine) the steam goes to the reheater (8) and is reheated to a temperature of 560 °C. Afterwards the reheated steam is expanded to a pressure of 4 bar in the intermediate pressure steam turbine (25). The exit temperature of this turbine is 280 °C. Before this exit steam enters the low-pressure steam turbine (26), it is mixed with low-pressure steam. The low-pressure stream starts at the splitter after the deaerator (29). The low-pressure stream with a mass flow of 12.5 kg/s is vaporised in the low-pressure steam generator (12) and superheated in the low-pressure superheater (11). The low-pressure steam leaves this superheater at a temperature of about 260 °C. It is then mixed with the exit steam of the intermediate pressure steam turbine as mentioned before. At a temperature after mixing of about 277 °C, the steam enters the low-pressure steam turbine (26) and is expanded there to a pressure of 0.021 bar. The exit steam of the low-pressure steam turbine has a temperature of about 18 °C and is condensed in the condenser (27). Afterwards it is pumped to the deaerator (19) via the condensate preheater (13) by the condensate pump (28). In the condensate preheater the condensate is heated up to a temperature of about 159 °C. Then the water is used again in the high-pressure or low-pressure steam cycle.

The principle T-s-diagram of the CO₂ cycle of Naki III is depicted in *Figure 32*. The marked kinks in the lines of the HRSG and the recuperative heat exchanger are the starting points of the condensation of combustion-generated water. The principle T-s-diagram of the double pressure steam cycle of Naki III is shown in *Figure 33*.

4.3.2 Thermodynamic balance

Table 12 gives an overview of the power balance of Naki III. The IPSEpro schematic with calculation data is depicted in *Figure 36*. The main mass flows of the cycle are shown in *Table 13*. The working fluid mass flow of 400 kg/s is chosen to achieve a low number of stages of the cooled CO₂ turbine. The TIT of the HPT is 1 400 °C and the TIP is about 186.2 bar. The working fluid is expanded to 4 bar by the LPT and then piped to the heat recovery steam generator. With these parameters Naki III reaches a thermal cycle efficiency of 64.7 %. Considering the auxiliary losses, methane and oxygen supply, and the compression of the captured CO₂ to 100 bar, the net efficiency is about 50.5 %. Thus Naki III with a heat input of 714.9 MW has an electrical output of 361.2 MW. The cooled CO₂ turbines (HPT and IPT)

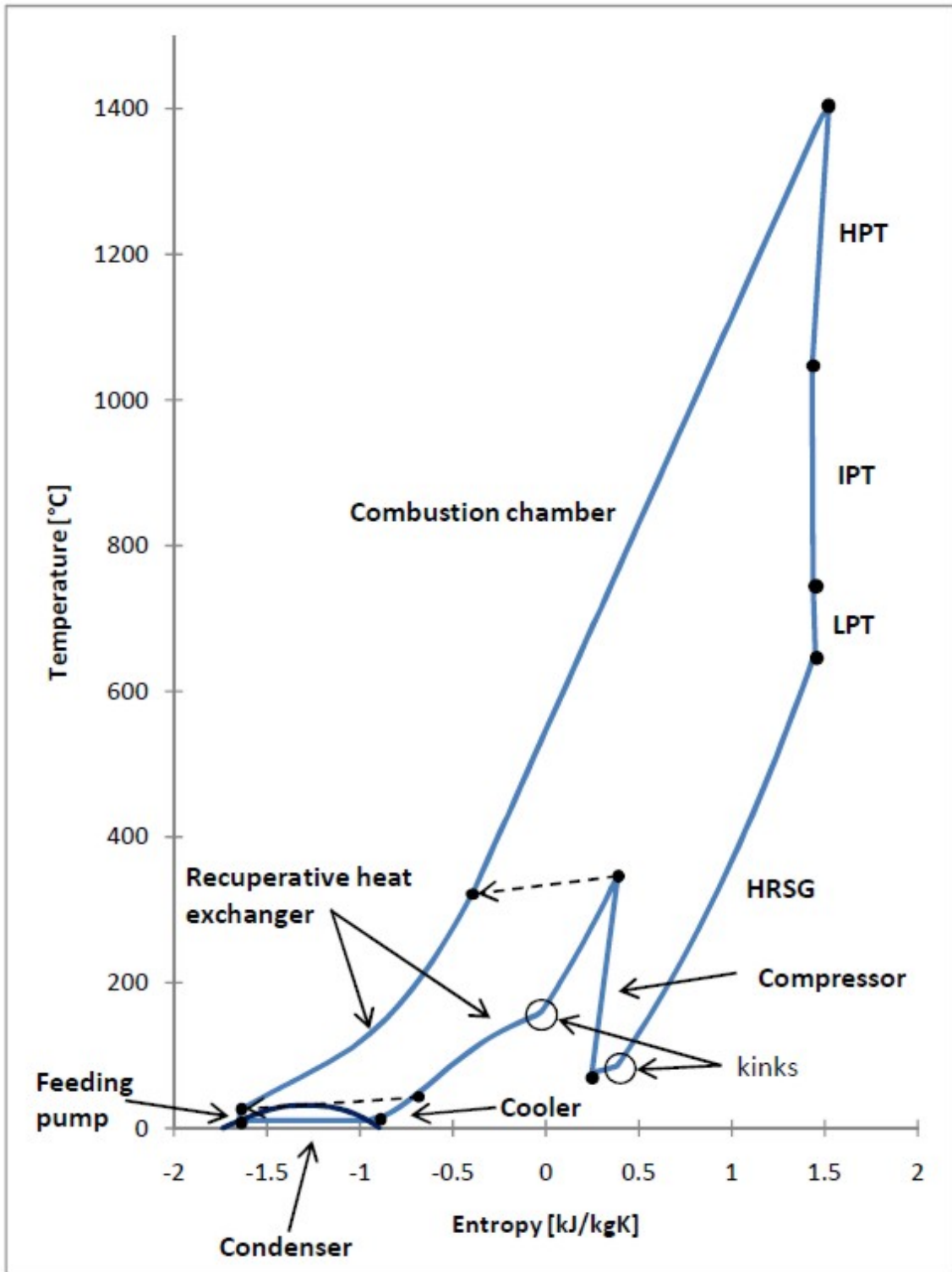


Figure 32: Principle T-s-diagram of the CO₂ cycle of Naki III

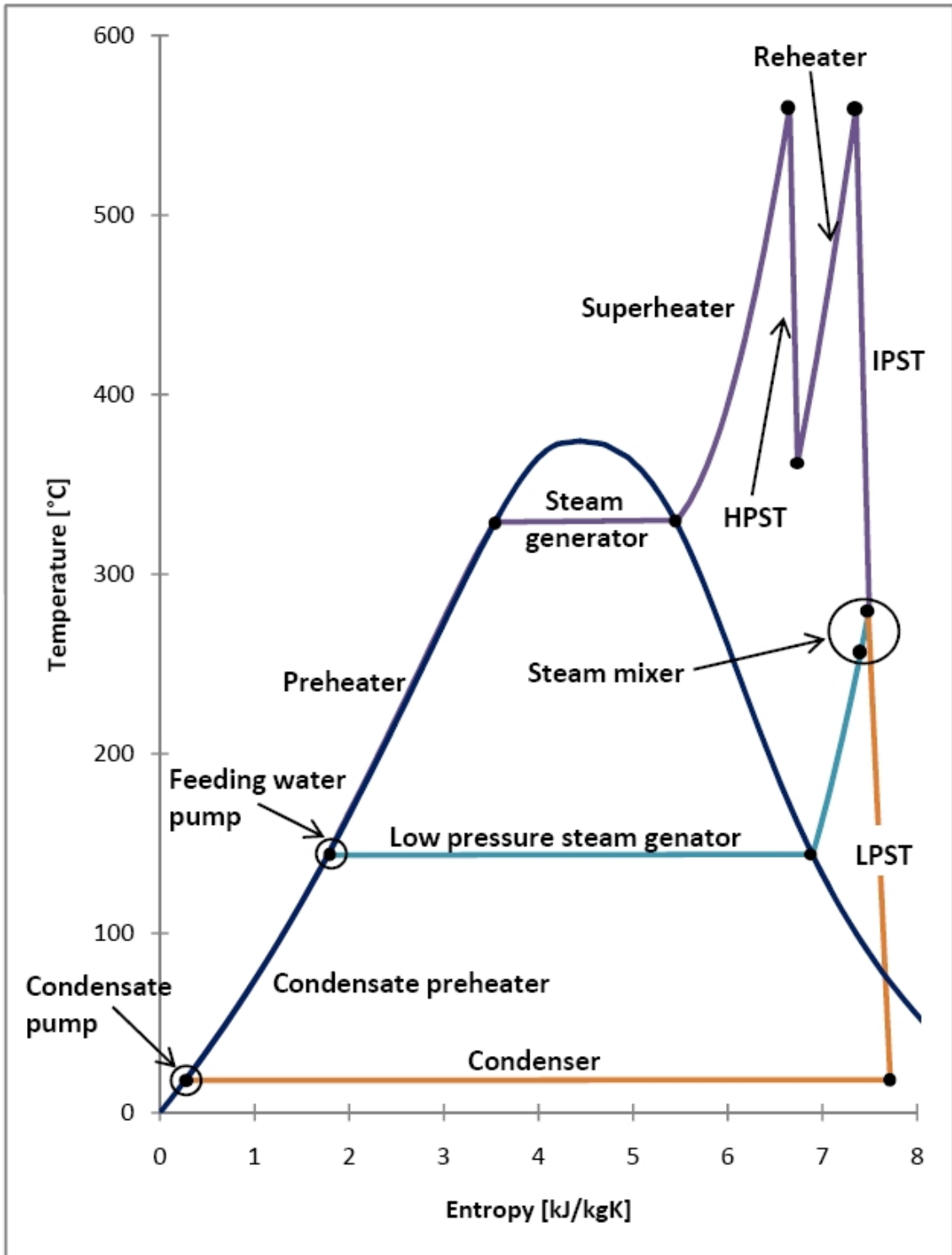


Figure 33: Principle T-s-diagram of the double pressure steam cycle of Naki III

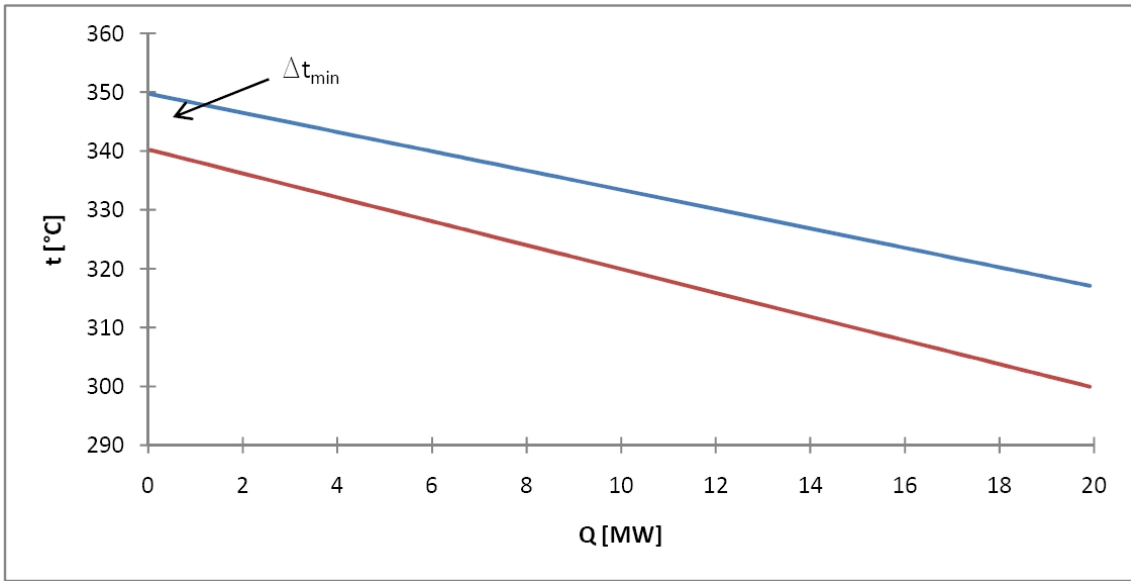


Figure 34: Q-t-diagram of recuperative heat exchanger 3

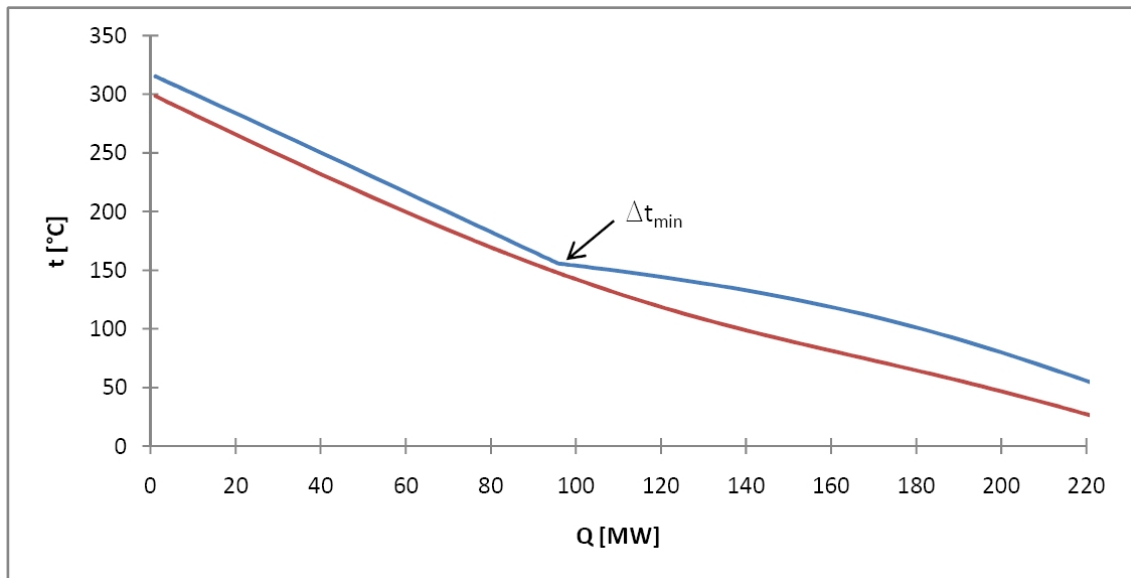


Figure 35: Q-t-diagram of recuperative heat exchanger 2

Table 12: Power balance of Naki III

Heat input	714.9	MW
High-pressure turbine	192.0	MW
Intermediate pressure turbine	200.3	MW
Low-pressure turbine	67.3	MW
High-pressure steam turbine	30.9	MW
Intermediate pressure steam turbine	47.3	MW
Low-pressure steam turbine	74.5	MW
Feeding pump (CO ₂)	9.4	MW
Working fluid compressor	138.3	MW
Condensate pump	0.1	MW
Feeding water pump	1.7	MW
Thermal cycle efficiency	64.7	%
Auxiliary losses	2.50	MW
Net electrical efficiency	61.8	%
Methane compression	3.29	MW
O ₂ generation	51.2	MW
O ₂ compression	26.1	MW
Efficiency considering O₂ and methane supply	50.6	%
CO ₂ compression	0.29	MW
Net efficiency	50.5	%
Net electrical power	361.2	MW

have a cooling mass flow demand of 59.6 kg/s. This is about 12.6 % of the main mass flow of these turbines. The HRSG produces 83.6 kg/s high-pressure steam and 12.5 kg/s low-pressure steam. Naki III with an electrical output of 361.2 MW needs 14.3 kg/s methane as fuel and 56.9 kg/s oxygen. Thus it produces 32 kg/s combustion-generated water and captures 39.2 kg/s CO₂, as shown in *Table 13*.

4.3.3 IPSEpro schematic of Naki III

The IPSEpro schematic depicted in *Figure 36* shows all thermodynamic data (pressure, enthalpy, temperature, and mass flow) of the calculation with methane as fuel.

4.3.4 Turbomachinery arrangement and dimensions

The turbomachinery arrangement of the CO₂ cycle of Naki III is depicted in *Figure 37*. The double pressure steam cycle has a conventional turbomachinery arrangement. It is thus not considered in detail in this work. The CO₂ turbines and their dimensions are the same as in Naki II variant 1a (see *Table 15*). The HPT has two cooled stages and a speed of 20 000 rpm. The first stage is the HPT of the thermodynamic calculation. The second stage is called IPT in the thermodynamic calculation. On every side of the HPT in the turbomachinery arrangement there is a power gear unit. Each has a power of about 196 MW and transfers half of the

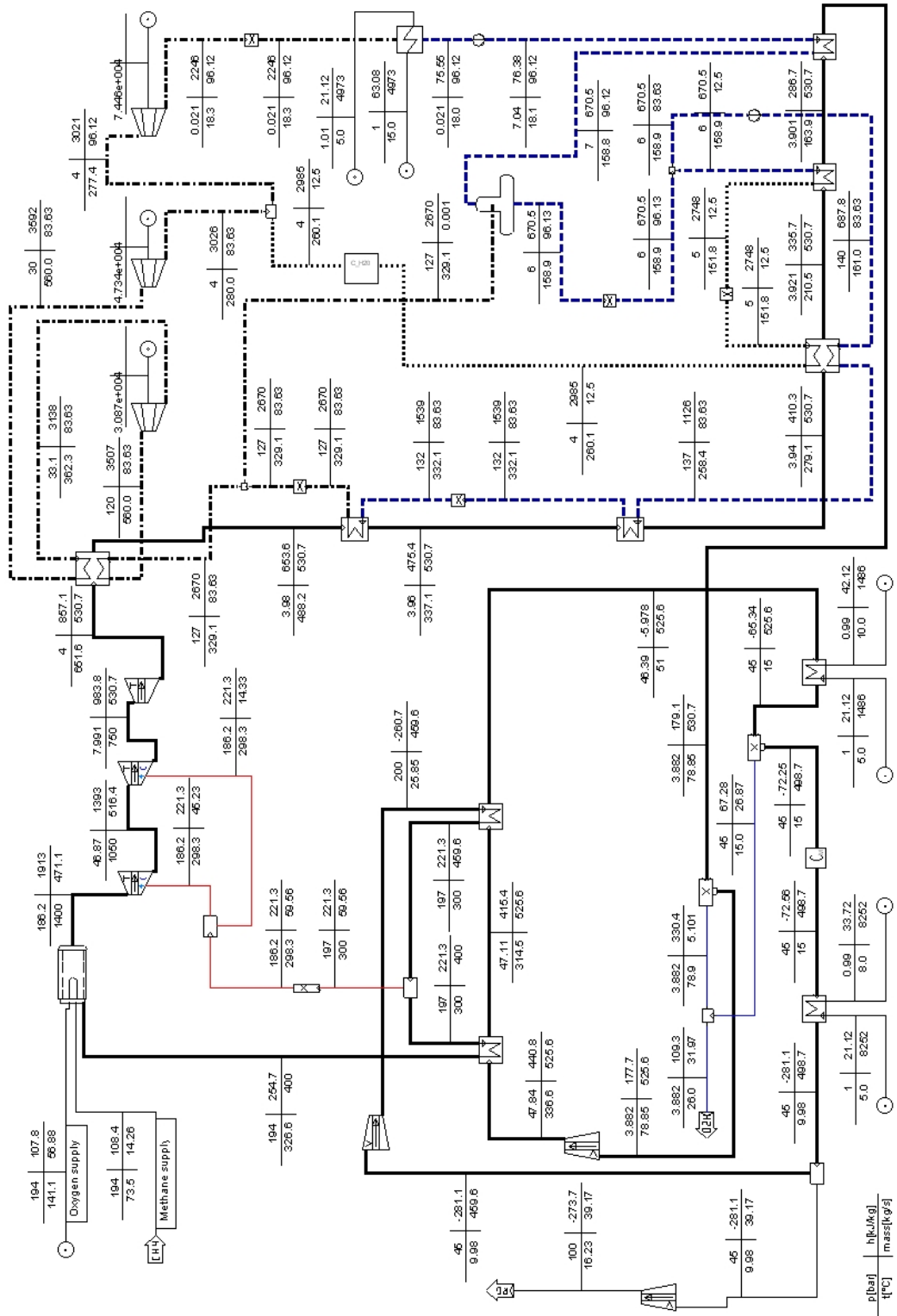


Figure 36: IPSEpro schematic of Naki III with calculation data

Table 13: Mass flows of Naki III

Working fluid (CO ₂)	400.0	kg/s
Turbine cooling	59.6	kg/s
Turbine inlet mass flow	471.1	kg/s
Ratio of turbine cooling to inlet mass flow	12.6	%
High-pressure steam	83.6	kg/s
Low-pressure steam	12.5	kg/s
Mass flow of LPST	96.1	kg/s
Methane	14.3	kg/s
Oxygen	56.9	kg/s
Captured CO ₂	39.2	kg/s
Separated H ₂ O	32.0	kg/s

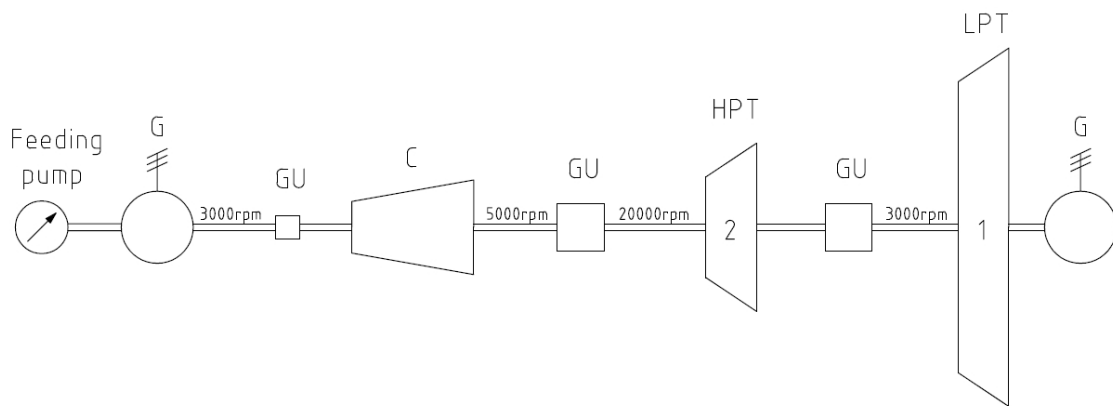


Figure 37: **Turbomachinery arrangement of the CO₂ cycle of Naki III:**
HPT ... High-pressure turbine; LPT ... Low-pressure turbine; GU ... Gear unit;
G ... Generator; C ... Compressor

HPT power. The right power gear unit reduces the speed to 3 000 rpm and drives a generator via the LPT. The LPT has one uncooled stage and is directly coupled to the generator. The left power gear unit reduces the speed to 5 000 rpm and drives the compressor, a small generator, and the feeding pump. The generator and the feeding pump have a speed of 3 000 rpm. An additional small gear unit with a power of about 58 MW is thus necessary.

The compressor has a speed of 5 000 rpm because of the Mach number limitation (see *Chapter 5.2*). The tip Mach number of the first stage is 1.16. The compressor is designed as axial compressor with one radial stage at the outlet side. With a mass flow of 525.6 kg/s and a pressure ratio of 12.3 it has a power of 138 MW. The work coefficient is 0.85 and the enthalpy drop 263 kJ/kg. The compressor thus has 11 axial stages and 1 radial stage.

5 Turbomachinery Dimensions

A rough layout of the turbomachinery dimensions was performed using [17]. For more details see [21, 22]. The main dimensions of the turbomachinery like temperature, mass flow, density of the fluid, and the enthalpy drop can be calculated using the data of the IPSEpro simulation. For turbomachineries with more than two stages, only the dimensions of the first and last stage are calculated.

5.1 Layout of turbines

The dimensioning of turbines is generally difficult for working fluids with a high CO₂ content because of the low speed of sound and the high density of CO₂. The high density causes low volume flows and therefore short blade lengths. To obtain longer blades it is necessary to have small mean diameters. To handle enthalpy drops with a small number of stages at low diameters, a high rotational speed of the turbine is necessary. Higher values in mass flows make the dimensioning of turbines easier because of the higher volume flows. The low speed of sound results in high Mach numbers or leads to low velocities of gases for given Mach numbers (if the Mach number is limited).

To reduce the heating up of the rotor through the hot working fluid, it is necessary to strongly reduce the temperature of the working fluid in the first turbine stage. This is achieved by a high pressure ratio of this turbine stage. If CO₂ is used as working fluid, the pressure ratio must be higher than for other gases (e.g., air) as mentioned before. Hence the increase in volume flow through the first turbine stage (for CO₂) is also very high and causes a high enlargement of the flowing duct.

Because of the efficiency penalties caused by the film cooling of turbine blades, the cooling mass flow should be as small as possible. This can be achieved by a low number of cooled stages. It is thus also necessary to strongly reduce the temperature of the working fluid through the first stages by a high pressure ratio.

The main dimensions of the turbine (e.g., diameter and blade length) are calculated with data from IPSEpro (enthalpy drop, mass flow, and density) and with some parameters that can be estimated reasonably (rotational speed n , work coefficient ψ , degree of reaction r , nozzle exit angle α , and the relation $(\frac{D_{mean}}{l})$). This method is valid for axial flow turbines.

The flow factor f as defined in *Equation 2* describes the effect of work coefficient and degree of reaction on the velocity triangle.

$$f = \frac{\psi}{4} + (1 - r) \quad (2)$$

The mean diameter is calculated according to *Equation 3* for the first and last stage of a turbine. [17]

$$D_{mean} = \sqrt[3]{\frac{\dot{V} * (\frac{D_{mean}}{l}) * 60}{f * \pi^2 * n * \tan \alpha}} \quad (3)$$

Δh_{stage} (*Equation 4*) is the enthalpy drop of one stage. It is calculated for the first and last stage of a turbine.

$$\Delta h_{stage} = \frac{\psi}{2} * \left(\frac{D_{mean} * \pi * n}{60} \right)^2 \quad (4)$$

The stage number z is calculated with *Equation 5*. Δh_{inlet} is the enthalpy drop of the first, Δh_{outlet} of the last stage and Δh the total enthalpy drop of the turbine.

$$z = \frac{\Delta h * 2}{\Delta h_{inlet} + \Delta h_{outlet}} \quad (5)$$

5.2 Layout of compressors

The speed of a compressor is limited by the inlet tip Mach number, which should not exceed $M=1.3$. In this work a maximum value of 1.2 is assumed. Δh , mass flow, and density from the IPSEpro calculation as well as rotational speed n , work coefficient ψ , factor f , and $\left(\frac{D_{mean}}{l}\right)$ as variable parameters are used for the dimensioning. The inlet dimensions are calculated according to *Equation 3*. The inner diameter and the axial velocity are kept constant through the compressor. Hence the outlet dimensions and further parameters can be calculated. With *Equation 4* and *5* the number of stages is defined. This method is valid only for axial flow compressors. If a radial exit stage is employed, it is assumed to replace two axial stages in this rough layout.

5.3 Calculation of Mach number

The Mach number in turbomachinery should not exceed certain limits. In this work the Mach number for turbines is limited to 1.4 (at mean diameter) for efficiency reasons. For compressors it is 1.2 (inlet tip Mach number). The Mach number is calculated as shown in *Equation 6*. c_1 is used for turbines and $w_{1\ Tip}$ for compressors.

$$M = \frac{c_1 \text{ or } w_{1\ Tip}}{a} \quad (6)$$

The speed of sound in critical areas is calculated according to *Equation 7* using IPSEpro.

$$a^2 = \left. \frac{\partial p}{\partial \rho} \right|_{s=const.} \quad (7)$$

In turbines the critical area is the stator exit. The velocity at the stator exit is normally the highest gas velocity in turbines. It is estimated as shown in *Equation 8*.

$$c_1 = \sqrt{2 * (1 - r) * \Delta h_{stage}} \quad (8)$$

Table 14: Dimensions of the uncooled turbine of Naki I

Inlet mass flow	294.6	kg/s
Inlet volume flow	3.5	m ³ /s
Outlet mass flow	294.6	kg/s
Outlet volume flow	11.1	m ³ /s
Power	74.2	MW
Speed	20 000	rpm
Stage number	3	-
Enthalpy drop	252.0	kJ/kg
Work coefficient	2.800	-
Inlet inner diameter	0.189	m
Inlet mean diameter D	0.221	m
Inlet outer diameter	0.252	m
Inlet blade length l	0.032	m
Inlet D/l	7.0	-
Outlet inner diameter	0.164	m
Outlet mean diameter D	0.246	m
Outlet outer diameter	0.328	m
Outlet blade length l	0.082	m
Outlet D/l	3.0	-

In compressors the critical area is the inlet blade tip. There the speed of sound has the lowest value and the relative velocity $w_{1 \text{ Tip}}$ (see *Equation 9*) has the highest value. u_{Tip} is the circumferential velocity of the blade tip and c_{ax} the axial velocity.

$$w_{1 \text{ Tip}} = \sqrt{u_{\text{Tip}}^2 + c_{ax}^2} \quad (9)$$

5.4 Main turbomachinery dimensions of Naki I

Table 14 gives an overview of the dimensions of the uncooled turbine for Naki I. It has a speed of 20 000 rpm. Because of the high speed and a mass flow of 294.6 kg/s, it has only 3 stages with a work coefficient of 2.8. All gas velocities in the turbine are lower than the speed of sound. The highest Mach number is 0.8. The high-speed turbine allows small diameters despite an enthalpy drop of 252.0 kJ/kg.

5.5 Main turbomachinery dimensions of Naki II

The turbomachinery dimensions were achieved for the fuel methane. *Table 15* shows the main turbomachinery dimensions for variant 1a. The HPT is the first stage of the high-pressure turbine, the IPT the second stage, and they are in the same casing as shown in *Figure 16*. HPT and IPT are supersonic stages with a Mach number of about 1.3. The speed of 20 000 rpm is necessary to get feasible blade lengths and to reach high enthalpy drops, which result in a low number of cooled turbine stages.

The LPT has a Mach number of 0.9 and one subsonic stage at a speed of 3 000 rpm. All inlet dimensions in *Table 15* are for the stator because of the one-stage turbines.

All compressors are designed as axial compressors with one radial stage at the outlet side. C1 and C2 have the same speed of 3 000 rpm because they are directly coupled to the generator. To reduce the number of stages in C3, it has a higher speed of 10 000 rpm. However, as a result, an additional gear unit is needed. The outlet diameters of all compressors are given for the last axial stage.

The main turbomachinery dimensions for variant 1b are shown in *Table 16* and are also calculated for the fuel methane. The HPT has a speed of 17 000 rpm and one supersonic stage with a Mach number of 1.3. The IPT in its own casing as shown in *Figure 16* has a speed of 15 000 rpm and also has one supersonic stage with a Mach number of 1.3. At a speed of 3 000 rpm the LPT needs one subsonic stage (Mach number 0.9). Because of the three casings, the diameter of each turbine is independent from the others. The inlet dimensions in *Table 16* are for the stator because of the single-stage turbines.

The last stage of all compressors is a radial stage. The double-flow compressor C3 has the same speed as the HPT of 17 000 rpm and an inlet tip Mach number of 1.21. Compressors C1 and C2, which have a speed of 5 000 rpm, have an inlet tip Mach number of 1.14 (C1) and 0.86 (C2).

The results for the main turbomachinery dimensions of variant 2 fired with methane are given in *Table 17*. The HPT has one subsonic stage (Mach number 0.8) and a speed of 14 500 rpm. IPT and LPT are on the same shaft and in the same casing and have a speed of 3 000 rpm. The IPT needs 8 cooled stages because of its low speed and the small volume flow. To achieve feasible blade lengths at small volume flows, the diameters of the IPT have to be small. The low speed and the small diameters of this turbine lead to the high number of stages. All stages are subsonic. The first stage has a Mach number of 0.3 and the last stage of 0.4. The high cooling mass flow demand of the IPT is the reason why the temperature of 750 °C is reached at a higher pressure level. This leads to a lower inlet volume flow of the LPT, and hence the diameters of this turbine have to be smaller. Thus it needs 5 stages, more stages than in variant 1a and 1b with higher volume flows and therefore larger diameters. The first stage of the LPT has a Mach number of 0.5 and the last stage of 0.7.

The dimensions of the double-flow compressor C3 allow a speed of 14 500 rpm. C1 and C2 run with a speed of 5 000 rpm because of the Mach number limitation of C1. All compressors have one radial stage at the exit side.

Table 18 shows the main turbomachinery dimensions for variant 3. The HPT has a speed of 16 167 rpm and one cooled supersonic stage with a Mach number of 1.5. The first stage of the LPT (in the thermodynamic calculation it is called IPT) has a speed of 3 000 rpm. This cooled turbine stage has a Mach number of about 1.0. The second stage of the LPT (called LPT in the thermodynamic calculation) has cooled blade roots and also a Mach number of about 1.0. The inlet dimensions of the turbines are given for the stator because of the single-stage turbines.

Table 15: Main turbomachinery dimensions of variant 1a

		HPT ¹	IPT ¹	LPT ¹	C1 ²	C2 ²	C3 ²
Inlet mass flow	kg/s	464.6	508.6	522.5	499.7	499.2	499.0
Inlet volume flow	m ³ /s	8.7	29.4	137.7	66.6	29.4	12.0
Outlet mass flow	kg/s	508.6	522.5	522.5	499.7	499.2	499.0
Outlet volume flow	m ³ /s	29.4	137.7	225.9	35.9	15.5	6.3
Power	MW	186.52	194.57	54.91	27.11	27.31	25.21
Speed	rpm	20 000	20 000	3 000	3 000	3 000	10 000
Stage number	-	1	1	1	4+1rad.	5+1rad.	2+1rad.
Enthalpy drop	kJ/kg	395.2	380.5	105.1	54.2	54.7	50.5
Work coefficient	-	2.771	1.994	2.658	0.850	0.960	0.814
Inlet tip Mach number	-				0.81	0.67	1.06
Inlet c_{ax}/u_m	-				0.60	0.60	0.60
Outlet c_{ax}/u_m	-				0.64	0.63	0.62
Inlet inner diameter	m	0.450	0.430	1.590	0.737	0.701	0.260
Inlet mean diameter D	m	0.505	0.580	1.780	0.974	0.842	0.356
Inlet outer diameter	m	0.560	0.730	1.970	1.211	0.982	0.452
Inlet blade length l	m	0.055	0.150	0.190	0.237	0.140	0.096
Inlet D/l	-	9.2	3.9	9.4			
Inlet D_{in}/D_{out}	-				0.61	0.71	0.57
Outlet inner diameter	m	0.450	0.430	1.590	0.737	0.701	0.260
Outlet mean diameter D	m	0.510	0.590	1.790	0.917	0.801	0.343
Outlet outer diameter	m	0.570	0.750	1.990	1.097	0.901	0.426
Outlet blade length l	m	0.060	0.160	0.200	0.180	0.100	0.083
Outlet D/l	-	8.5	3.7	9.0			
Outlet D_{in}/D_{out}	-				0.67	0.78	0.61

Compressor C1 allows a speed of 5 000 rpm because of the limitation of the inlet tip Mach number. At this speed it needs one axial and one radial stage. Compressor C2 is coupled to C1 and hence it has the same speed. This speed results in two axial stages and one radial stage. Compressor C3 is designed as double-flow compressor and so its diameter becomes smaller, allowing a speed of 16 167 rpm with an inlet tip Mach number of 1.19. With this speed compressor C3 can be directly coupled to the HPT and needs one axial and one radial stage on each side. The outlet diameters of all compressors are given for the last axial stage.

The advantage of the double-flow design of C3 in variants 1b, 2, and 3 is that it can be directly coupled to the HPT and no further gear unit is needed. In variant 1a the speed of the HPT is so high that a directly coupled double-flow compressor C3 is not possible. This design concept is thus not used in that variant.

¹Inlet dimensions are given for the stator because of the single-stage turbine

²Outlet dimensions are given for the last axial stage

Table 16: Main turbomachinery dimensions of variant 1b

		HPT ¹	IPT ¹	LPT ¹	C1 ²	C2 ²	C3 ²
Inlet mass flow	kg/s	464.6	508.6	522.5	499.7	499.2	249.5
Inlet volume flow	m ³ /s	8.7	29.4	137.7	66.6	29.4	6.0
Outlet mass flow	kg/s	508.6	522.5	522.5	499.7	499.2	249.5
Outlet volume flow	m ³ /s	29.4	137.7	225.9	35.9	15.5	3.2
Power	MW	186.52	194.57	54.91	27.11	27.31	25.21
Speed	rpm	17 000	15 000	3 000	5 000	5 000	17 000
Stage number	-	1	1	1	1+1rad.	4+1rad.	1+1rad. double-flow
Enthalpy drop	kJ/kg	395.2	380.5	105.1	54.2	54.7	50.5
Work coefficient	-	2.966	2.136	2.658	0.850	0.814	0.814
Inlet tip Mach number	-				1.14	0.86	1.21
Inlet c_{ax}/u_m	-				0.66	0.60	0.60
Outlet c_{ax}/u_m	-				0.60	0.64	0.60
Inlet inner diameter	m	0.520	0.620	1.590	0.629	0.440	0.179
Inlet mean diameter D	m	0.575	0.750	1.780	0.826	0.604	0.241
Inlet outer diameter	m	0.630	0.880	1.970	1.024	0.767	0.303
Inlet blade length l	m	0.055	0.130	0.190	0.198	0.163	0.062
Inlet D/l	-	10.5	5.8	9.4			
Inlet D_{in}/D_{out}	-				0.61	0.57	0.59
Outlet inner diameter	m	0.520	0.620	1.590	0.629	0.440	0.179
Outlet mean diameter D	m	0.580	0.760	1.790	0.826	0.564	0.241
Outlet outer diameter	m	0.640	0.900	1.990	1.024	0.687	0.303
Outlet blade length l	m	0.060	0.140	0.200	0.198	0.123	0.062
Outlet D/l	-	9.7	5.4	9.0			
Outlet D_{in}/D_{out}	-				0.61	0.64	0.59

Table 17: Main turbomachinery dimensions of variant 2

		HPT ¹	IPT	LPT	C1 ²	C2 ²	C3 ²
Inlet mass flow	kg/s	451.3	499.4	645.3	620.4	619.8	309.8
Inlet volume flow	m ³ /s	8.6	17.5	65.5	82.8	36.5	7.5
Outlet mass flow	kg/s	499.4	645.3	645.3	620.4	619.8	309.8
Outlet volume flow	m ³ /s	17.5	65.5	240.9	44.6	19.2	3.9
Power	MW	110.87	183.94	165.02	33.65	33.90	31.30
Speed	rpm	14 500	3 000	3 000	5 000	5 000	14 500
Stage number	-	1	8	5	1+1rad.	2+1rad.	1+1rad. double-flow
Enthalpy drop	kJ/kg	241.4	307.6	255.7	54.2	54.7	50.5
Work coefficient	-	2.981	3.000	3.000	0.814	0.860	0.814
Inlet tip Mach number	-				1.21	0.98	1.19
Inlet c_{ax}/u_m	-				0.60	0.60	0.60
Outlet c_{ax}/u_m	-				0.60	0.62	0.60
Inlet inner diameter	m	0.470	0.810	0.935	0.618	0.565	0.215
Inlet mean diameter D	m	0.525	0.900	1.091	0.850	0.711	0.281
Inlet outer diameter	m	0.580	0.990	1.247	1.082	0.858	0.347
Inlet blade length l	m	0.055	0.090	0.156	0.232	0.146	0.066
Inlet D/l	-	9.5	10.0	7.0			
Inlet D_{in}/D_{out}	-				0.57	0.66	0.62
Outlet inner diameter	m	0.470	0.886	0.846	0.618	0.565	0.215
Outlet mean diameter D	m	0.530	1.108	1.270	0.850	0.690	0.281
Outlet outer diameter	m	0.590	1.330	1.693	1.082	0.816	0.347
Outlet blade length l	m	0.060	0.222	0.423	0.232	0.126	0.066
Outlet D/l	-	8.8	5.0	3.0			
Outlet D_{in}/D_{out}	-				0.57	0.69	0.62

Table 18: Main turbomachinery dimensions of variant 3

		HPT ¹	1 st stage LPT ¹	2 nd stage LPT ¹	C1 ²	C2 ²	C3 ²
Inlet mass flow	kg/s	463.6	513.6	523.6	500.9	500.4	250.1
Inlet volume flow	m ³ /s	8.7	58.6	111.5	66.8	29.5	6.0
Outlet mass flow	kg/s	513.6	523.6	523.6	500.9	500.4	250.1
Outlet volume flow	m ³ /s	58.6	111.5	226.2	36.0	15.5	3.2
Power	MW	275.98	78.56	79.74	27.17	27.37	25.27
Speed	rpm	16 167	3 000	3 000	5 000	5 000	16 167
Stage number	-	1	1	1	1+1rad.	2+1rad.	1+1rad. double- flow
Enthalpy drop	kJ/kg	585.0	152.3	152.3	54.2	54.7	50.5
Work coefficient	-	2.458	3.086	2.778	0.814	0.850	0.814
Inlet tip Mach number	-				1.16	0.95	1.19
Inlet c_{ax}/u_m	-				0.60	0.60	0.60
Outlet c_{ax}/u_m	-				0.60	0.61	0.60
Inlet inner diameter	m	0.740	1.868	1.868	0.652	0.591	0.193
Inlet mean diameter D	m	0.790	1.990	2.058	0.843	0.710	0.252
Inlet outer diameter	m	0.840	2.112	2.248	1.033	0.829	0.312
Inlet blade length l	m	0.050	0.122	0.190	0.191	0.119	0.059
Inlet D/l	-	15.8	16.3	10.8			
Inlet D_{in}/D_{out}	-				0.63	0.71	0.62
Outlet inner diameter	m	0.740	1.868	1.868	0.652	0.591	0.193
Outlet mean diameter D	m	0.815	2.000	2.108	0.843	0.693	0.252
Outlet outer diameter	m	0.890	2.132	2.348	1.033	0.794	0.312
Outlet blade length l	m	0.075	0.132	0.240	0.191	0.101	0.059
Outlet D/l	-	10.9	15.2	8.8			
Outlet D_{in}/D_{out}	-				0.63	0.74	0.62

6 Turbomachinery Design Details

A detailed design of the turbomachinery is performed for the turbines of Naki II variant 3. The design presented is a recommendation as to how the turbines could be designed. All drawings are true to scale, but most dimensions (besides the diameters of the stator and rotor and the blade length) are reasonably estimated and not calculated.

6.1 High-pressure turbine (HPT)

The HPT is characterised by a high inlet pressure of about 190 bar and a high inlet temperature of 1 400 °C. Because of these high parameters it is advantageous to include the combustion chambers in the turbine casing. Otherwise there would be transition lines with flanges that have to withstand the high pressure and temperature. To tighten these flanges would be very difficult. The high pressure level in the turbine casing will not allow the design of the casing to be divided. The undivided design has the advantage that the casing has no horizontal flange which would cause sealing problems under these demanding operating conditions. A constant wall thickness around the perimeter of the undivided casing design leads to a constant temperature distribution around the perimeter, and thus there are no shape distortions around the perimeter of the casing. A divided turbine casing with a horizontal flange has no constant wall thickness around the perimeter (because of the flange). This leads to shape distortion of the casing during heating up (start up) and cooling down (shut down) of the turbine because of a non-uniform temperature distribution around the perimeter. Such a shape distortion (the turbine casing has no exact round shape under these transient operating conditions) may lead to leakages in the horizontal flange of the turbine casing. Another consequence of the shape distortion around the perimeter of the turbine casing is a reduction in the clearances of the labyrinth sealings in the turbine. The clearance between the rotor blades and the stator is also reduced. Such a shape distortion may lead to rubbing of the seal tips of the balance piston and of the rotor blade tips if not operated carefully, which causes high repair costs.

In summary, the undivided design of the HPT casing avoids all the problems mentioned above and allows very low labyrinth sealing clearances. Furthermore the clearance between the rotor blades and the stator can be kept low which results in lower leakage streams. For this HPT which has a very small blade length in relation to the mean diameter of the rotor, this is very important to keep leakage losses low.

An overview of the HPT is depicted in *Figure 38*. This drawing shows all components of the turbine in a section. This means that not all parts that are shown in this drawing are placed in this plane. For example the star bolt, in which cooling CO₂ is supplied to the stator, is located at about 45 ° to the section shown. In the description below such parts are mentioned and their correct position is given. The red arrows in this drawing show the coolant flow in the turbine.

The description of the HPT starts at the helical inlet header of this turbine.

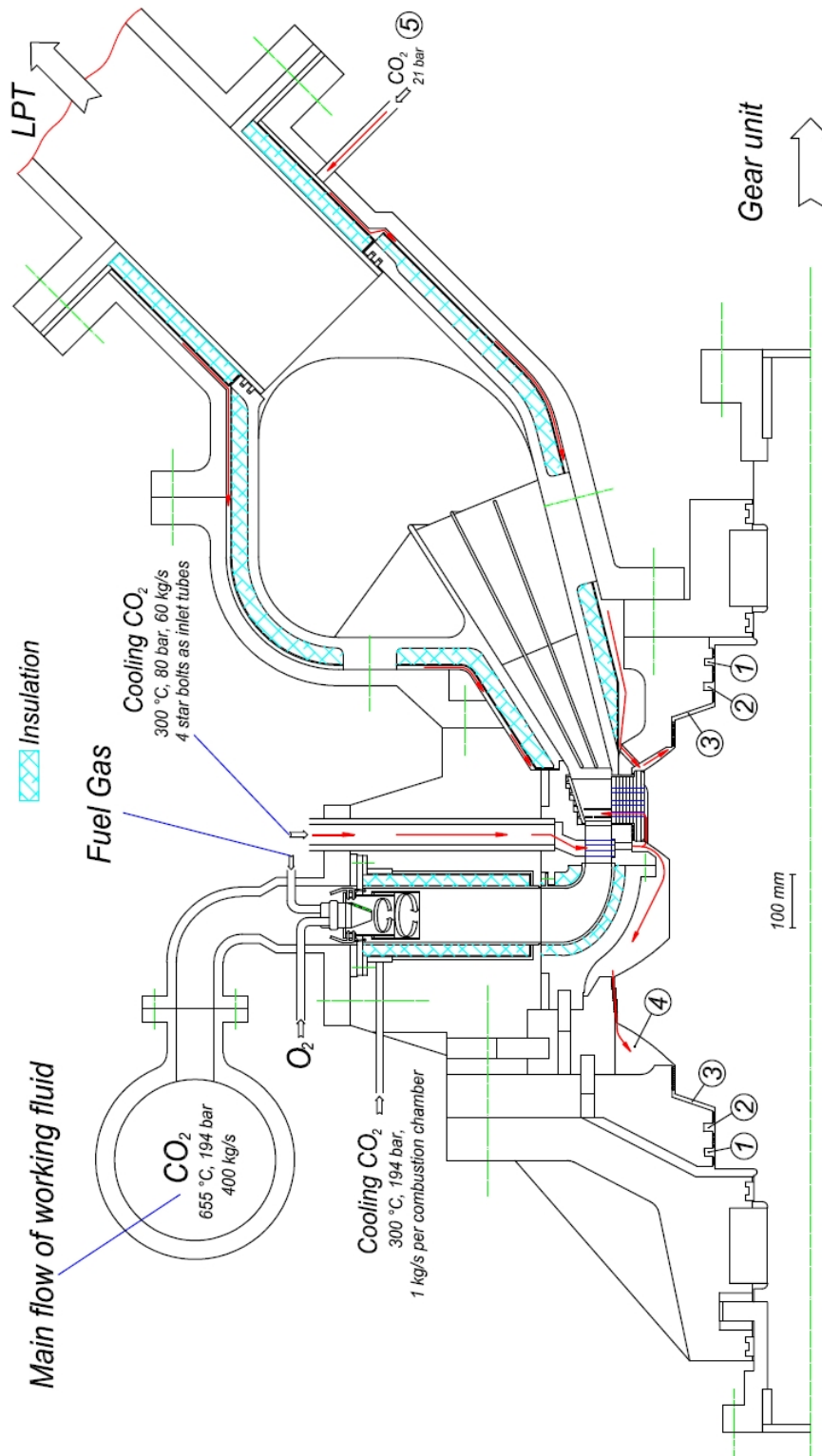


Figure 38: High-pressure turbine (HPT) - overview

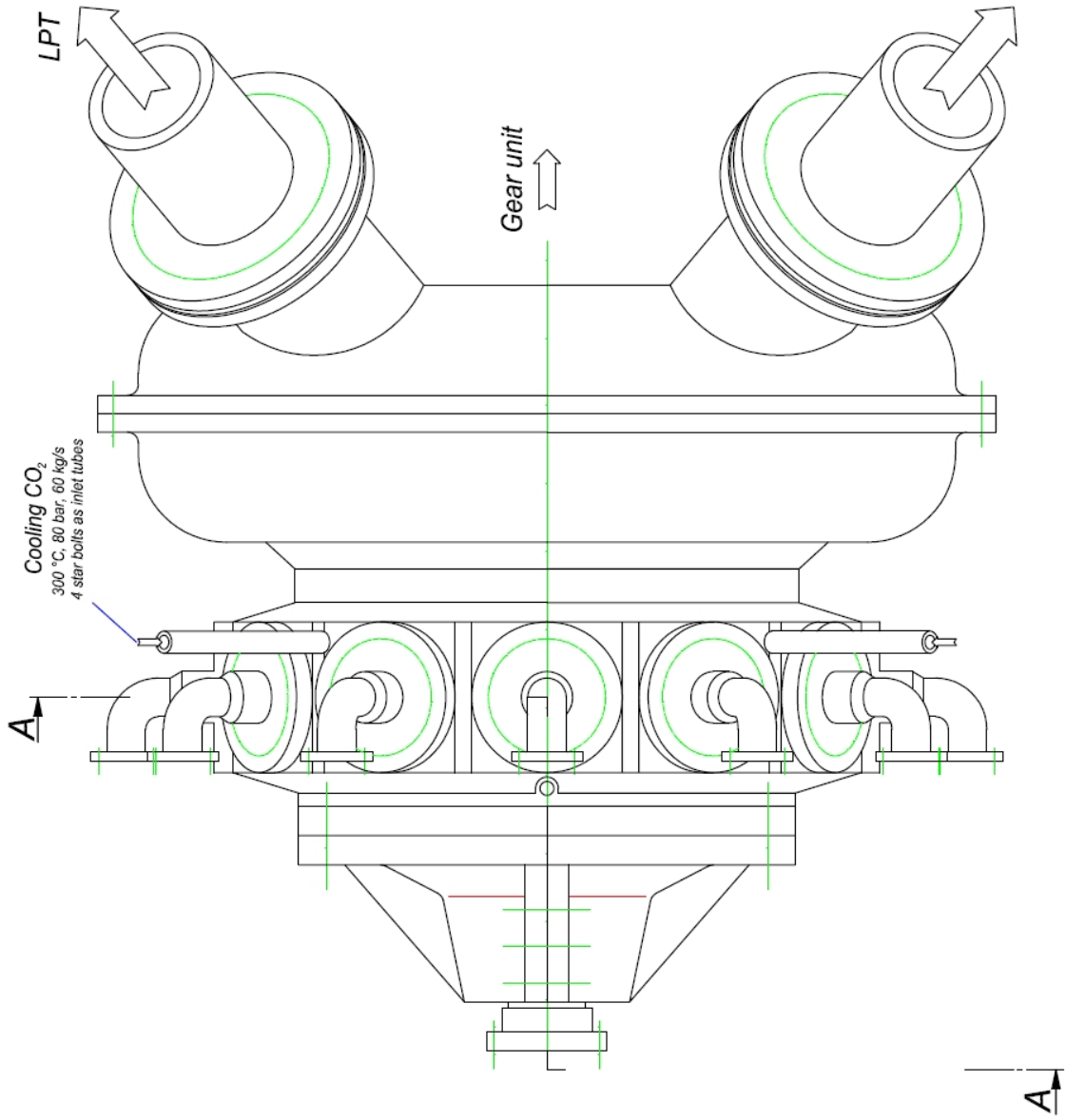


Figure 39: HPT exterior view

Section A-A

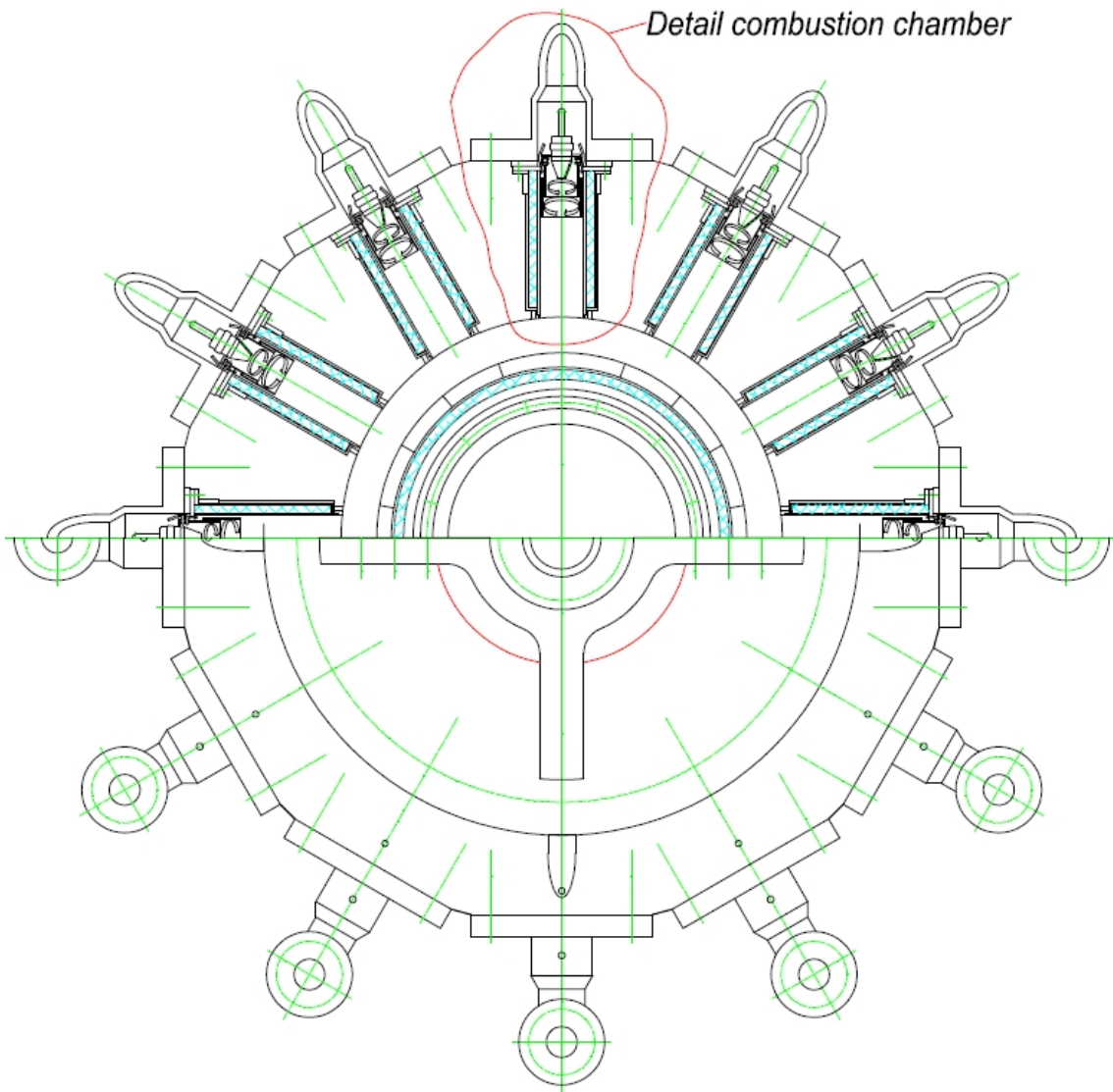
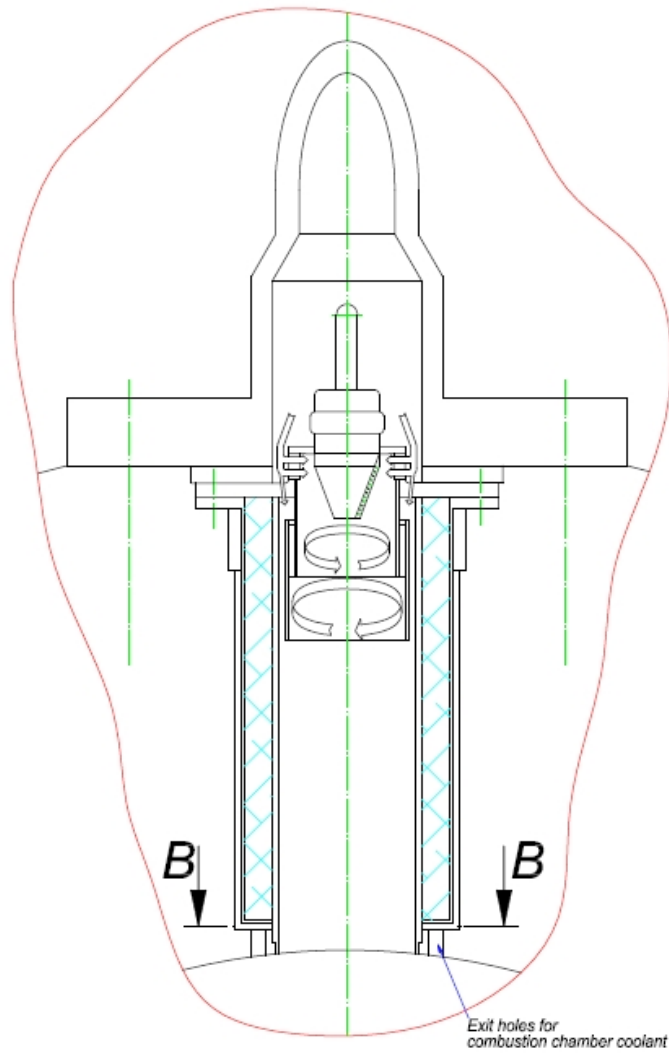


Figure 40: HPT section A-A



Section B-B

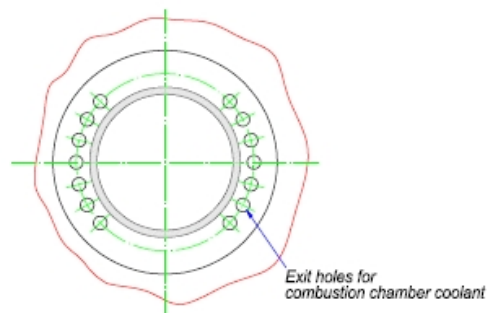


Figure 41: Detail combustion chamber

Working fluid with a pressure of 194 bar and a temperature of 655 °C is delivered from the recuperative heat exchanger to the helical inlet header. This header is connected to the 12 combustion chambers that are placed on the perimeter of the HPT. In each combustion chamber a burner is placed. Details of the burner are shown in *Chapter 6.1.2*. Each burner is fed with fuel gas and O₂. The working fluid is fed around the burner and forms a vortex. The inner wall of the combustion chamber is made of ceramic rings that are placed in a borehole in the turbine casing. Insulation is placed around the ceramic rings. A thin perforated sheet of metal surrounds the insulation and keeps it in position. The perforation is necessary because the ceramic rings are not designed to withstand the pressure of the inner side. The outer side of these ceramic rings is thus also exposed to the same pressure by the cooling stream. Cooling CO₂ (300 °C, 194 bar), used for the cooling of the combustion chamber, is fed to the duct that is formed by the borehole and the sheet of metal that surrounds the insulation. To sum up 12 kg/s CO₂ are used to cool the 12 combustion chambers. At the end of the cooling duct the cooling stream is mixed in with the mainstream through holes. These holes can be seen in *Figure 41*. The hot working fluid is then conducted to the stator by two rings. These rings consist of high temperature material with a thermal barrier coating. The upper ring is mounted on the stator and the cavity between the ring and the stator is filled with insulation material. The lower ring is also mounted on the stator. There is also insulation material between the high temperature metal with a thermal barrier coating and the massive ring that has to withstand the pressure between the inner and the outer side.

The stator blades are cooled with cooling CO₂ (300 °C, 80 bar, 60 kg/s), which is supplied through the 4 star bolts that hold the stator. The pressure of this cooling stream has a value of about 194 bar in the thermodynamic design. It thus has to be throttled to 80 bar to reduce both the leakage stream through the labyrinth sealing and the coolant consumption of the rotor blade cooling system. The pressure of 80 bar should be sufficient for this cooling system. The star bolt shown in this drawing is positioned at about 45 ° to this section. Its correct position can be seen in *Figure 39*. After the inner cooling of the stator blades, most of this cooling flow is used for the film cooling of the rotor blades. The rest passes the labyrinth seal of the balance piston into cavity ④. After passing through the rotor blade, the mixed main mass flow and cooling flow (from film cooling) flow to the outlet header via the diffuser. From the header 4 pipes conduct the working fluid to the LPT. The pipe in this drawing is also located at about 45 ° to this section. The correct position is shown in *Figure 39*. The inner part of the header and tube socket are made of high temperature steel. They are also surrounded by insulation material and perforated sheets of metal. A cooling flow with a pressure of 21 bar passes through the duct between the sheets of metal and the casing. This cooling CO₂ is taken from cavity ④ and fed into this duct by pipes ⑤.

Explanation of the cavities marked

The cooling CO₂ fed to the stator through 4 star bolts with a pressure of 80 bar is split into two streams as shown by the red arrows in *Figure 38*. Most is fed into the

rotor blades and used for the film cooling of these blades. The rest flows through the labyrinth sealing of the balance piston into cavity ④ where it reaches a pressure of 21 bar. Most of this mass flow is taken out of this cavity by pipes and split up. A small amount is fed to the outlet header of the HPT through pipe ⑤ as mentioned. Most is fed to the LPT (see *Chapter 6.2*). Cavity ④ is sealed to cavity ③ with a pressure of 4.2 bar by a labyrinth sealing. All leakage flows entering cavity ③ are fed to compressor C1, as cavity ③ is connected with the suction side of this compressor. There the leakage stream is mixed into the main working fluid stream. Cavity ② has a pressure level of 4.5 bar and is fed with steam (H₂O). Therefore, a small steam generator is required. The connection pipes of the cavities are not shown in the drawings. Steam leakage from ② to ③ is mixed there with CO₂ leakage from ④ and fed to compressor C1 as mentioned. The pressure in cavity ① is below the ambient pressure in the turbine building. The extraction removal by suction of cavity ① is done in order to prevent sealing steam entering the turbine building. If there were no cavity ② with sealing steam, there would be CO₂ leakage in the stream that is taken out of ①. From this stream consisting of air and CO₂ leakage careful removal of the CO₂ is necessary as, otherwise, it would lead to CO₂ emissions if this stream is released to the atmosphere.

The right-hand side sealing of the turbine is in principle the same as the sealing on the left-hand side as described before.

6.1.1 Rotor design

The rotor of the high-pressure turbine is shown in *Figure 42*. The disc and balance piston are designed according to Traupel's formula (see *Equation 10*)

$$\frac{h}{h_0} = e^{-\frac{\rho * R^2 * \Omega^2}{2 * \sigma}}, \quad (10)$$

where h is the width of the disc at the radius, R , h_0 is the width at the middle of the rotor ($R=0$), and ρ is the density of steel used for this rotor. The angular speed of the rotor is given by Ω . σ is the stress of the disc and constant because of the design according to Traupel's formula.

A value of 717 MPa for σ leads to the disc contours shown in *Figure 42*. This very high value of 717 MPa is caused by the high rotational speed of the rotor (16 167 rpm). Due to the high rotor stresses a high-alloy steel is necessary, for example, T200 from Böhler Edelstahl [24]. However, for this steel to be used as rotor material it needs a higher carbon content than usual [25]. The temperature of the rotor is kept below 380 to 400 °C by the cooling stream (see *Figure 38*).

A rough estimation of the eigenfrequency of the rotor leads to a first eigenfrequency of about 0.53 times the rotational speed (16 167 rpm). The next eigenfrequency is estimated to 1.52 times the rotational speed. [25]

6.1.2 Burner details

Figure 43 shows a burner as it is integrated in each of the 12 combustion chambers of the HPT. The burner was developed for the Graz cycle and published amongst

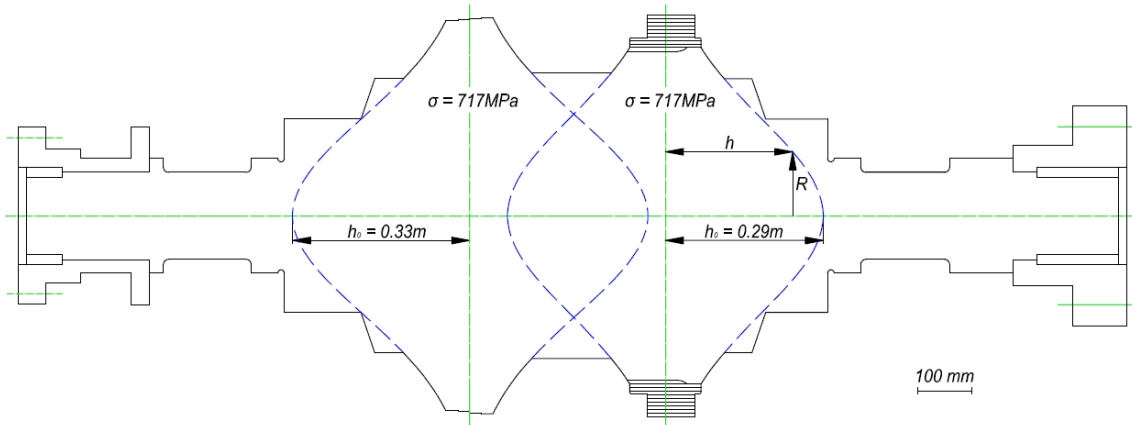


Figure 42: Rotor design of the HPT

others in [27]. Only the flange and the size of the burner were adapted to fit into the combustion chamber of the HPT of the Naki II cycle. The design principles and mode of operation are still the same. Fuel gas and O_2 are fed to the burner cone shown in *Figure 44*. Two coaxial cylindrical ducts pipe fuel gas and O_2 to the outlet nozzles. The inner duct is filled with fuel gas and the outer duct with O_2 . An outlet nozzle is shown in Section C-C. Around the burner core there is a vortex formed by working fluid (CO_2). To achieve this, CO_2 is guided along the burner through swirler blades. A small amount of CO_2 flows through holes in the flange and cools the outer side of the combustor wall. This stream forms a second vortex rotating in the opposite direction thus leading to a vortex breakdown, which results in a stable combustion. In the drawing, vortices are shown by arrows.

6.1.3 Layout of stator blades

The layout of the stator blades of the HPT is shown in *Figure 45*. The blade section is from the mean diameter of the stator. The stator consists of 24 (2x12 because of the split stator) guide vanes. Hence the spacing is 103 mm. The nozzles are designed for supersonic flow with a downstream flow angle of 18° . Each guide vane has three cooling bore holes, through which cooling CO_2 is guided to the inside. c_1 is the exit gas velocity (see *Chapter 6.1.5*).

6.1.4 Rotor blades with ICS (Innovative Cooling System)

A rotor blade with cooling flow is depicted in *Figure 46*. 35 blades are placed on the rotor with a spacing of 71.9 mm at the mean diameter of 800 mm. There is a slot milled into the rotor under the fir tree root of each rotor blade. These slots are made to guide cooling CO_2 into the hollow rotor blades. The cavities there are called CO_2 chambers. Near the leading edge of the rotor blade two cooling slits, as shown in the drawing, are placed on the pressure side. These slits extend over the whole blade length and are interrupted by ligaments to hold the stress. Each slit is 0.9 mm wide. Cooling CO_2 is supplied to the cooling slits by the CO_2 chambers. In the slits the CO_2 expands to sound velocity and further it covers all the outside

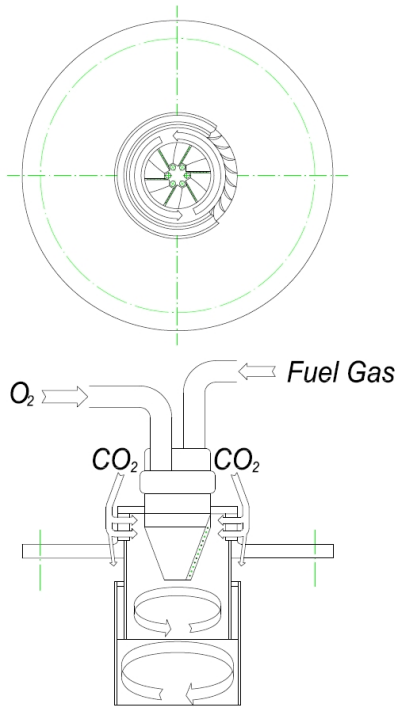


Figure 43: Burner

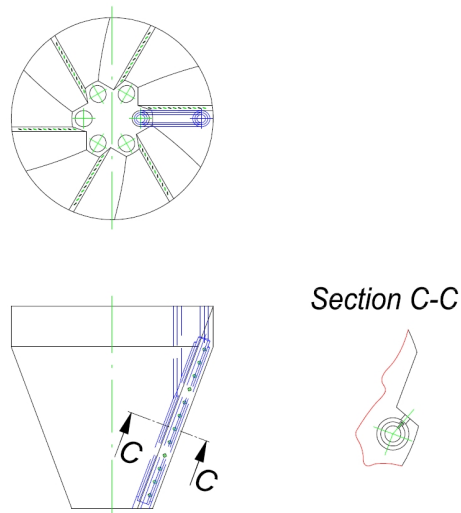


Figure 44: Burner cone

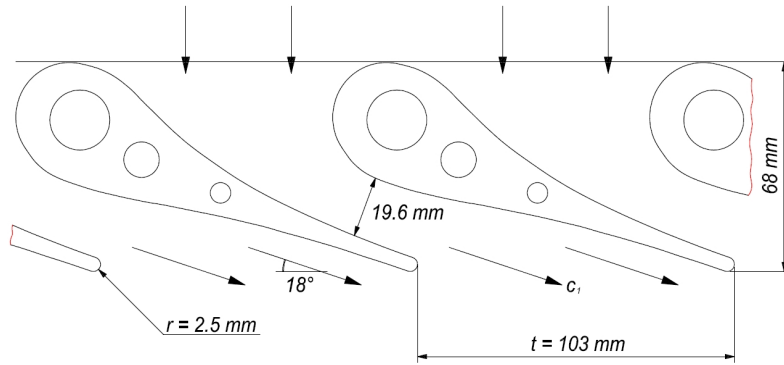


Figure 45: Guide vanes

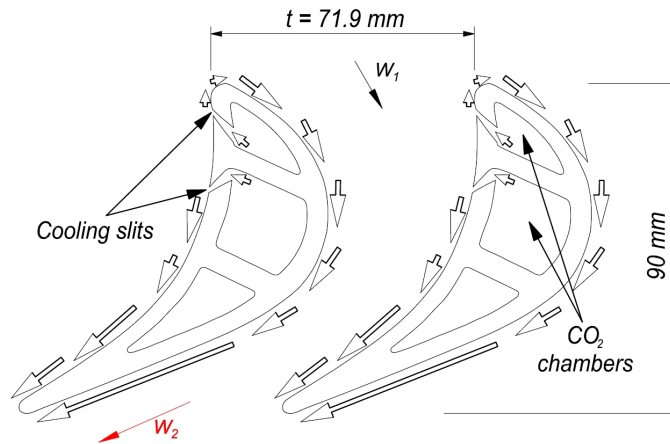


Figure 46: Rotor blade with ICS (innovative cooling system)

of the blade, creating an actually coherent layer of cold CO₂ inside the hot working gas [27]. The cooling flow is shown by arrows in the drawing.

This cooling system is called ICS (Innovative Cooling System) and has been developed for the high temperature turbine of the Graz cycle. The contour of this blade is originally from the Graz cycle turbine and, with small modifications, fits into the high-pressure turbine of the Naki II cycle. The design of the turbine blade with ICS used in the high temperature turbine of the Graz cycle was published among others in [26] and [27].

w_1 is the relative gas velocity at the entry side and w_2 the relative gas velocity at the exit side of the rotor (see *Chapter 6.1.5*).

6.1.5 Velocity triangle of the HPT

Figure 47 shows the velocity triangle of the HPT. The black triangle is for the rotor entry and the red triangle for the rotor exit. c_1 is the exit velocity of the stator and has a value of about 892 m/s. The direction of c_1 is given by the angle α_{in} (18 °) (see *Figure 45*). u means the circumferential velocity of the rotor blade at its mean diameter and is about 690 m/s. w_1 (317 m/s) is the relative velocity of the gas to

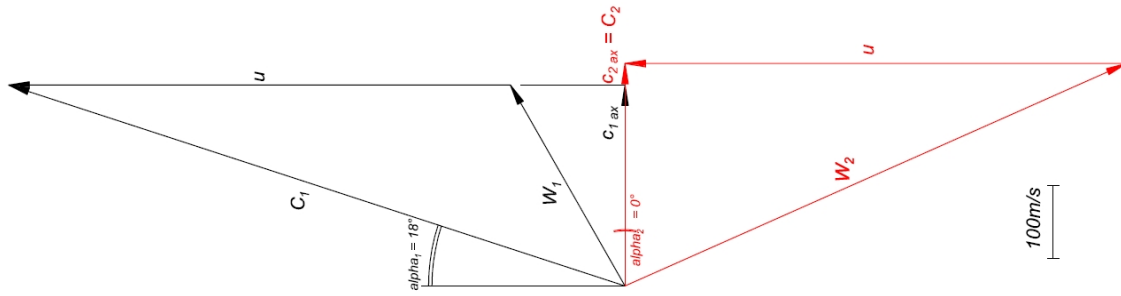


Figure 47: Velocity triangle of the HPT

the rotor blades. $c_{1\text{ ax}}$, which has a value of about 276 m/s, represents the axial velocity at the rotor entry.

c_2 , the exit velocity of the rotor, is 305 m/s and is in axial direction. The velocity w_2 (754 m/s) is the relative velocity between the exit gas flow and the rotor blades.

6.1.6 Assembly of HPT

In this short description the main steps of assembling the HPT are mentioned. The internals of the combustion chambers can be mounted later.

In addition to this explanation, the sequence of assembly is shown in *Figure 48* by numbers. At first the split stator with the mounted inflow duct is placed around the rotor. The inflow duct consists of high temperature material and its surface next to the hot gas is coated with a thermal barrier coating. On the other side it is insulated. The upper ring of the inflow duct is fixed on the stator. The lower ring is also fixed on the stator but it has a further massive ring that has to withstand the pressure difference between the pressure in the inflow duct (194 bar) and the pressure in the inner casing of the turbine (80 bar). After the stator has been placed around the rotor, step 2 follows. On each side of the stator a ring is shrunk on as shown in the drawing. These rings fix the stator when the rotor and stator, together, are pushed axially into the one-piece casing of the turbine in step 3. The casing is warmed up in order to get a tight fit of the stator in the casing during operation. It is important so ensure that the position of the stator vis-à-vis the rotor is fixed with an assembly attachment during assembly, as any movement between them could damage the labyrinth sealing. The stator is fixed with four star bolts in the turbine casing (step 4). These bolts provide perfect centering of nozzle and rotor blade arrangement during thermal strains. The undivided ring with the labyrinth sealing for the balance piston is then pushed axially into its position (5) and is fixed with four star bolts. With four axial bolts it supports the massive ring of the inflow duct. The axial bolt shown in the drawing is located at about 45° to this section. In step 6 the split sealing ring is mounted. Its position is fixed to the ring assembled in step 5 by four axial bolts. Fixing the bearing with the turbine casing in step 7 completes the left side of this turbine.

On the right side the split rings which include the labyrinth sealing (8) and the bearing (9) are placed on the rotor. A part of the outer casing of the outlet header is

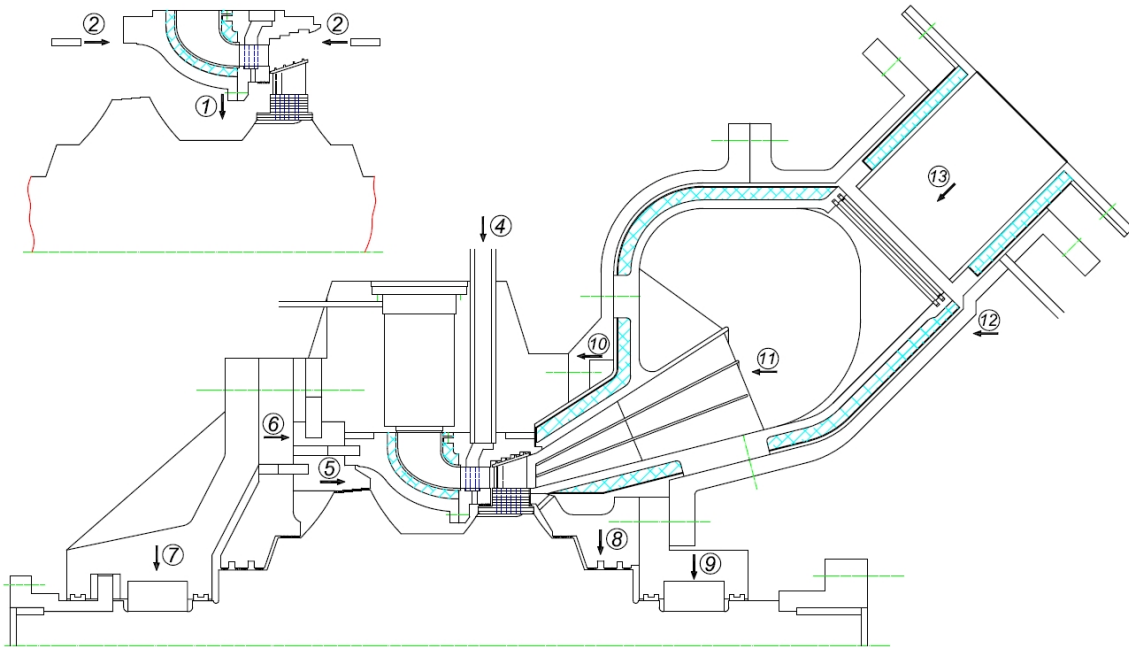


Figure 48: Assembly of HPT

then mounted on the turbine casing (10). In this part of the header casing, the one-piece inner header with surrounding insulation is axially pushed into position and fixed (11). In step 12 the second part of the outer casing is mounted. The bearing is connected through this part to the casing. Lastly, the liner with insulation is positioned in the outlet tube socket of the exhaust pipe (13).

6.2 Low-pressure turbine (LPT)

The requirements on the LPT in relation to inlet pressure (21 bar) and temperature (911 °C) are lower compared to the HPT. Therefore a horizontally split casing design is chosen to facilitate assembly of the turbine. However, the hot parts of the inlet side like the nozzle box and the first stator are also undivided to avoid non-uniform wall thickness and thus non-uniform temperature distribution during heating up and cooling down of the turbine, as mentioned in *Chapter 6.1 (HPT)*.

Figure 49 depicts an overview of the LPT. The red arrows show the coolant flow through the turbine. On the left side of the turbine is the nozzle box. Its insulation is the same as that used for the HPT. Working fluid from the HPT is fed into the nozzle box through four pipes. The pipe shown in this drawing is located at about 45 ° to this section. This position is the same as for the HPT outlet pipe. The one-piece nozzle box is fixed at the stator of the first turbine stage. This stator is fixed by four star bolts which are used to guide cooling CO₂ into the stator blades. The star bolt shown is also located at about 45 ° to this section. Cooling CO₂ is taken from cavity ④ of the HPT (21 bar) and throttled to 16 bar. After flowing

through the guide vanes of the stator a small amount streams along the duct formed by the insulation of the nozzle box and the outer casing. This stream is taken out with pipe⑥ for further usage as mentioned below. Most of the cooling flow streams through slots under the fir tree roots of the rotor blades. From there it is guided by boreholes through the rotor blades in order to cool them. The outlet of these boreholes is on the tip of the blades in the clearance of the labyrinth sealing. The slot, as mentioned, extends over the whole width of the blade root. It thus connects the cavity on the left of the disc with the cavity between this disc and the second stator.

The guide vanes of the second stator are also cooled by a cold CO₂ flow through boreholes. This cooling CO₂ is also taken from cavity④ and throttled to a pressure of 6.5 bar. It is then guided through four star bolts which fix the second stator. The star bolt shown is located at 45 ° to this section. After passing through the guide vanes of the stator the cooling flow enters the cavity between the second stator and the second rotor disc. From there it is also fed into the rotor blade boreholes by slots under the fir tree roots. This turbine stage is designed with a blade root cooling facility. The coolant flows through the blade roots and leaves the blades via small holes in the root plate. The coolant is then mixed with the main flow. The cavity between the second rotor disc and the casing is also fed by the slots mentioned above.

On the left side of the turbine there is not enough space to arrange a balance piston because of the undivided nozzle box. It is thus designed to be on the right side with cavity⑦. This cavity is fed with CO₂ at a pressure level of 16 bar via pipe⑥. Another advantage of the balance piston on the right side is the nearly symmetric rotor.

Cavities①,②, and③ have the same pressure levels and functions as in the HPT.

6.2.1 Assembly of LPT

Most parts of the LPT are horizontally split. Thus the LPT can be opened by lifting the upper part of the casing and is easier to assemble than the HPT. The insulated one-piece nozzle box is fixed on the undivided stator of the first stage. First, the left ring that includes the labyrinth sealing is positioned on the rotor. Its position has to be fixed with an assembly attachment so as not to cause damage to the sealing due to relative movements between this ring and the rotor. Then the first stator with the mounted nozzle box is pushed axially into its position on the rotor. It also has to be fixed with an assembly attachment during assembly. Afterwards, the rotor with the fixed parts can be integrated into the lower part of the turbine casing, in which the lower part of the second stator and of the right sealing ring are already positioned. The lower bearing parts are also fixed in the lower turbine casing at this time. When the rotor is positioned in the lower turbine casing, the upper parts of the second stator, the right sealing ring, and the turbine casing are mounted. Both nozzle stators are fixed with four star bolts in the turbine casing. When the turbine casing is closed, the upper part of the left and right bearing are fixed. The liner with the surrounding insulation is then pushed into the inlet tube socket. Lastly, the outlet scroll on the right side of the turbine is mounted.

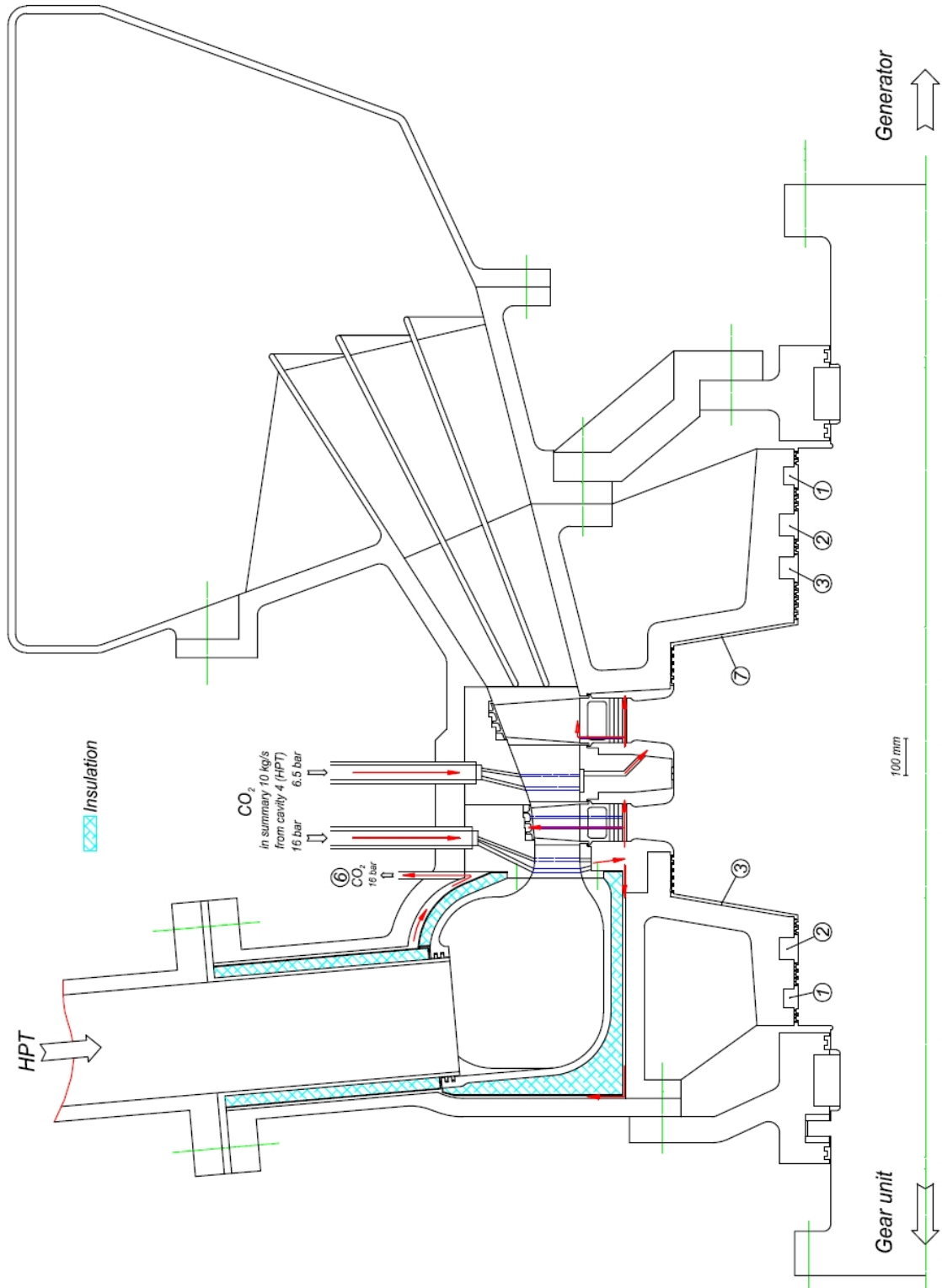


Figure 49: Low-pressure turbine (LPT) - overview

Table 19: General economic assumptions

Yearly operating hours (f) [13]	8 500	hrs/yr
Capital charge rate (a) [13]	12	%/yr
Fuel costs: methane (C_{fuel}) [29]	5.5	€/GJ _{th}
Fuel costs: anthracite (C_{fuel})	3.0	€/GJ _{th}
O&M (b) [29]	7	% of capital costs

7 Economic Evaluation

In this rough economic evaluation a comparison between the Naki cycles and corresponding reference systems were done. The reference systems are conventional power plants without CO₂ capture. The results of this evaluation heavily depend on the reference systems. Therefore state-of-the-art power cycles, as mentioned below, are used as reference systems.

The main results of this evaluation are the CO₂ mitigation costs of the three Naki cycles. These are the costs for one tonne CO₂ that is avoided. The COE (cost of electricity) for power plants with CO₂ capture are higher than for conventional power plants without CO₂ capture. This is because of higher capital costs for the same electrical output and the lower net efficiency. Another reason is the higher operation and maintenance (O&M) costs of power plants with CO₂ capture.

7.1 Assumptions

The economic evaluation is based on a comparison of the Naki cycles with conventional state-of-the-art power plants. A coal plant with a net efficiency of 46 % [30] and a combined cycle plant (CC plant) with a net efficiency of 59.2 % [31] are used as reference plants. Naki I and the coal plant are fired with anthracite. Naki II, Naki III, and the CC plant use methane (natural gas) as fuel. Naki I is compared with the coal plant and also with the CC plant. Naki II and Naki III are compared with the CC plant. General economic assumptions are shown in *Table 19*. The yearly operating hours are assumed to be 8500 hrs/yr. The capital charge rate is 12 %/yr. This corresponds to an interest rate of 8 % over a depreciation period of 15 years [13]. The fuel costs for methane are 5.5 €/GJ_{th} [29]. The anthracite price is taken from [32] and increased by an additional charge for transport by railway, assumed to be 3.0 €/GJ_{th}. For operation and maintenance (O&M), 7 % of the capital costs are assumed [29].

For the Naki cycles additional costs arise for CO₂ capture which are estimated according to [28] as shown in *Table 20*. The additional costs are split into costs for an air separation unit, other costs (piping. . .), and costs for CO₂-compression. The last point also refers to the treatment of the captured CO₂ in such a way that it causes no damage in the transport system. For example, dehumidification is needed, as humid CO₂ is corrosive. The costs of CO₂ transport and storage are not considered, as they largely depend on the site of the power plant.

The dollar exchange rate used is 1.27\$/€. Prices in power generation plants have

Table 20: Additional costs [28]

Air separation unit	1 500 000	\$/ (kg O ₂ /s)
Other costs (piping. . .)	100 000	\$/ (kg CO ₂ /s)
CO ₂ -compression	450 000	\$/ (kg CO ₂ /s)

risen in the last few years. Thus, a price rise factor of 2 is used to obtain actual prices for the additional costs.

7.1.1 Evaluation of the capital costs for a Naki I power plant

One reference plant for Naki I is a conventional coal power plant with a net efficiency of 46 % [30]. The investment costs of this reference plant are estimated at 1.250 €/kW [30]. To estimate the difference in investment costs between a Naki I and Naki II plant, the main components for a plant of 270 MW net power output are compared in *Table 21*.

As shown in *Table 21*, the CO₂ turbine of Naki I has a lower TIT and also lower power than the CO₂ turbine in the Naki II cycle. Furthermore, there are no CO₂ compressors required in a Naki I power plant. These aspects lead to lower investment costs needed for the Naki I plant. However, the recuperative heat exchanger of the Naki I plant compared to that of the Naki II plant has a higher power and also a higher pressure (45 bar) in the casing. Despite the lower volume flow, this has an adverse effect on the investment costs. The higher power of the CO₂ condenser also leads to increased costs. Both generators are in the same power range.

In summary, some components are more expensive and some cheaper. Thus, for a rough economic evaluation, the estimated investment costs of the Naki I power plant are assumed to be the same as for the Naki II plant. These investment costs in €/kW_{el} are shown in *Table 24* of *Chapter 7.1.2*.

7.1.2 Evaluation of the capital costs for a Naki II and Naki III power plant

The Naki II and Naki III power plants are compared with a conventional combined cycle power plant (CC plant) with a net efficiency of 59.2 % [31]. In *Table 23* assumed costs for the Naki II, Naki III, and conventional CC plant in 10⁶ € are given. The specific investment costs of the conventional CC plant are estimated to be 570 €/kW [31]. The assumed cost split of the conventional CC plant in terms of costs of the gas turbine, steam generator, etc. is shown in the third column. The component costs of the Naki plants are assumed on the basis of the component costs of the conventional CC plant taking into account the component parameters shown in *Table 22* of power plants with a net power output of 270 MW.

The TITs of the CO₂ turbines in the Naki plants are the same as the TIT of the gas turbine in the CC plant. The higher TIP in the Naki plants leads to higher costs. But the lower turbine powers have a contrary effect and in combination with the lower powers and pressure ratios of the compressors, used in the Naki plants,

Table 21: Comparison of equipment size for a Naki I plant of 270 MW net power output

			Naki II	Naki I
CO ₂ turbine	Power	MW	435	396
	TIP	bar	190	190
	TIT	°C	1 400	850
CO ₂ compressors	Power	MW	80	-
	Pressure ratio	-	12	-
Recuperative heat exchanger	Power	MW	403	1 098
	Pressure	bar	200 / 4	200 / 46
	Hot inlet temp.	°C	667	646
	Hot inlet volume flow	m ³ /s	226	59
CO ₂ condenser	Power	MW	104	380
	Pressure	bar	45	45
	Inlet volume flow	m ³ /s	4	16
Generator	Power	MW	333	354

this rise in cost is compensated for. The costs of the CO₂ turbines and compressors are thus estimated to be the same as the costs of the gas turbine in the CC plant.

In the Naki II plant, there is no steam turbine and thus no costs for it. The power of the steam turbine in the Naki III plant is about 27 % higher than in the CC plant. Hence, it is assumed that the costs also rise by about 27 %.

The recuperative heat exchangers used in the Naki plants are compared with the HRSG of the CC plant. For the Naki II plant, the costs are the same as for the HRSG of the CC plant because the hot inlet temperature is nearly the same. However, the pressure in the tubes is equal. The higher pressure of 4 bar in the casing and the higher power of the recuperative heat exchanger are compensated for by the lower inlet volume flow. The main differences in the HRSG used in the Naki III plant in comparison to the HRSG of the CC plant are the lower inlet volume flow and the higher pressure (4 bar) in the casing. The recuperative heat exchanger in the Naki III plant has a higher pressure (45 bar) in the casing, but a lower power, a lower inlet temperature, and lower volume flow. To sum up, these two components (recuperative heat exchanger and HRSG) of the Naki III plant are assumed to be about 30 % more expensive than in the reference CC plant.

The power of the generator of the Naki plants is about 23 % higher and hence the costs are estimated to rise at about the same percentage rate.

The estimated costs of the buildings for the Naki II plant are 16 Mio€ and lower than the 23 Mio€ estimated for the CC plant. This is because there is no boiler house needed in the Naki II plant. The dimensions of the Naki III plant are the same as for a conventional CC plant and the same costs for building are thus used.

In summary, the investment or capital costs for a conventional CC plant of 270 MW are estimated to be 154 Mio€ (the specific costs are 570 €/kW_{el}). The costs for the Naki II plant of 136 Mio€ (specific costs of 504 €/kW_{el}) are lower than the costs for the reference plant. The capital costs of 180 Mio€ (specific costs of 667

Table 22: Comparison of equipment size for a Naki II and Naki III plant of 270 MW net power output

			Conventional CC plant	Naki II	Naki III
Turbine of “gas turbine”/ CO ₂ turbine	Power	MW	450	435	344
	TIP	bar	25 to 30	190	190
	TIT	°C	1 400	1 400	1 400
Compressor of “gas turbine”/ CO ₂ compres- sors	Power	MW	270	80	103
	Pressure ratio	-	25 to 30	12	12.3
Steam turbines	Power	MW	90	-	114
Recuperative heat exchanger	Power	MW	-	403	176
	Pressure	bar	-	200 / 4	200 / 45
	Hot inlet temp.	°C	-	667	337
	Hot inlet volume flow	m ³ /s	-	226	10
HRSG	Power	MW	257	-	269
	Pressure	bar	200 / 1	-	160 / 4
	Hot inlet temp.	°C	620	-	652
	Hot inlet volume flow	m ³ /s	930	-	188
Generator	Power	MW	270	333	335

€/kW_{el}) for the Naki III plant are higher. The Naki III plant is more expensive than the Naki II plant because of the additional steam cycle.

Table 24 gives an overview of the investment costs of the reference plants and the Naki plants. The costs for additional equipment (air separation unit...) are also shown. The scale parameter given is used to adapt these costs to the size needed. The mass flows that are required as scale parameters for the Naki plants of 270 MW net power output are shown in Table 25.

7.2 Basics of economic calculations

This chapter gives a summary of the equations used in the economic evaluation.

- **Additional capital costs**

The additional capital costs include additional components of the Naki power plants that are not used in the reference power plant. These are calculated as shown in Equation 11. The specific additional costs for the air separation unit (C_{asu}), other equipment (C_{oth}), and for CO₂-compression (C_{comp}) (see Table 20) multiplied by the corresponding mass flows (\dot{m}_{O_2} or \dot{m}_{CO_2}) (Table 25) are the absolute additional capital costs in €. This sum divided by the electrical net power output (P_{el}) leads to the additional capital costs (C_{addit}) in €/kW_{el}.

Table 23: Estimated costs for a Naki II, Naki III, and conv. CC plant of 270 MW net power output

		Conventional CC plant	Naki II	Naki III
Gas turbine / CO ₂ turbine and compressor	10 ⁶ €	28	28	28
Steam turbine	10 ⁶ €	23	0	29
HRSG / recuperative heat exchanger	10 ⁶ €	27	27	35
Electrical equipment	10 ⁶ €	53	65	65
Buildings	10 ⁶ €	23	16	23
Sum	10 ⁶ €	154	136	180
Specific investments costs	€/kW _{el}	570	504	667

Table 24: Investment costs of the different power plants

Component	Scale parameter	Specific costs	
Investment costs of the reference plants (C_C)			
Conventional CC plant [31]	Electric power	570	€/kW _{el}
Conventional coal plant [30]	Electric power	1 250	€/kW _{el}
Investment costs of the Naki plants (C_C)			
Naki I	Electric power	504	€/kW _{el}
Naki II	Electric power	504	€/kW _{el}
Naki III	Electric power	667	€/kW _{el}
Air separation unit (C _{asu})	O ₂ mass flow	2 362 205	€/(kg O ₂ /s)
Other costs (piping. . .) (C _{oth})	CO ₂ mass flow	157 480	€/(kg CO ₂ /s)
CO ₂ -compression (C _{comp})	CO ₂ mass flow	708 661	€/(kg CO ₂ /s)

Table 25: Mass flows of the Naki plants with a net power output of 270 MW

		Naki I	Naki II	Naki III
Fuel	kg/s	21.4	10.5	10.7
O ₂	kg/s	56.8	41.9	42.5
CO ₂	kg/s	78.2	28.9	29.3

$$C_{addit} = \frac{C_{asu} * \dot{m}_{O_2} + (C_{oth} + C_{comp}) * \dot{m}_{CO_2}}{P_{el}} \quad (11)$$

- **COE for plant amortization**

This is the COE (cost of electricity) due to the capital costs of the power plant. The capital charge rate (a) multiplied by the specific capital costs for the reference plant (C_C) and divided by the yearly operating hours (f) results in the cost of electricity for the reference plant ($COE_{C(R)}$), as shown in *Equation 12*. The $COE_{C(N)}$ as calculated in *Equation 13* gives the cost of electricity for the Naki plant. It is the sum of the specific capital costs for the Naki plant (C_C) and the additional capital costs (C_{addit}) multiplied by the capital charge rate and divided by the yearly operating hours.

$$COE_{C(R)} = \frac{a * C_C}{f} \quad (12)$$

$$COE_{C(N)} = \frac{a * (C_C + C_{addit})}{f} \quad (13)$$

- **COE due to fuel**

The COE due to the fuel consumption (COE_{fuel}) is defined in *Equation 14* and the result of the fuel costs (C_{fuel}) divided by the net efficiency (η) of the considered power plant.

$$COE_{fuel} = \frac{C_{fuel}}{\eta} \quad (14)$$

- **COE due to O&M**

The COE caused by the costs of operation and maintenance ($COE_{O\&M}$) is calculated as in *Equation 15*. It is the product of COE for plant amortization of the power plant under consideration ($COE_{C(R)}$ or $COE_{C(N)}$) and the percentage rate for O&M (b).

$$COE_{O\&M} = COE_C * b \quad (15)$$

- **Total COE**

The total COE is the sum of all calculated COEs of the power plant under consideration (see *Equation 16*).

$$COE_{total} = COE_C + COE_{fuel} + COE_{O\&M} \quad (16)$$

- **Differential COE**

The difference between the total COE of the Naki plant ($COE_{total N}$) and the reference plant ($COE_{total R}$) is the differential COE (COE_{diff}) (*Equation 17*).

$$COE_{diff} = COE_{total N} - COE_{total R} \quad (17)$$

- **Mitigation costs**

The additional costs arising from the capture of CO₂ are the mitigation costs (MC). The MC are the ratio of the differential COE and the difference between the emitted CO₂ of the reference plant (E_R) and of the Naki plant (E_N) related to one kWh_{el}. Inserting the difference between the total COE of the Naki and the reference plant for the differential COE gives *Equation 18*.

$$MC = \frac{COE_{totalN} - COE_{totalR}}{E_R - E_N} \quad (18)$$

7.3 Results of the economic evaluation

The economic comparison for a 270 MW Naki I plant with a conventional coal plant is given in *Table 26*. Compared to the reference plant, the capital costs of the Naki I plant are nearly the same if the additional costs are considered. This results in the same COE for plant amortization. The difference in the COE due to fuel consumption is caused by the lower net efficiency of the Naki I plant. The COE due to O&M of both plants is also the same because the costs for O&M are assumed to be 7 % of the capital costs, which are the same for these plants. To sum up, the differential COE of the Naki I plant is 0.55 ct/kWh_{el}, an increase of 13.0 %. This results in mitigation costs of 6.5 €/tCO₂ avoided for CO₂ capture.

Table 26: Economic comparison for a 270 MW Naki I plant

		Reference plant: Coal plant	Naki I plant
Plant capital costs (C _C)	€/kW _{el}	1 250	504
Additional capital costs (C _{addit})	€/kW _{el}	-	748
CO ₂ emitted (E)	kg/kWh _{el}	0.846	0.0
Net efficiency (η)	%	46.0	37.3
COE for plant amortisation (COE _C)	ct/kWh _{el}	1.76	1.77
COE due to fuel (COE _{fuel})	ct/kWh _{el}	2.35	2.90
COE due to O&M (COE _{O&M})	ct/kWh _{el}	0.12	0.12
Total COE (COE_{total})	ct/kWh_{el}	4.24	4.79
Comparison			
Differential COE (COE_{diff})	ct/kWh_{el}		0.55
Mitigation costs (MC)	€/t CO₂		6.5

In *Table 27* the economic comparison for a conventional CC plant, a Naki I, Naki II, and Naki III plant with an electrical net power output of 270 MW is shown. Compared to the reference plant the capital costs are about 119 % higher for the Naki I plant, 69 % higher for the Naki II plant, and about 99 % higher for the Naki III plant if the additional costs are taken into account. Thus the COE for plant amortization of these three plants are also higher. The COE due to O&M of the Naki plants is higher because it is linked to the capital costs. The COE due to fuel

Table 27: Economic comparison for a 270 MW Naki I, Naki II, and Naki III plant

		Conv. CC plant	Naki I plant	Naki II plant	Naki III plant
Plant capital costs (C_C)	€/kW _{el}	570	504	504	667
Additional capital costs (C_{addit})	€/kW _{el}	-	748	459	466
CO ₂ emitted (E)	kg/kWh _{el}	0.335	0.0	0.0	0.0
Net efficiency (η)	%	59.2	37.3	51.3	50.5
COE for plant amortisation (COE_C)	ct/kWh _{el}	0.81	1.77	1.36	1.60
COE due to fuel (COE_{fuel})	ct/kWh _{el}	3.34	2.90	3.86	3.92
COE due to O&M ($\text{COE}_{\text{O\&M}}$)	ct/kWh _{el}	0.06	0.12	0.10	0.11
Total COE ($\text{COE}_{\text{total}}$)	ct/kWh_{el}	4.21	4.79	5.31	5.63
Comparison					
Differential COE (COE_{diff})	ct/kWh_{el}		0.58	1.11	1.43
Mitigation costs (MC)	€/t CO₂		17.3	33.1	42.6

consumption which is the major contributor to the total COE is influenced by the net efficiency. In the case of Naki I plant, the COE due to fuel consumption in comparison to the CC plant is lower because the price of anthracite is considerably lower than of methane. In the case of Naki II and Naki III the lower net efficiencies in comparison to the reference plant lead to a higher COE due to fuel consumption. In summary the total COEs for the Naki plants are higher than for the CC plant which result in differential COEs of 0.58 ct/kWh_{el} (an increase of 13.7 %) for Naki I, of 1.11 ct/kWh_{el} (an increase of 26.3 %) for Naki II, and of 1.43 ct/kWh_{el} (an increase of 33.9 %) for Naki III. The differential COEs lead to mitigation costs of 17.3 €/tCO₂ avoided for the Naki I plant, of 33.1 €/tCO₂ avoided for the Naki II plant, and of 42.6 €/tCO₂ avoided for the Naki III plant.

The difference in the mitigation costs between Naki I and the two other Naki plants is caused by the different fuel costs, as mentioned. However, the costs of transport and storage of the captured CO₂ are not considered in this economic evaluation. The Naki I plant produces 78.2 kg CO₂/s (see Table 25) which results in 2.39 m tonnes of CO₂ per year for 8 500 operating hours per year. These 2.39 m tonnes of CO₂ per year have to be transported and stored. Naki II with 28.92 kg CO₂/s (0.88 m tonnes of CO₂ per year) produces 63 % less CO₂ than Naki I. In the Naki III plant 29.3 kg CO₂/s are produced, which results in 0.90 m tonnes of CO₂ per year. Hence the costs of transport and storage of the captured CO₂ of the Naki I plant will be about 63 % higher than those of Naki II.

7.4 Cost-sensitivity analysis

The results of the economic evaluation heavily depend on the assumptions, especially on the investment costs, capital charge rate, fuel costs, and the efficiencies of the cycles. Unfortunately, however, there is a large uncertainty involved in these costs.

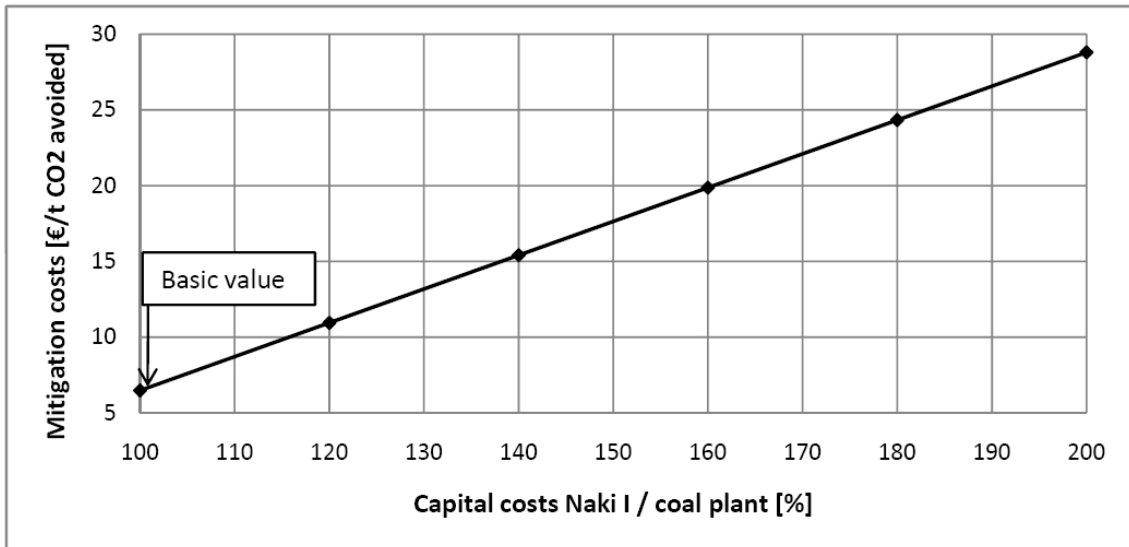


Figure 50: Influence of capital costs on mitigation costs for Naki I

Therefore, a cost sensitivity analysis was performed. Naki I is compared only with the coal plant in this cost-sensitivity analysis. The trend of the mitigation costs is similar for the Naki I, Naki II, and Naki III plants. Thus, only the results of the sensitivity analysis of the Naki I plant are shown below. The results for the Naki II and Naki III plants are given in *Appendix D*.

- **Capital costs**

The sum of plant capital costs and additional costs of the Naki I plant is nearly the same as the capital costs of the coal plant. In case of the Naki II and Naki III plants, the sum of these costs is higher than the capital costs of the reference plant. This results in increased cost of electricity. The calculation of the influence of the capital costs on the mitigation costs is performed by calculating the ratio of the capital costs of the Naki plant to the capital costs of the reference plant. In *Figure 50* the influence is shown for a ratio of 100 % (both plants have the same capital costs) to 200 % (the Naki I plant costs twice as much as the reference plant) for the Naki I and the coal plant. At 100 % the mitigation costs of 6.5 €/tCO₂ avoided are caused mainly by the lower net efficiency of the Naki I plant. With rising capital costs, the mitigation costs also increase and at 200 % they have a value of 28.8 €/tCO₂ avoided. The mitigation costs for a Naki II plant compared with a CC plant are 15.4 €/tCO₂ avoided for 100 % and 41.1 €/tCO₂ avoided for 200 %. In the case of the Naki III plant, compared with a CC plant, the mitigation costs are 17.2 €/tCO₂ avoided for 100 % and 42.9 €/tCO₂ avoided for 200 %.

- **Capital charge rate**

Economic life-time and interest payments result in the capital charge rate. In the literature capital charge rates of between 7 % and 16 % are given. To demonstrate the influence of the capital charge rate, it is varied between 5 %/yr and 25 %/yr (12 % is used in the economic evaluation). For these values

the mitigation costs rise from 6.49 to 6.53 €/tCO₂ avoided as shown in *Figure 51* for the Naki I plant compared with a coal plant. The only low rise in the mitigation costs is because of the nearly same investment costs for the Naki I plant and the coal plant. The investment costs for the Naki II and Naki III plant are higher than for the CC plant. Hence the rise in mitigation costs from 22.7 to 52.2 €/tCO₂ avoided for Naki II and from 27.8 to 70.0 €/tCO₂ avoided for Naki III is higher than for the Naki I plant.

- **Fuel costs**

The influence of fuel costs on mitigation costs relates to the different net efficiency of the Naki plant and the reference plant. In *Figure 52* this influence is shown for a fuel cost ranging from 1€/GJ_{th} to 10 €/GJ_{th}, in which the mitigation costs rise from 2.2 to 21.6 €/tCO₂ avoided for the Naki I plant compared with a coal plant. In the case of the Naki II plant compared with a CC plant, mitigation costs from 20.5 to 45.6 €/tCO₂ avoided were calculated for the same price range of fuel. The mitigation costs of the Naki III plant rise from 28.5 to 56.6 €/tCO₂ avoided under the same conditions.

- **Net efficiency of the power plants**

The fuel demand of a power plant depends on its net efficiency for a given net power output. Decreasing net efficiency leads to increased fuel demand and hence increased cost of electricity due to fuel consumption. *Figure 53* depicts the influence of net efficiency of the coal plant on mitigation costs for the Naki I plant. The net efficiency is varied from 35 % to 55 %, which results in mitigation costs from -1.7 to 13.2 €/tCO₂ avoided. If the net efficiency of the coal plant is lower than the net efficiency of the Naki I plant, the mitigation costs have negative values because of the nearly same investment costs in both power plants. In *Figure 54* the cost sensitivity caused by the net efficiency of the Naki I plant is shown. The range of the net efficiency varies from 25 % to 45 % and results in decreasing mitigation costs from a value of 13.3 €/tCO₂ avoided to a value of 0.6 €/tCO₂ avoided.

The net efficiency of the CC plant is varied from 45 % to 65 %. This leads to mitigation costs from 1.2 to 46.1 €/tCO₂ avoided for the Naki II plant and from 8.4 to 56.5 €/tCO₂ avoided for the Naki III plant. A variation of the net efficiency of the Naki II plant from 40 % to 60 % results in mitigation costs from 65.6 to 16.4 €/tCO₂ avoided. For a net efficiency from 40 to 60 % for the Naki III plant, mitigation costs from 73.3 to 24.0 €/tCO₂ avoided were calculated.

These results show the importance of high efficiency for the CO₂-free power plant.

Capital costs and fuel costs have the largest influence on the mitigation costs. Unfortunately, these values have the highest uncertainties, as it is difficult to predict future fuel and capital costs, as a large amount of development work is needed.

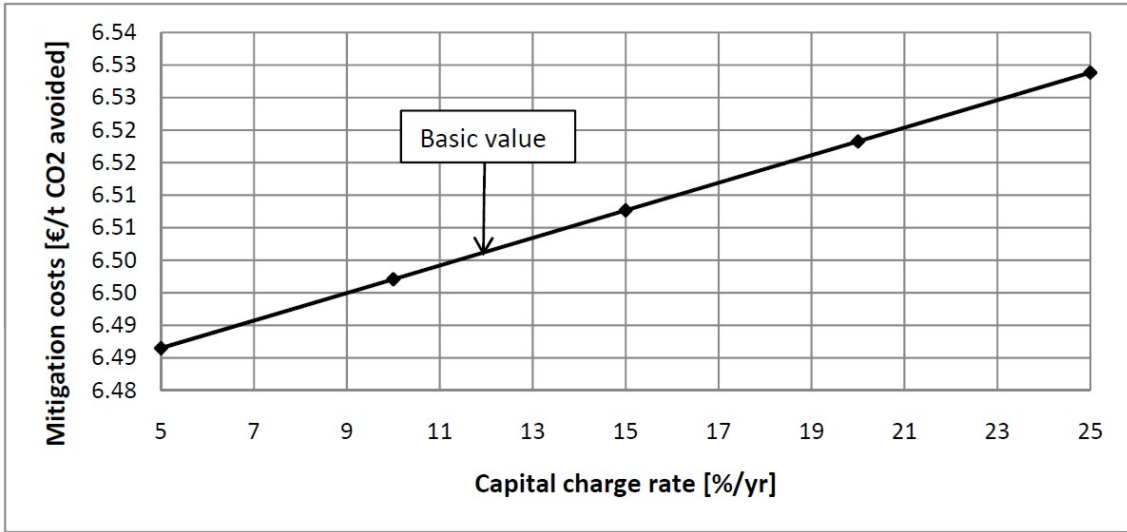


Figure 51: Influence of capital charge rate on mitigation costs for Naki I

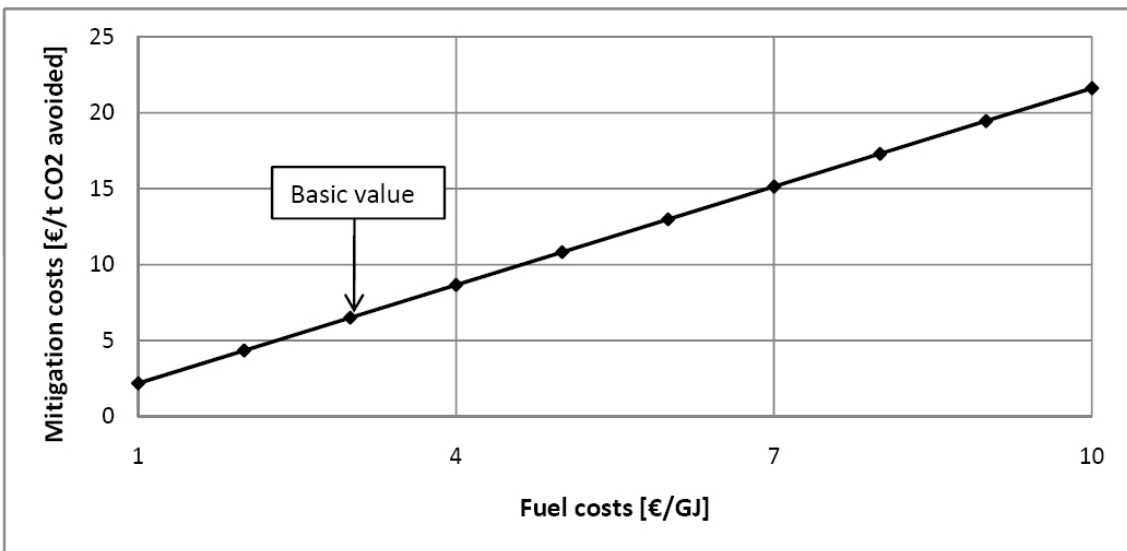


Figure 52: Influence of fuel costs on mitigation costs for Naki I

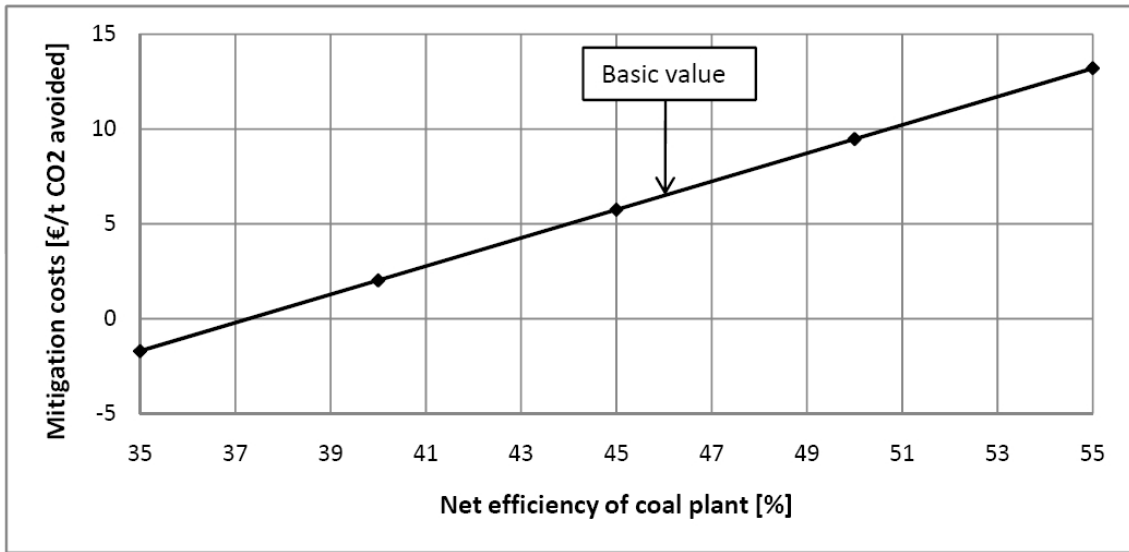


Figure 53: Influence of net efficiency of the reference plant on mitigation costs (Naki I)

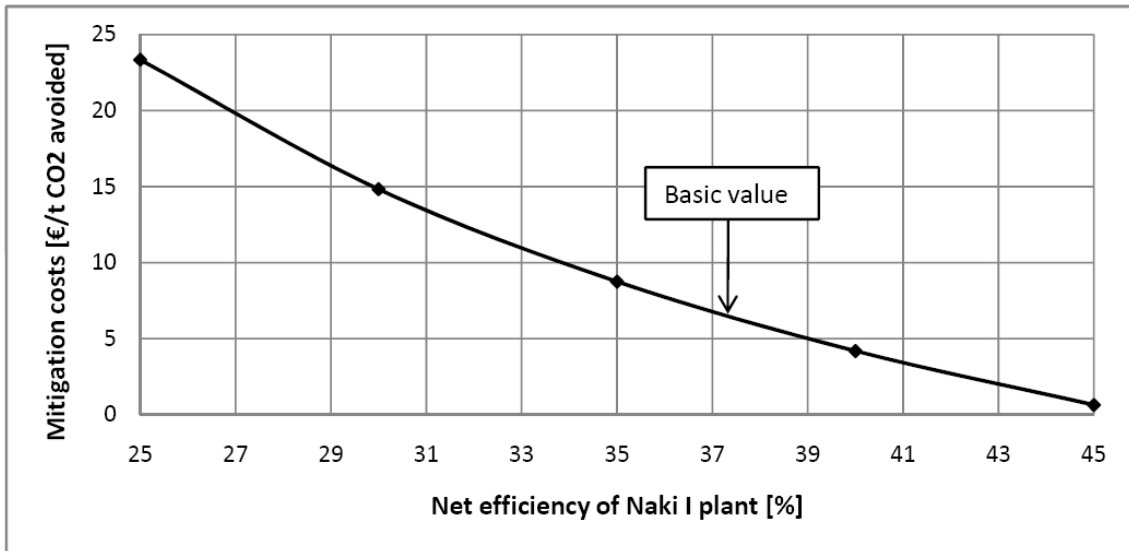


Figure 54: Influence of net efficiency of the Naki I plant on mitigation costs

8 Conclusion and Outlook

In the present work new oxyfuel cycles with inherent CO₂ capture were investigated. The so-called Naki cycle is in principle a closed cycle gas turbine with a recuperative heat exchanger. The main difference between the Naki cycle and conventional gas turbine cycles is the pressure rise in liquid state instead of the compression in gaseous state. This leads to a reduced power demand for the pressure rise. CO₂ is used as the working fluid in these supercritical cycles with internal combustion. Because of the pressure rise in liquid state, the working fluid has to be condensed.

The less favorable properties of the working fluid CO₂, like high density and low speed of sound, make the overall dimensioning of turbines difficult. The high density leads to low volume flows and therefore to small diameters and blade lengths of the turbines. High turbine inlet temperatures (Carnot) lead to cooled turbine blades (film cooling) and this cooling causes efficiency penalties. To minimize the efficiency penalties due to turbine cooling, the number of cooled stages should be low. Hence, high enthalpy drops of the turbine stages are necessary. There are different ways to obtain these high enthalpy drops in combination with small turbine diameters. High rotational speed of turbines, high mass flows of working fluid (which causes higher volume flows and increased turbine diameters), or a combination of the two is necessary. However, a high mass flow of working fluid causes high turbine power that has to be transferred by gear units, if the turbine has a higher speed than the generator. Another property of CO₂ is that it needs a higher pressure ratio of turbines than, for example, air, to reach the same exit temperature for a given turbine inlet temperature.

The aim of this work was to investigate three variants (Naki I, Naki II, and Naki III) of the Naki cycle in terms of their thermodynamic aspects, with taking into consideration the technical feasibility of the turbomachinery, especially the turbines. A rough economic evaluation of these cycles was also performed.

- **Naki I**

Naki I is the simplest cycle of this investigation and fired with pure carbon (coal dust). The working fluid is cooled in the recuperative heat exchanger after driving the turbine. It is then directly fed to the condenser without water separation. If there are some substances like water in the working fluid, the condensation process will not work in the pressure and temperature range of 45 bar and about 10 °C. Thus it is not possible to use hydrogen-containing fuels in the Naki I cycle.

A TIT of 850 °C is chosen because the cycle is designed with an uncooled turbine (no film cooling of the turbine blades). The working fluid is expanded from a TIP of about 190 bar to a pressure of about 46 bar in a three-stage turbine with a speed of 20 000 rpm. These parameters result in a net efficiency of 37.3 %.

The economic evaluation was performed for a 270 MW net power output plant. A conventional coal power plant with a net efficiency of 46 % was used as the

first reference plant. In comparison to this reference plant, mitigation costs of 6.5 €/tCO₂ avoided were calculated for a Naki I power plant with a net efficiency of 37.3 %. The second reference plant was a conventional combined cycle plant with a net efficiency of 59.2 %. Compared to this reference plant mitigation costs of 17.3 €/tCO₂ avoided were calculated because of the cheaper costs of anthracite compared to natural gas.

- **Naki II**

Naki II is designed to be fired with hydrogen-containing fuels like natural gas (methane) or syngas from coal gasification. To remove the combustion-generated water a three-stage intercooled compression with water separation is used. It is thus possible to condense the CO₂ at the same conditions as in Naki I (45 bar at about 10 °C). A TIT of 1 400 °C is envisaged so that all turbine stages with a working fluid temperature above 750 °C have film-cooled blades. The TIP is about 186 bar and the exit pressure of the last turbine is 4.4 bar.

To achieve a low number of cooled turbine stages, large dimensions are necessary; thus, the mass flow of working fluid was chosen to be about 400 kg/s. This mass flow leads to high power in the high-speed turbine which has to be transferred by gear units. Alternative concepts of turbomachinery arrangements with four different targets (variant 1a, 1b, 2, and 3) were investigated. Variant 1a and 1b are equal in the thermodynamic point and, fired with methane, they have a net efficiency of 51.2 %. Because of the complex turbomachinery arrangement of both variants, these concepts are not very promising. Variant 2 needs a high number of cooled turbine stages (in sum, 9 cooled turbine stages) because of the low speed (3 000 rpm) of the power turbine. The only advantage is that it needs no power gear unit to drive the generator. However, the efficiency penalty due to the high number of stages leads to a net efficiency of 46.8 %. This value is about 4.4 % points lower than for variant 1. Another disadvantage is the high manufacturing effort needed for the high number of cooled turbine stages with film-cooled blades. The cooling of the rotor is also more complex in comparison to turbines with a lower number of cooled stages. These unsatisfactory results lead to variant 3. The HPT of this variant has one stage with film-cooled blades and a speed of 16 167 rpm. The first stage of the LPT has also film-cooled blades; the second stage uses blade root cooling. The LPT has a speed of 3 000 rpm and is directly coupled to the generator. With the same parameters (TIT, TIP...) variant 3 reaches a net cycle efficiency of about 51.3 %.

Syngas from coal gasification was also investigated as fuel in the Naki II cycle. The calculation was performed for variant 1. The lower net efficiency of 49.8 % for syngas as fuel in comparison to 51.2 % for methane is caused by the different assumptions regarding fuel supply. It is assumed that methane is delivered at a pressure of 50 bar and syngas at a pressure of 1 bar. It is the additional power demand in fuel compression for syngas that mainly leads to this difference in net efficiency. In the calculation of net efficiency, the process of coal gasification is not considered.

The economic evaluation was performed for variant 3 and methane as fuel (51.3 % net efficiency). It was compared with a conventional combined cycle plant with a net efficiency of 59.2 % as reference plant. For a plant size of 270 MW net power output, the calculated mitigation costs are 33.1 €/tCO₂ avoided.

- **Naki III**

Naki III is a modification of Naki II and can also be fired with hydrogen-containing fuels. The main difference is a conventional bottoming steam cycle. This double pressure reheat steam cycle replaces the recuperative heat exchanger. With a TIT of 1 400 °C, a TIP of 186 bar, and an exit pressure of the last turbine of 4 bar (the condensation conditions are 45 bar at a temperature of about 10 °C) Naki III reaches a net cycle efficiency of 50.5 %. The fuel used was methane.

Naki III is also compared with a conventional combined cycle plant with a net efficiency of 59.2 % in a rough economic evaluation. A plant size of 270 MW net power output leads to 42.6 €/tCO₂ avoided. This value is higher than the value of Naki II because of the additional costs of the bottoming steam cycle and the lower net efficiency.

In summary Naki II seems to be the most promising cycle of this investigation because it promises the highest net efficiency. In comparison to Naki I it can be fired with hydrogen-containing fuels. Naki II in combination with a coal-to-gas-plant is able to use the same fuel as Naki I. Naki I needs pure carbon as fuel and thus requires a fuel treatment that removes hydrogen and water. Naki III with its additional steam cycle is more complex than Naki II and needs the same additional development work of the CO₂ turbine and power gear unit as Naki II. The lower net efficiency and the higher investment costs, which result in higher CO₂ mitigation costs, are other disadvantages of this variant.

Regarding Naki II, variant 3 is preferred because of the simplified turbomachinery arrangement in comparison to variant 1a and 1b. In comparison to variant 2 it has a higher net efficiency and a lower manufacturing effort, given that the number of cooled turbine stages with film-cooled blades is lower.

A further variant of the Naki II cycle with the turbomachinery arrangement variant 3 could include a steam cycle or an ORC (Organic Rankine Cycle) that uses the heat from the intercooled compression of the working fluid to increase the net efficiency. The three-stage compression of the working fluid could thus be replaced by a two-stage compression to reach higher compressor outlet temperatures.

Furthermore, a coal-to-gas-plant could be included in the simulation; hence heat transfer between the gasification process and the power cycle could be considered. Such a cycle with CO₂ capture could be compared with an IGCC plant (integrated gasification combined cycle).

Appendix A: Tables corresponding to diagrams of Chapter 4

Naki I: For Chapter 4.1.5

Table 28: Influence of TIT and pressure after feeding pump on net efficiency for Naki I

Net efficiency [%]					
	160 bar	180 bar	200 bar	220 bar	240 bar
700 °C	30.4	32.0	33.2	34.2	35.0
720 °C	31.0	32.6	33.8	34.8	35.6
740 °C	31.6	33.2	34.4	35.4	36.2
760 °C	32.1	33.7	35.0	36.0	36.8
780 °C	32.6	34.3	35.5	36.5	37.3
800 °C	33.1	34.8	36.1	37.1	37.9
820 °C	33.7	35.3	36.6	37.6	38.4
840 °C	34.2	35.8	37.1	38.1	38.9
860 °C	34.6	36.3	37.6	38.6	39.5
880 °C	35.1	36.8	38.1	39.1	40.0
900 °C	35.6	37.3	38.6	39.6	40.4

Table 29: Influence of cooling water temperature on net efficiency for Naki I

Cooling water temperature	Condenser pressure	Net efficiency
°C	bar	%
5	45	37.3
10	51	36.4
15	57	35.5
20	64	34.5
25	72	33.7

Naki II: For Chapter 4.2.7

Table 30: Influence of TIT and pressure after feeding pump on net efficiency for Naki II

	Net efficiency [%]				
	160 bar	180 bar	200 bar	220 bar	240 bar
1 100 °C	46.2	46.0	46.0	45.9	45.9
1 150 °C	47.3	47.1	47.0	47.0	47.0
1 200 °C	48.2	48.0	48.0	47.9	47.9
1 250 °C	49.1	48.9	48.9	48.8	48.8
1 300 °C	50.0	49.7	49.7	49.6	49.6
1 350 °C	50.6	50.5	50.4	50.4	50.4
1 400 °C	50.2	50.8	51.1	51.0	51.1
1 450 °C	49.9	50.5	51.0	51.4	51.7
1 500 °C	49.5	50.2	50.7	51.1	51.5

Table 31: Influence of expansion pressure on net efficiency for Naki II

Expansion pressure	Net efficiency
bar	%
2	49.6
3	50.5
4	51.1
5	51.1
6	50.8
7	50.5
8	50.1
9	49.8
10	49.5

Table 32: Influence of cooling water temperature on net efficiency for Naki II

Cooling water temperature	Condenser pressure	Net efficiency
°C	bar	%
5	45	51.1
10	51	50.1
15	57	49.0
20	64	47.9
25	72	46.7

Appendix B: Influence of thermodynamic parameters for Naki I

Basic values

Table 33: Basic values for the variation of parameters for Naki I

TIT	TIP	Feeding pump pressure	Condenser pressure	Mass flow	Cooling water temperature
°C	bar	bar	bar	kg/s	°C
850	189	200	45	280	5

Influence of cooling water temperature

Table 34: Influence of cooling water temperature on efficiency for Naki I

Cooling water temperature	Thermal cycle efficiency	Net electrical efficiency	Efficiency considering O ₂ supply	Net efficiency
°C	%	%	%	%
5	50.7	48.1	37.4	37.3
10	49.8	47.2	36.5	36.4
15	48.8	46.3	35.5	35.5
20	47.9	45.4	34.6	34.5
25	47.0	44.6	33.7	33.7

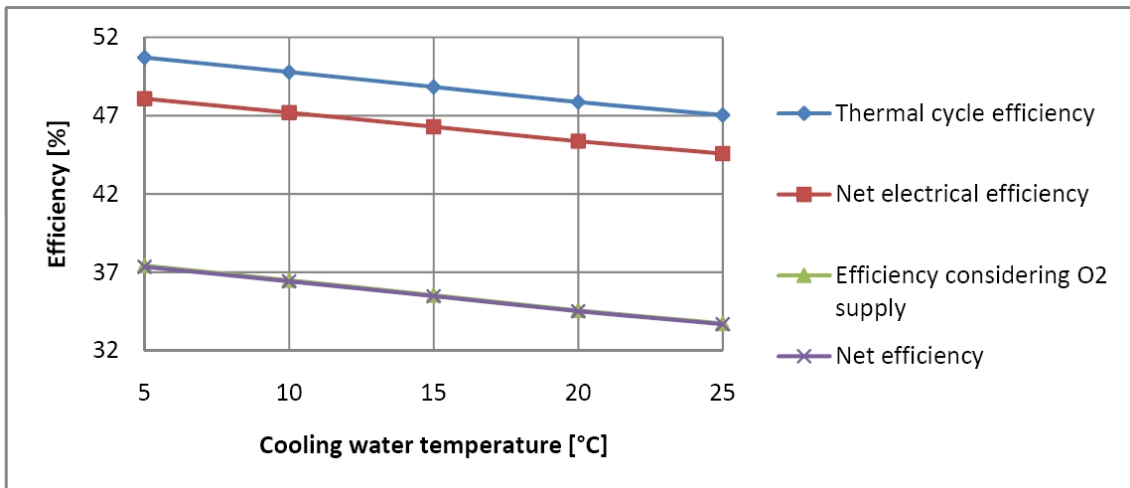


Figure 55: Influence of cooling water temperature on efficiency for Naki I

Table 35: Influence of cooling water temperature on thermal power (Naki I)

Cooling water temperature	Condenser pressure	Heat input	HTEX	Condenser
°C	bar	MW _{th}	MW _{th}	MW _{th}
5	45	135.1	204.8	71.4
10	51	125.5	209.4	67.4
15	57	115.8	213.7	63.2
20	64	105.7	217.4	58.5
25	72	94.2	219.1	52.7

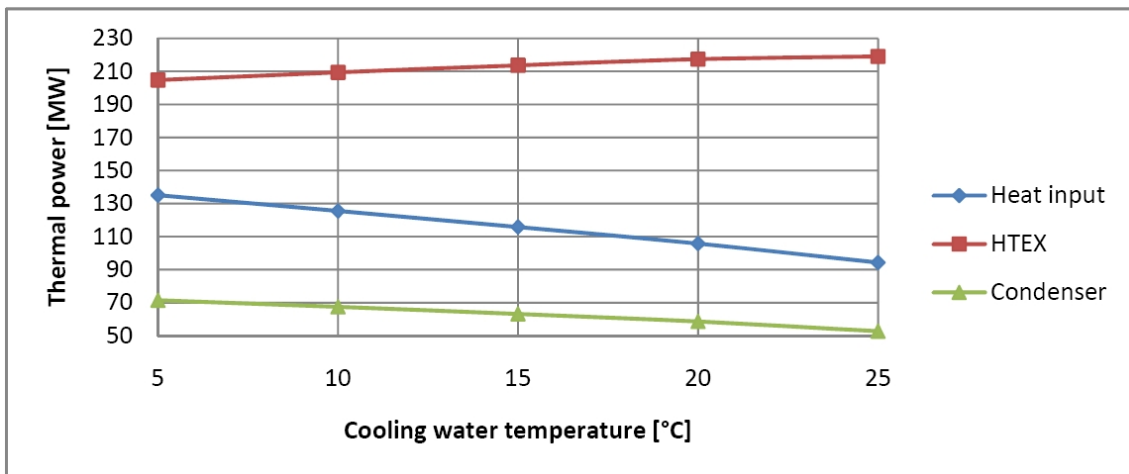


Figure 56: Influence of cooling water temperature on thermal power (Naki I)

Table 36: Influence of cooling water temperature on power (Naki I)

Cooling water temperature °C	Turbine MW	Feeding pump MW	O ₂ generation MW	O ₂ compression MW	CO ₂ compression (to 100 bar) MW	Net power output MW
5	74.22	5.73	9.53	4.87	0.11	50.44
10	68.22	5.74	8.85	4.58	0.09	45.71
15	62.31	5.76	8.17	4.28	0.08	41.08
20	56.46	5.85	7.46	3.96	0.07	36.49
25	50.59	6.26	6.65	3.57	0.05	31.74

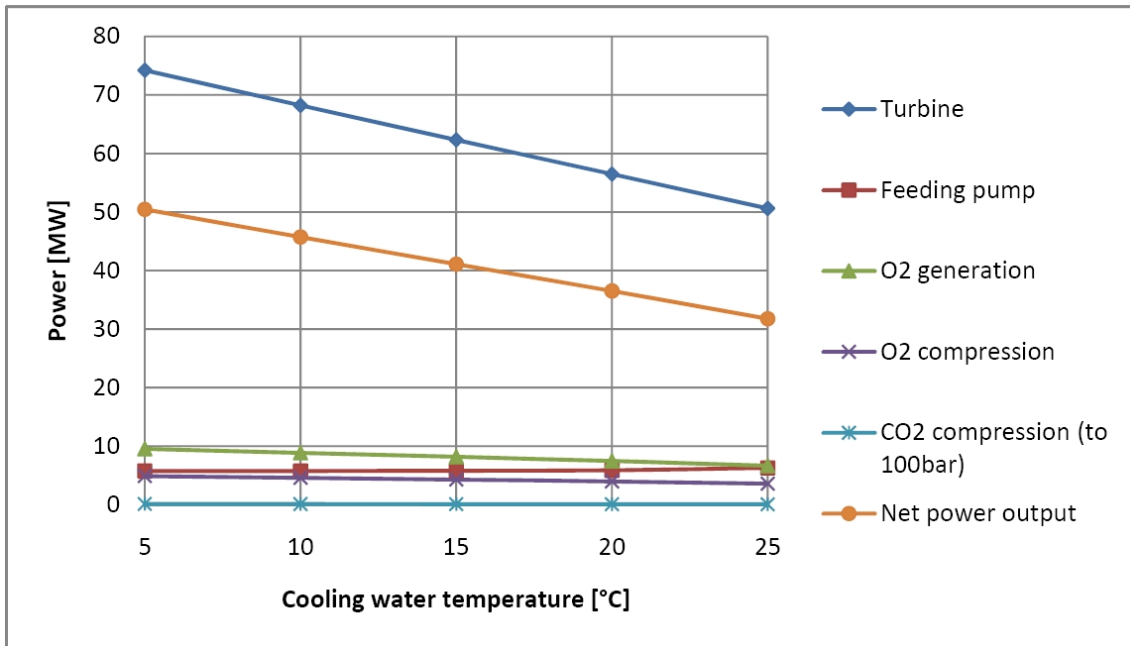


Figure 57: Influence of cooling water temperature on power (Naki I)

Influence of TIT

Table 37: Influence of TIT on efficiency (Naki I)

TIT	Thermal cycle efficiency	Net electrical efficiency	Efficiency considering O ₂ supply	Net efficiency
°C	%	%	%	%
700	46.4	44.0	33.3	33.2
720	47.0	44.6	33.9	33.8
740	47.6	45.1	34.5	34.4
760	48.2	45.7	35.1	35.0
780	48.8	46.3	35.6	35.5
800	49.4	46.8	36.1	36.1
820	49.9	47.3	36.7	36.6
840	50.4	47.8	37.2	37.1
860	51.0	48.3	37.7	37.6
880	51.5	48.8	38.2	38.1
900	52.0	49.3	38.6	38.6

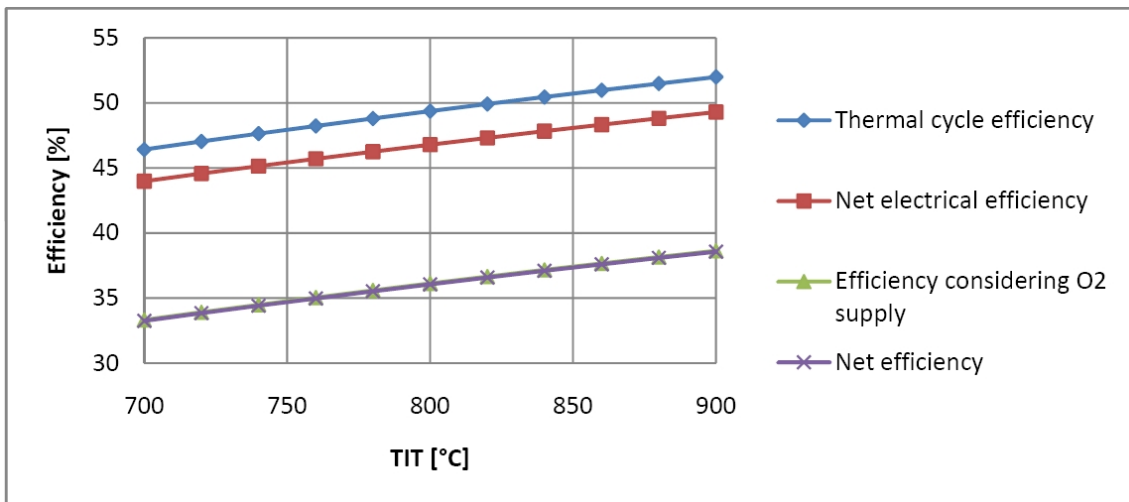


Figure 58: Influence of TIT on efficiency (Naki I)

Table 38: Influence of TIT on thermal power (Naki I)

TIT	Heat input	HTEX	Condenser
°C	MW _{th}	MW _{th}	MW _{th}
700	124.5	158.2	71.1
720	125.9	164.3	71.2
740	127.3	170.5	71.2
760	128.7	176.6	71.3
780	130.1	182.9	71.3
800	131.5	189.1	71.3
820	133.0	195.4	71.4
840	134.4	201.7	71.4
860	135.8	208.0	71.4
880	137.2	214.4	71.5
900	138.6	220.8	71.5

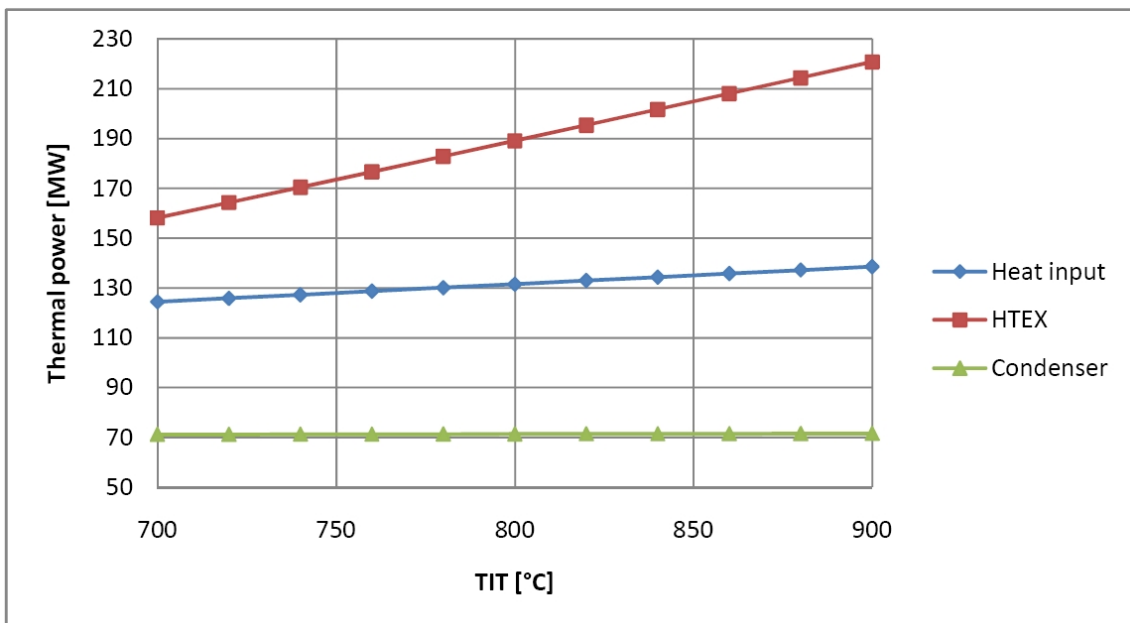


Figure 59: Influence of TIT on thermal power (Naki I)

Table 39: Influence of TIT on power (Naki I)

TIT	Turbine	Feeding pump	O ₂ generation	O ₂ compression	CO ₂ compression (to 100 bar)	Net power output
°C	MW	MW	MW	MW	MW	MW
700	63.50	5.73	8.78	4.49	0.10	41.38
720	64.94	5.73	8.88	4.54	0.10	42.59
740	66.37	5.73	8.98	4.59	0.10	43.81
760	67.80	5.73	9.08	4.64	0.10	45.02
780	69.23	5.73	9.18	4.69	0.10	46.23
800	70.66	5.73	9.28	4.74	0.10	47.43
820	72.09	5.73	9.38	4.79	0.11	48.64
840	73.51	5.73	9.48	4.84	0.11	49.84
860	74.93	5.73	9.57	4.89	0.11	51.04
880	76.35	5.73	9.67	4.94	0.11	52.25
900	77.78	5.73	9.77	4.99	0.11	53.45

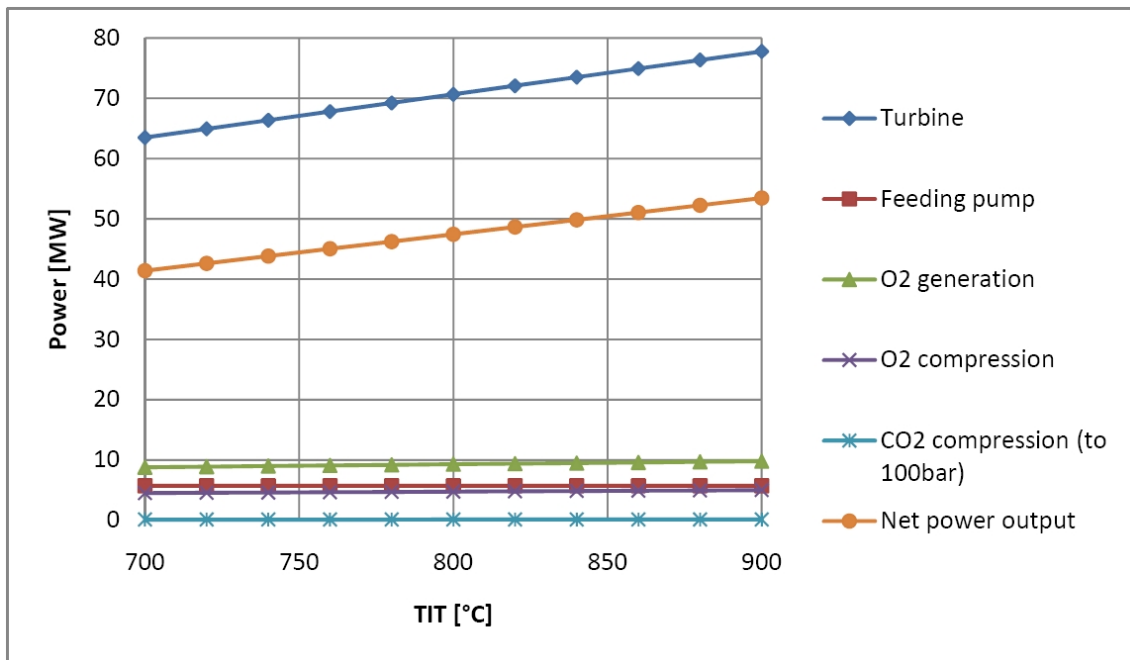


Figure 60: Influence of TIT on power (Naki I)

Influence of TIP

Table 40: Influence of TIP on efficiency (Naki I)

Feeding pump pressure	TIP	Thermal cycle efficiency	Net electrical efficiency	Efficiency considering O ₂ supply	Net efficiency
bar	bar	%	%	%	%
160	151	47.4	44.9	34.5	34.4
180	170	49.3	46.7	36.1	36.1
200	189	50.7	48.1	37.4	37.3
220	208	51.9	49.2	38.5	38.4
240	227	52.8	50.1	39.3	39.2

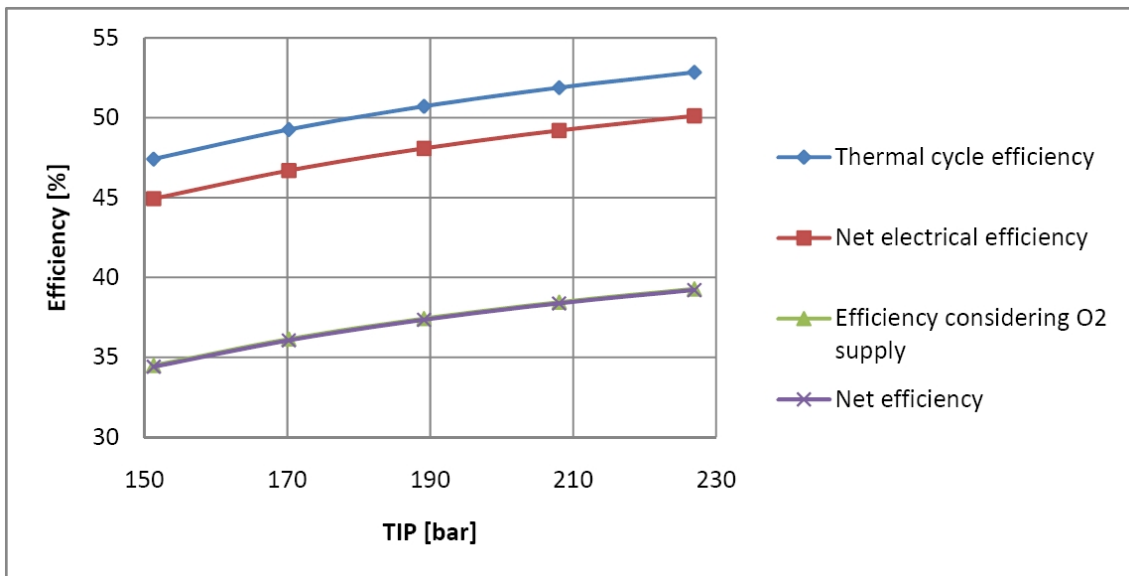


Figure 61: Influence of TIP on efficiency (Naki I)

Table 41: Influence of TIP on thermal power (Naki I)

Feeding pump pressure	TIP	Heat input	HTEX	Condenser
bar	bar	MW _{th}	MW _{th}	MW _{th}
160	151	124.0	216.5	69.6
180	170	129.9	210.4	70.5
200	189	135.1	204.8	71.4
220	208	139.7	199.8	72.3
240	227	143.8	195.3	73.1

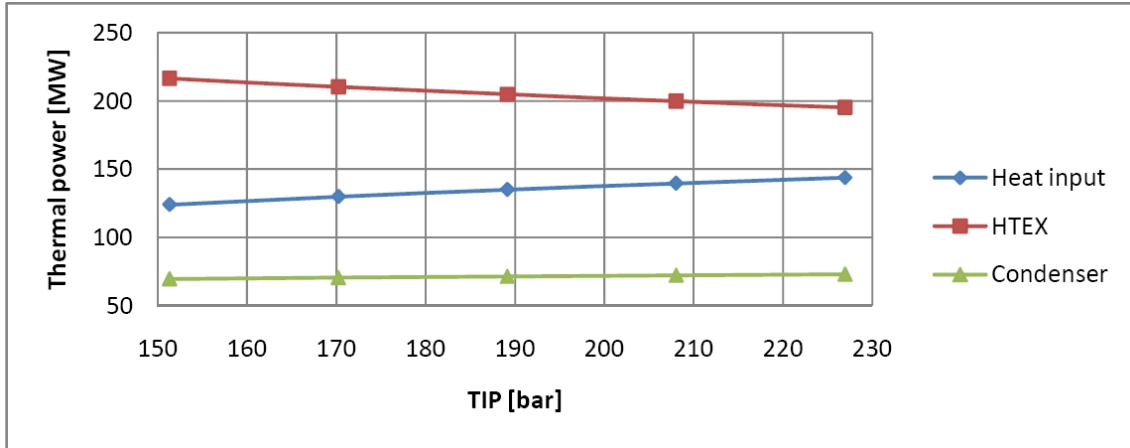


Figure 62: Influence of TIP on thermal power (Naki I)

Table 42: Influence of TIP on power (Naki I)

Feeding pump pressure	TIP	Turbine	Feeding pump	O ₂ generation	O ₂ compression	CO ₂ compression (to 100 bar)	Net power output
bar	bar	MW	MW	MW	MW	MW	MW
160	151	63.09	4.28	8.75	4.21	0.10	42.67
180	170	68.99	5.01	9.16	4.55	0.10	46.84
200	189	74.22	5.73	9.53	4.87	0.11	50.44
220	208	78.91	6.44	9.85	5.16	0.11	53.60
240	227	83.16	7.15	10.14	5.43	0.11	56.40

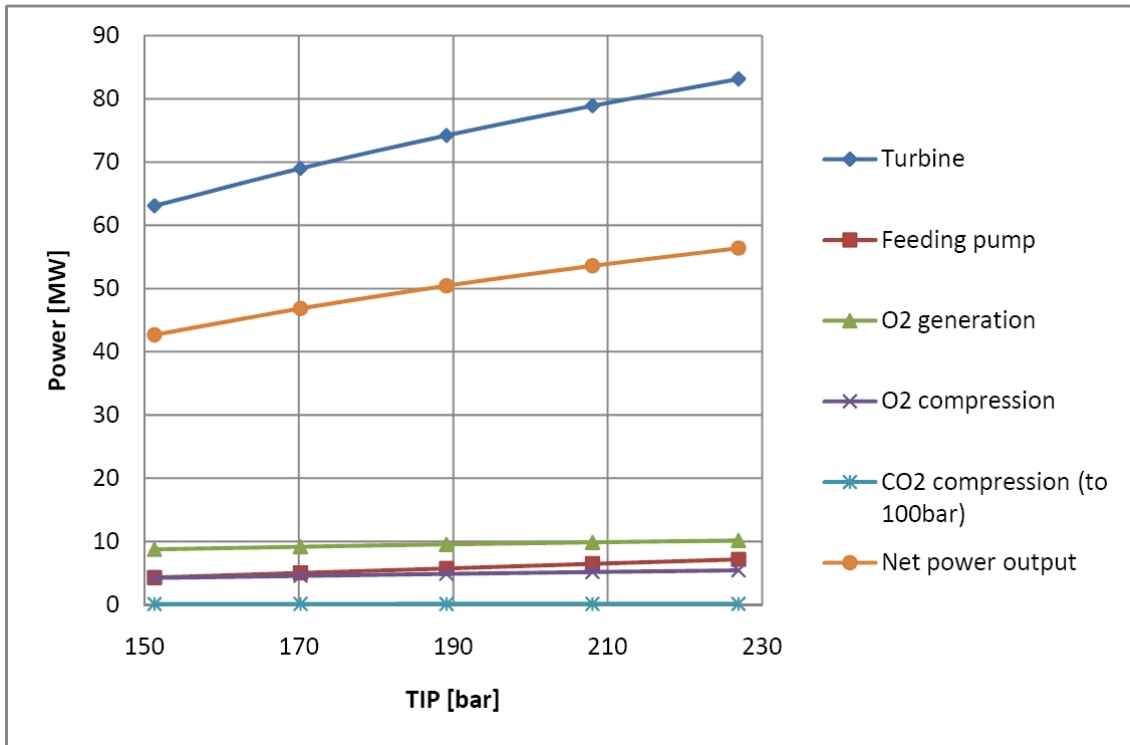


Figure 63: Influence of TIP on power (Naki I)

Appendix C: Influence of thermodynamic parameters for Naki II

Basic values

Table 43: Basic values for the variation of parameters for Naki II

TIT	1 400	°C
Pressure after feeding pump	200	bar
TIP	186	bar
LPT exit pressure	4	bar
Condenser pressure	45	bar
Main mass flow	400	kg/s
Cooling water temperature	5	°C

Influence of cooling water temperature

Table 44: Influence of cooling water temperature on efficiency for Naki II

Cooling water temperature °C	Thermal cycle efficiency %	Net electrical efficiency %	Efficiency considering O ₂ and fuel supply %	Net efficiency %
5	65.6	62.4	51.2	51.1
10	64.6	61.4	50.1	50.1
15	63.5	60.4	49.1	49.0
20	62.4	59.4	48.0	47.9
25	61.2	58.2	46.7	46.7

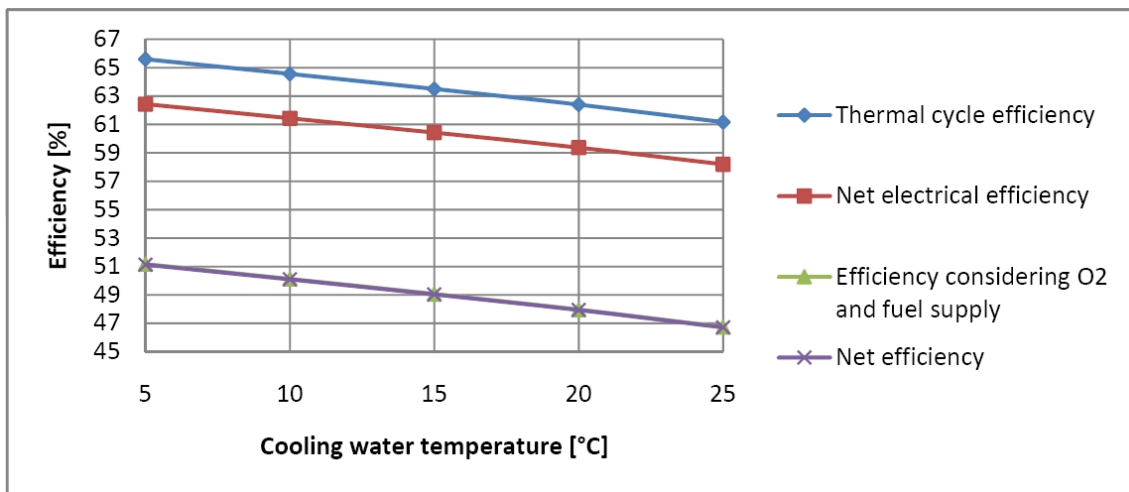


Figure 64: Influence of cooling water temperature on efficiency for Naki II

Table 45: Influence of cooling water temperature on thermal power (Naki II)

Cooling water temperature	Condenser pressure	Heat input	HTEX 2	HTEX 3	Working fluid cooler	Condenser
°C	bar	MW _{th}	MW _{th}	MW _{th}	MW _{th}	MW _{th}
5	45	528.9	226.9	174.5	146.6	104.2
10	50.87	528.3	219.9	174.7	160.4	94.9
15	57.29	527.7	212.1	174.9	175.6	84.3
20	64.34	527.0	202.9	175.1	193.1	71.5
25	72.14	526.4	188.0	175.3	217.2	52.4

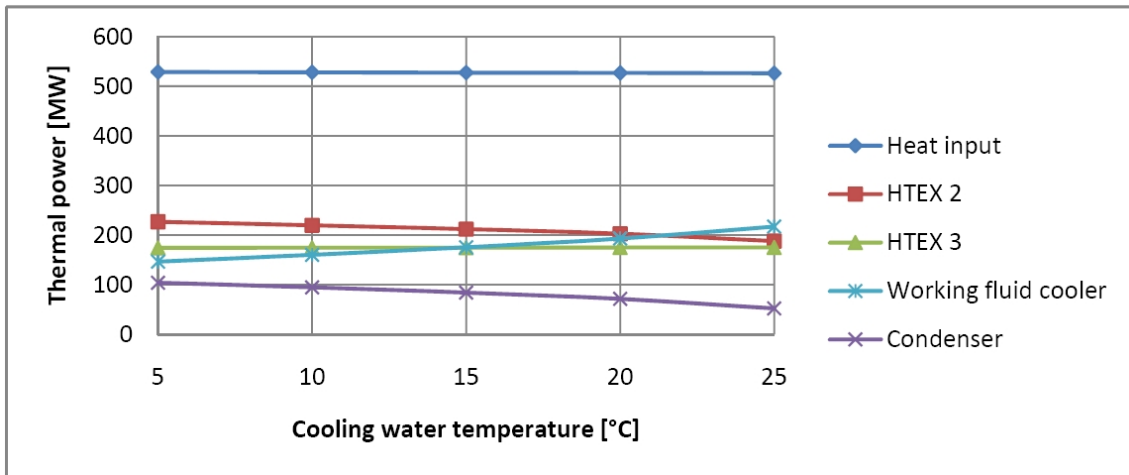


Figure 65: Influence of cooling water temperature on thermal power (Naki II)

Table 46: Influence of cooling water temperature on power, part 1 (Naki II)

Cooling water temperature	Condenser pressure	Turbine	Compressor (C1, C2, and C3)	Net power output
°C	bar	MW	MW	MW
5	45	436.37	79.78	270.40
10	51	436.12	85.41	264.61
15	57	435.88	91.11	258.72
20	64	435.62	96.91	252.64
25	72	435.37	102.86	245.90

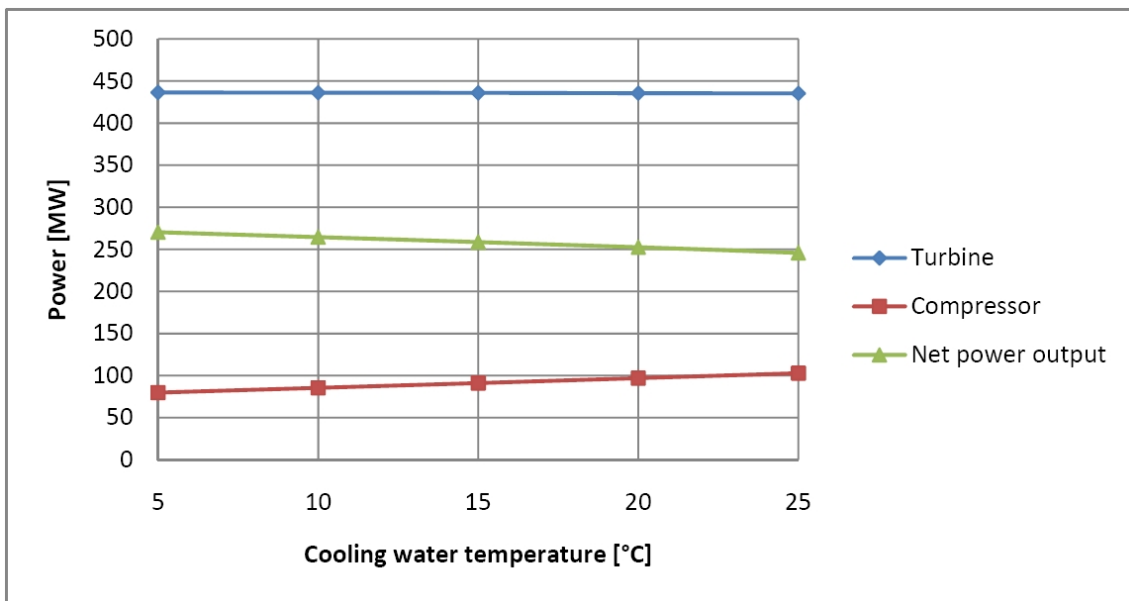


Figure 66: Influence of cooling water temperature on power, part 1 (Naki II)

Table 47: Influence of cooling water temperature on power, part 2 (Naki II)

Cooling water temperature	Feeding pump	O ₂ generation	O ₂ compression	Fuel compression	CO ₂ compression (to 100 bar)
°C	MW	MW	MW	MW	MW
5	9.63	37.87	19.28	2.43	0.21
10	9.63	37.83	19.51	2.43	0.20
15	9.67	37.78	19.73	2.43	0.18
20	9.81	37.74	19.96	2.43	0.17
25	10.47	37.69	20.18	2.42	0.15

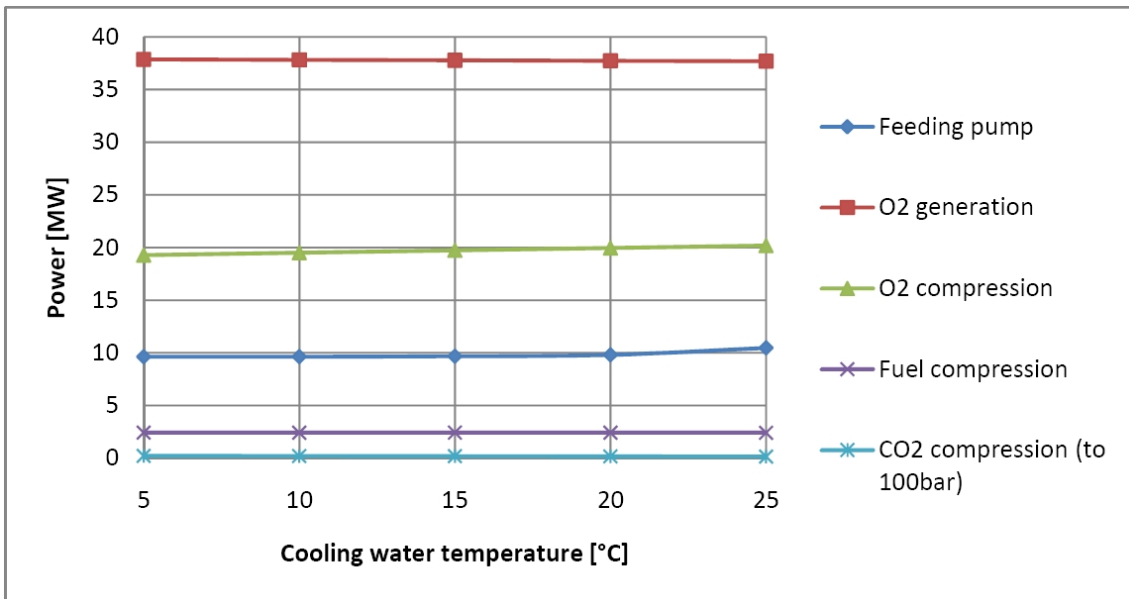


Figure 67: Influence of cooling water temperature on power, part 2 (Naki II)

Influence of TIT

Table 48: Influence of TIT on efficiency (Naki II)

TIT	Thermal cycle efficiency	Net electrical efficiency	Efficiency considering O ₂ and fuel supply	Net efficiency
°C	%	%	%	%
1 100	60.2	57.3	46.0	46.0
1 150	61.3	58.3	47.1	47.0
1 200	62.3	59.3	48.0	48.0
1 250	63.3	60.2	48.9	48.9
1 300	64.1	61.0	49.7	49.7
1 350	64.9	61.8	50.5	50.5
1 400	65.7	62.5	51.2	51.2
1 450	65.6	62.4	51.2	51.1
1 500	65.3	62.1	50.9	50.8

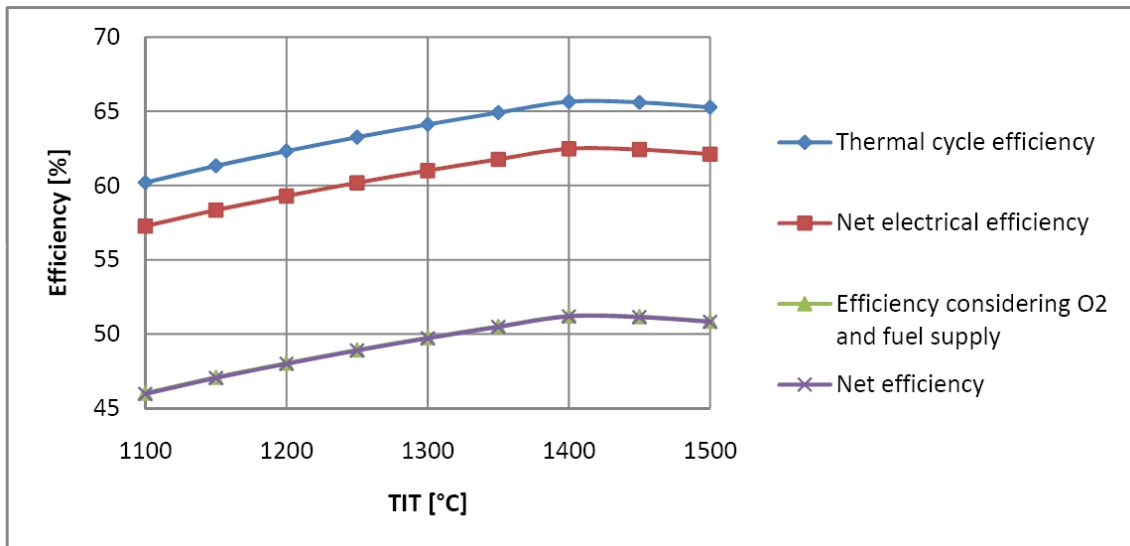


Figure 68: Influence of TIT on efficiency (Naki II)

Table 49: Influence of TIT on thermal power (Naki II)

TIT	Heat input	HTEX 2	HTEX 3	Working fluid cooler	Condenser
°C	MW _{th}	MW _{th}	MW _{th}	MW _{th}	MW _{th}
1 100	428.3	211.0	62.1	130.0	96.2
1 150	444.6	213.5	80.1	132.4	97.5
1 200	461.2	216.0	98.2	135.1	98.8
1 250	477.8	218.6	116.9	137.8	100.0
1 300	494.5	221.2	135.9	140.5	101.4
1 350	511.3	223.8	155.3	143.3	102.7
1 400	528.2	226.5	175.1	146.2	104.0
1 450	552.8	229.3	189.4	156.6	105.5
1 500	580.6	232.1	201.8	170.2	107.1

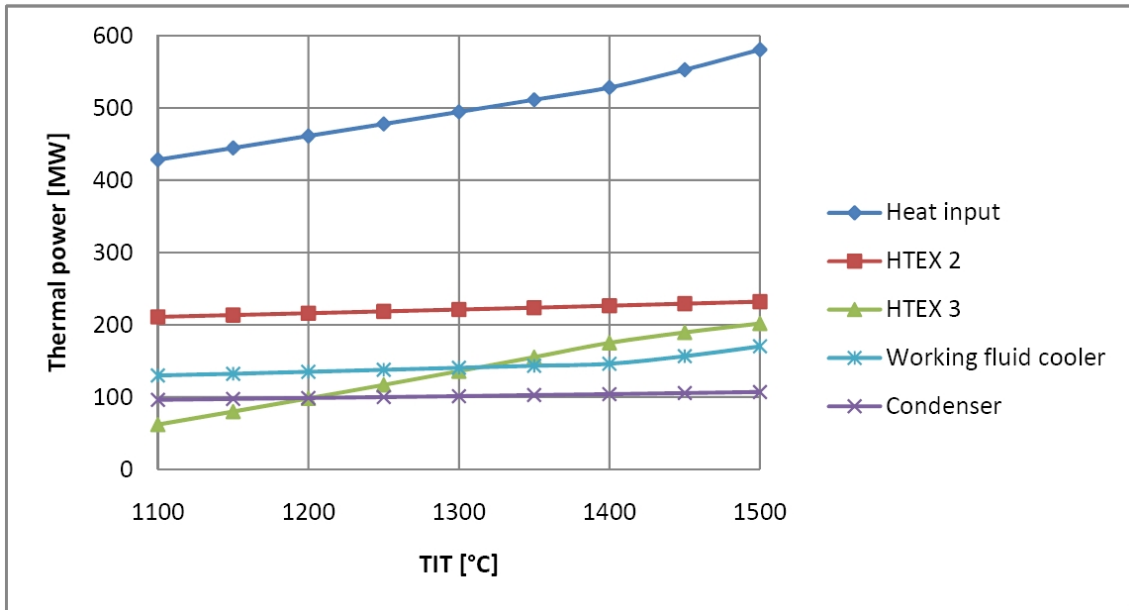


Figure 69: Influence of TIT on thermal power (Naki II)

Table 50: Influence of TIT on power, part 1 (Naki II)

TIT °C	Turbine MW	Compressor (C1, C2, and C3) MW	Net power output MW
1 100	340.5	73.6	196.9
1 150	356.3	74.6	209.1
1 200	372.2	75.6	221.3
1 250	388.1	76.6	233.6
1 300	404.0	77.6	245.8
1 350	420.0	78.6	258.0
1 400	436.0	79.6	270.3
1 450	453.1	80.8	282.6
1 500	470.8	82.0	295.0

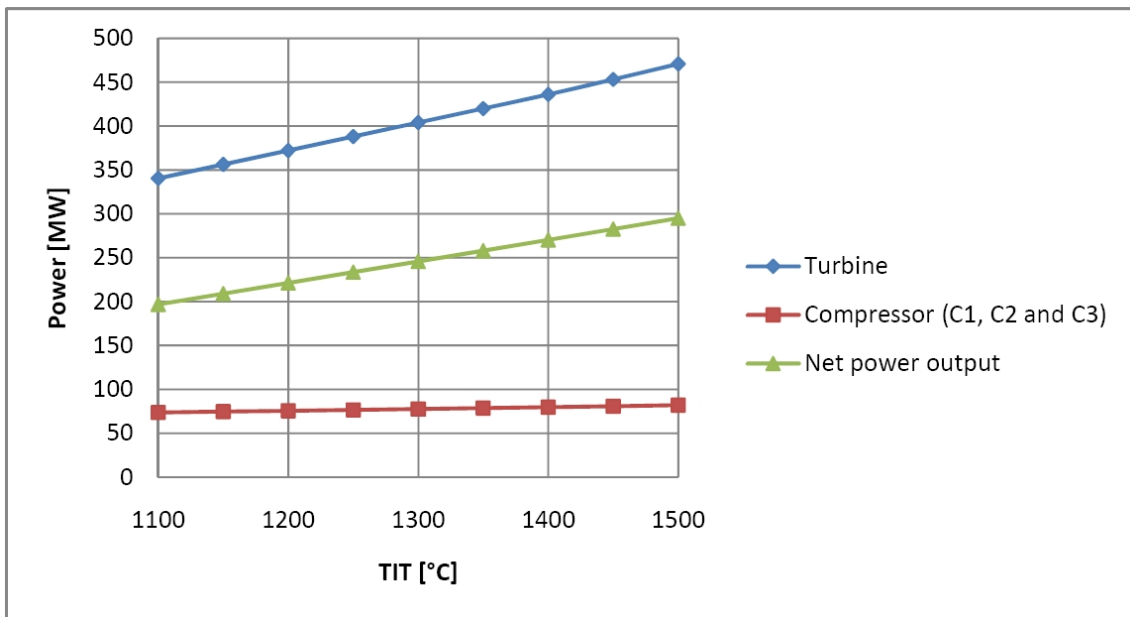


Figure 70: Influence of TIT on power, part 1 (Naki II)

Table 51: Influence of TIT on power, part 2 (Naki II)

TIT	Feeding pump	O ₂ generation	O ₂ compression	Fuel compression	CO ₂ compression (to 100 bar)
°C	MW	MW	MW	MW	MW
1 100	8.95	30.67	15.61	1.97	0.17
1 150	9.06	31.83	16.21	2.05	0.18
1 200	9.16	33.02	16.81	2.12	0.19
1 250	9.27	34.21	17.42	2.20	0.19
1 300	9.38	35.41	18.03	2.28	0.20
1 350	9.50	36.61	18.64	2.35	0.21
1 400	9.61	37.82	19.25	2.43	0.21
1 450	9.73	39.58	20.15	2.54	0.22
1 500	9.85	41.57	21.17	2.67	0.24

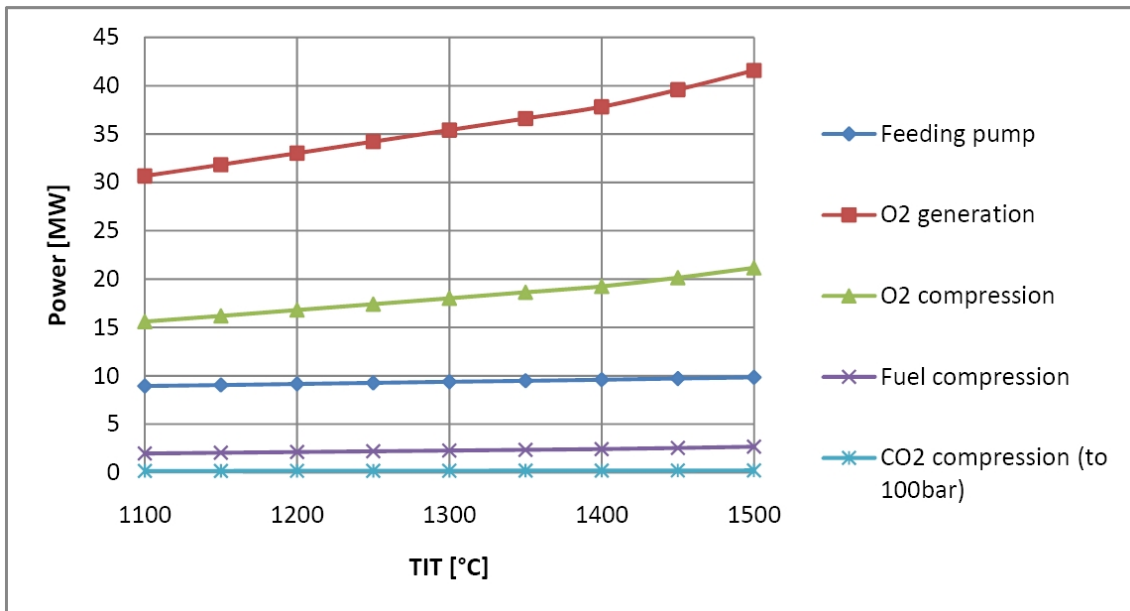


Figure 71: Influence of TIT on power, part 2 (Naki II)

Influence of TIP

Table 52: Influence of TIP on efficiency (Naki II)

Feeding pump pressure bar	TIP bar	Thermal cycle efficiency %	Net electrical efficiency %	Efficiency considering O ₂ and fuel supply %	Net efficiency %
160	149	64.4	61.3	50.3	50.3
180	168	65.2	62.0	50.9	50.9
200	186	65.7	62.5	51.2	51.2
220	205	65.7	62.5	51.1	51.1
240	224	65.8	62.6	51.1	51.1

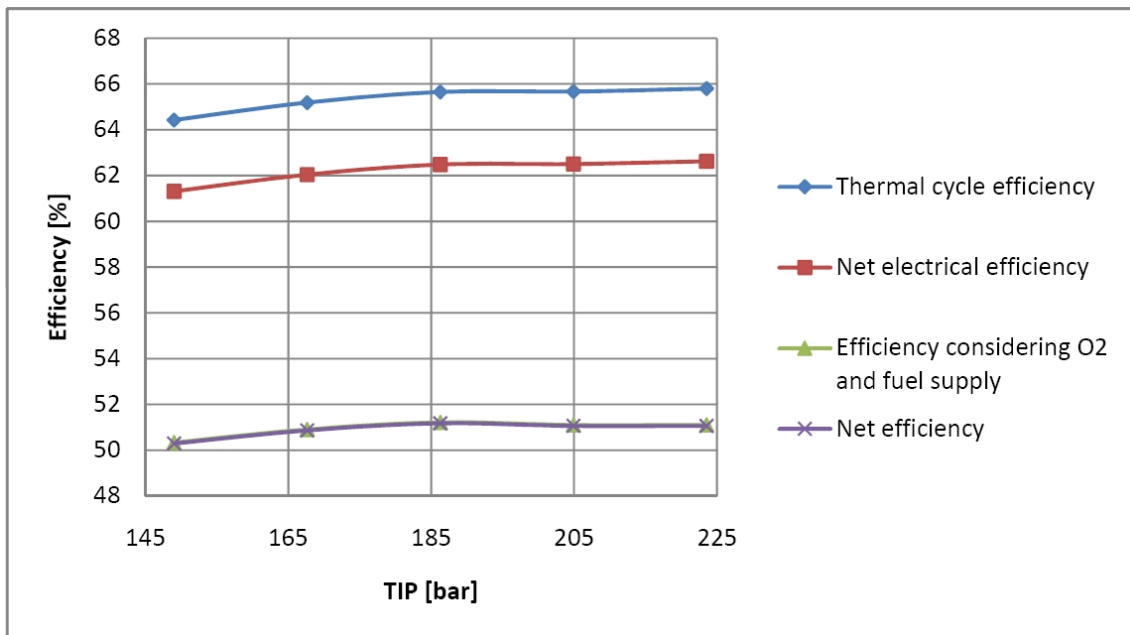


Figure 72: Influence of TIP on efficiency (Naki II)

Table 53: Influence of TIP on thermal power (Naki II)

Feeding pump pressure	TIP	Heat input	HTEX 2	HTEX 3	Working fluid cooler	Condenser
bar	bar	MW _{th}	MW _{th}	MW _{th}	MW _{th}	MW _{th}
160	149	504.9	232.9	189.7	141.2	103.9
180	168	516.4	229.6	182.5	142.9	104.0
200	186	528.2	226.5	175.1	146.2	104.0
220	205	542.4	223.4	165.7	152.8	104.2
240	224	554.0	220.4	158.3	157.7	104.2

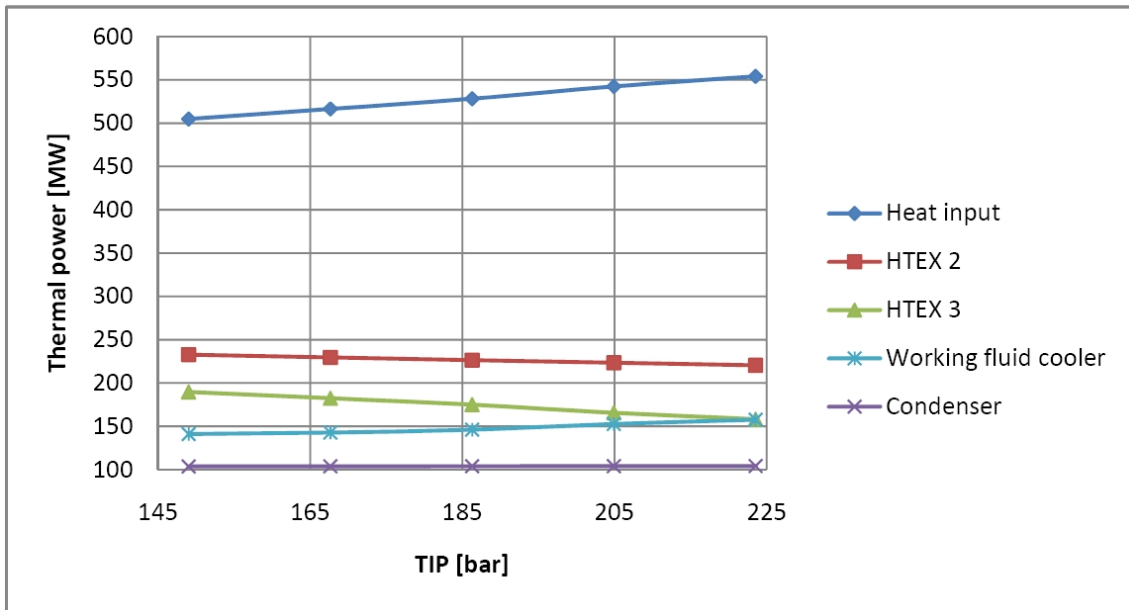


Figure 73: Influence of TIP on thermal power (Naki II)

Table 54: Influence of TIP on power, part 1 (Naki II)

Feeding pump pressure °C	TIP °C	Turbine MW	Compressor (C1, C2, and C3) MW	Net power output MW
160	149	412.0	79.5	253.9
180	168	424.6	79.6	262.7
200	186	436.0	79.6	270.3
220	205	446.8	79.7	277.0
240	224	456.3	79.8	282.9

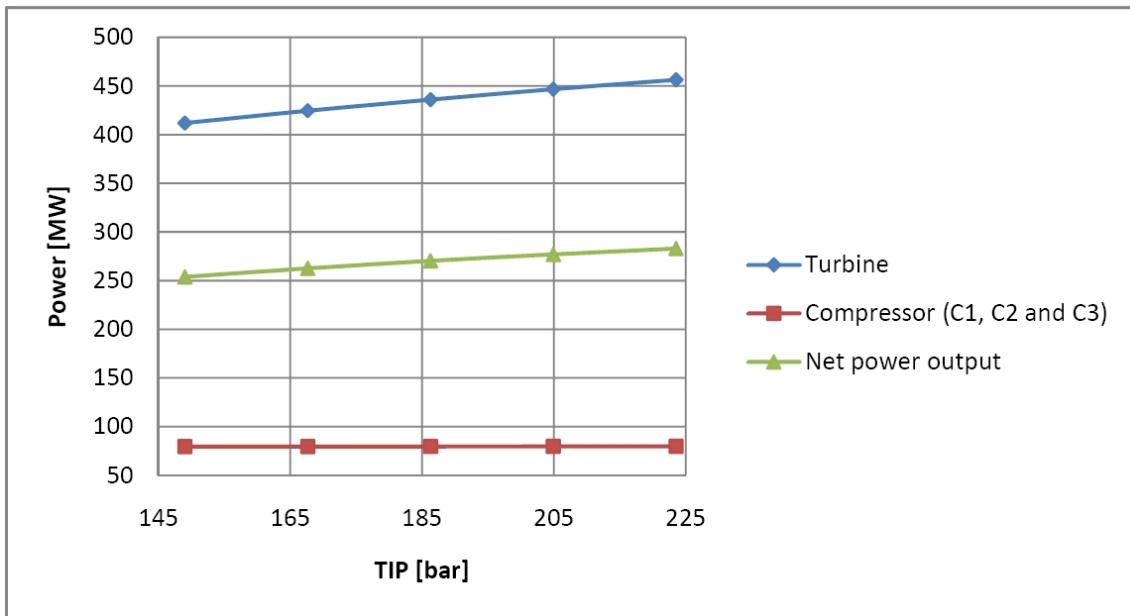


Figure 74: Influence of TIP on power, part 1 (Naki II)

Table 55: Influence of TIP on power, part 2 (Naki II)

Feeding pump pressure	TIP	Feeding pump	O ₂ generation	O ₂ compression	Fuel compression	CO ₂ compression (to 100 bar)
bar	bar	MW	MW	MW	MW	MW
160	149	7.19	36.15	17.36	1.90	0.20
180	168	8.40	36.97	18.33	2.19	0.21
200	186	9.61	37.82	19.25	2.43	0.21
220	205	10.81	38.84	20.30	2.69	0.22
240	224	12.00	39.67	21.19	2.94	0.22

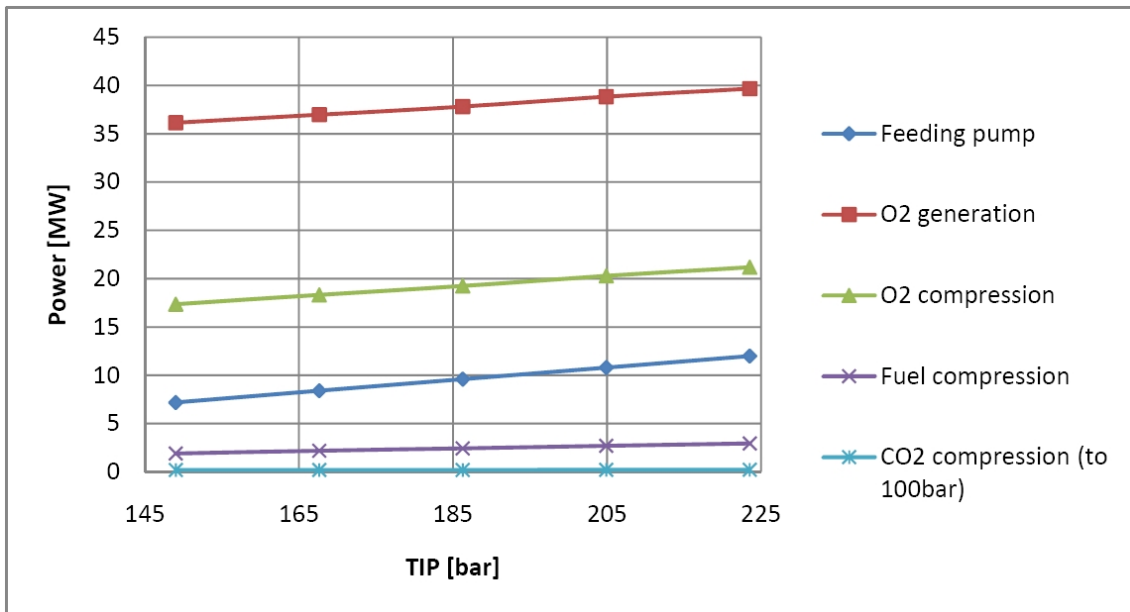


Figure 75: Influence of TIP on power, part 2 (Naki II)

Influence of LPT exit pressure

Table 56: Influence of the LPT exit pressure on efficiency (Naki II)

LPT exit pressure	Thermal cycle efficiency	Net electrical efficiency	Efficiency considering O ₂ and fuel supply	Net efficiency
bar	%	%	%	%
2	64.0	60.9	49.6	49.6
3	64.9	61.8	50.5	50.5
4	65.6	62.4	51.2	51.1
5	65.5	62.4	51.1	51.1
6	65.2	62.1	50.8	50.8
7	64.9	61.8	50.5	50.5
8	64.6	61.5	50.2	50.2
9	64.3	61.2	49.9	49.9
10	64.0	60.9	49.6	49.6

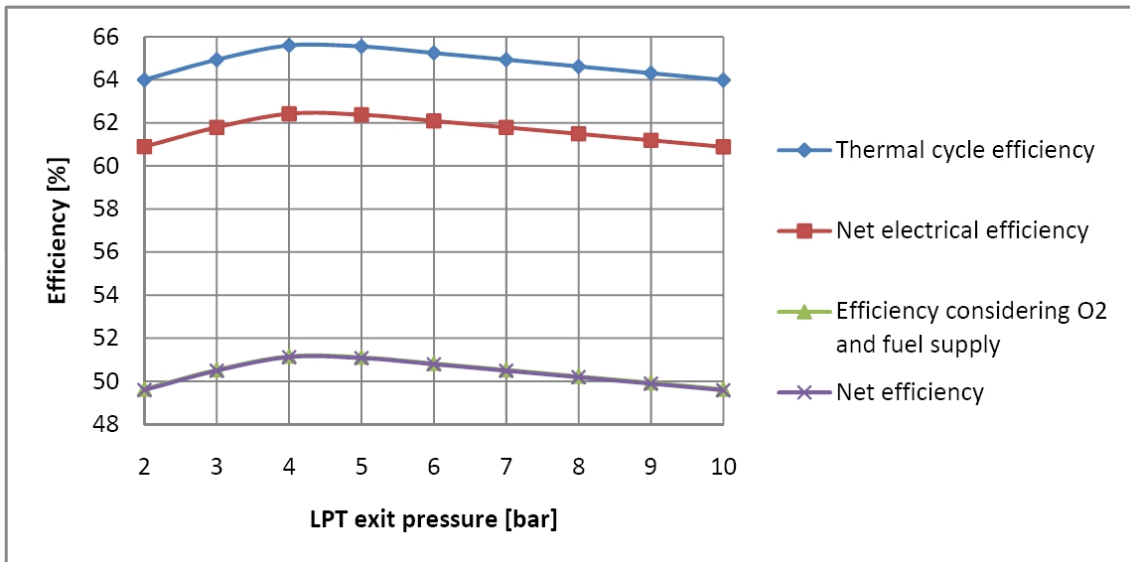


Figure 76: Influence of the LPT exit pressure on efficiency (Naki II)

Table 57: Influence of the LPT exit pressure on thermal power (Naki II)

LPT exit pressure	Heat input	HTEX 2	HTEX 3	Working fluid cooler	Condenser
bar	MW _{th}	MW _{th}	MW _{th}	MW _{th}	MW _{th}
2	609.8	226.4	111.8	194.1	104.9
3	563.3	226.7	147.9	166.3	104.5
4	529.0	226.9	174.4	146.7	104.2
5	506.8	227.1	191.6	136.6	104.1
6	490.1	227.2	204.5	130.2	103.9
7	475.8	227.4	215.7	125.0	103.8
8	463.0	227.5	225.6	120.4	103.7
9	451.5	227.6	234.4	116.3	103.6
10	441.1	227.6	242.5	112.7	103.5

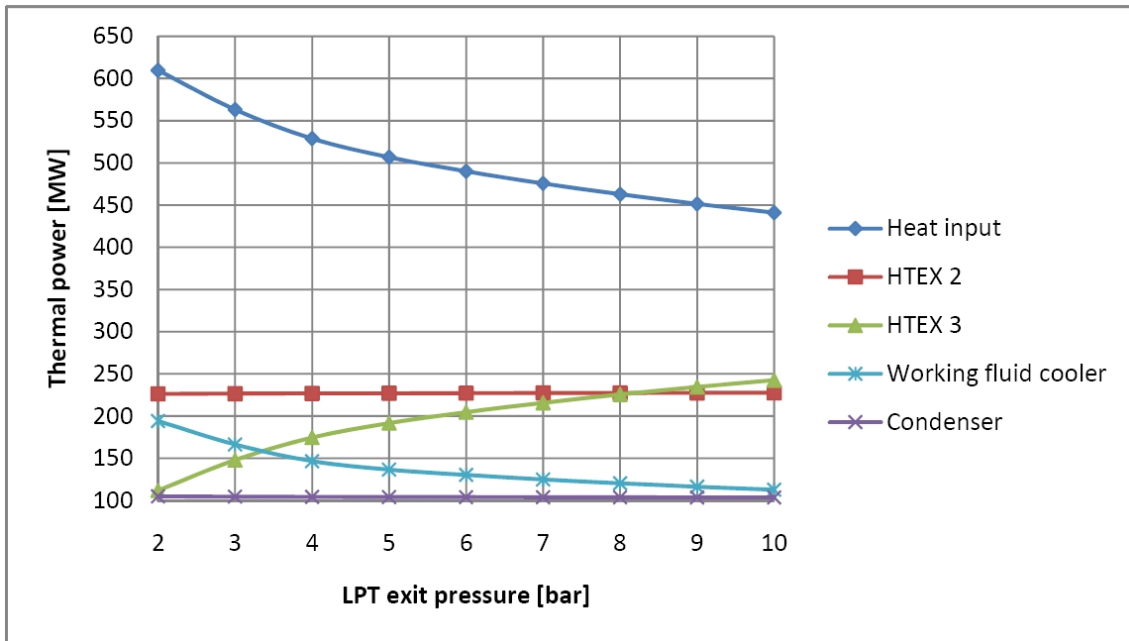


Figure 77: Influence of the LPT exit pressure on thermal power (Naki II)

Table 58: Influence of the LPT exit pressure on power, part 1 (Naki II)

LPT exit pressure bar	Turbine MW	Compressor (C1, C2, and C3) MW	Net power output MW
2	507.4	107.6	302.4
3	466.5	91.1	284.4
4	436.4	79.8	270.4
5	413.1	71.3	258.9
6	394.0	64.5	248.9
7	377.5	58.9	240.2
8	362.9	54.1	232.4
9	350.0	49.9	225.2
10	338.2	46.3	218.7

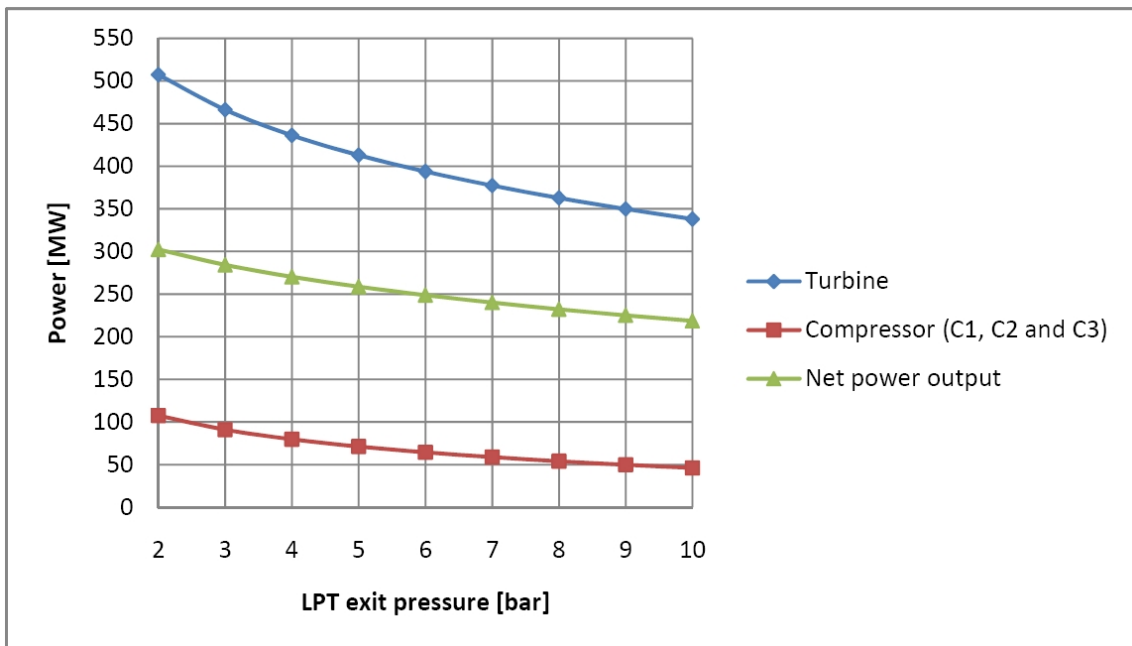


Figure 78: Influence of the LPT exit pressure on power, part 1 (Naki II)

Table 59: Influence of the LPT exit pressure on power, part 2 (Naki II)

LPT exit pressure	Feeding pump	O ₂ generation	O ₂ compression	Fuel compression	CO ₂ compression (to 100 bar)
bar	MW	MW	MW	MW	MW
2	9.61	43.66	22.23	2.81	0.25
3	9.62	40.33	20.53	2.59	0.23
4	9.63	37.87	19.28	2.43	0.21
5	9.63	36.29	18.48	2.33	0.21
6	9.64	35.09	17.87	2.26	0.20
7	9.65	34.07	17.34	2.19	0.19
8	9.65	33.15	16.88	2.13	0.19
9	9.65	32.33	16.46	2.08	0.18
10	9.66	31.58	16.08	2.03	0.18

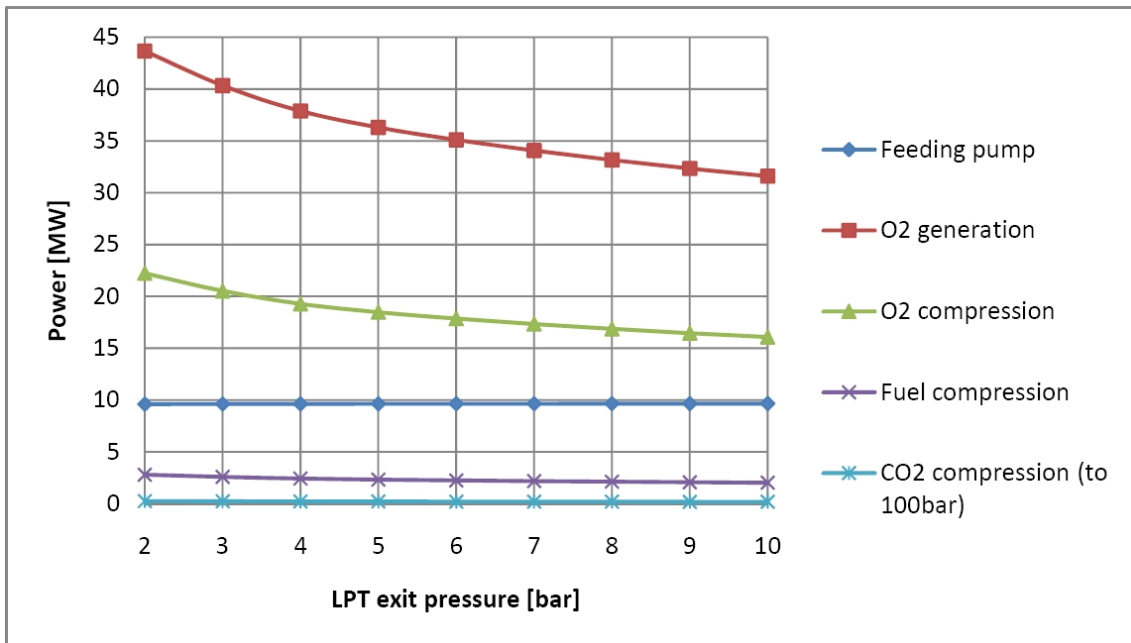


Figure 79: Influence of the LPT exit pressure on power, part 2 (Naki II)

Appendix D: Cost Sensitivity Analysis

Cost sensitivity analysis for Naki I

Table 60: Influence of fuel costs on mitigation costs for Naki I

$C_{C(\text{ref})}$ €/kW _{el}	$C_{C(\text{Naki I})}$ €/kW _{el}	a %/yr	η_{ref} %	$\eta_{\text{Naki I}}$ %	C_{fuel} €/GJ	COE_{ref} ct/kWh _{el}	$\text{COE}_{\text{Naki I}}$ ct/kWh _{el}	MC €/t CO ₂
1 250	1 251	12	46	37.3	1	2.67	2.86	2.2
1 250	1 251	12	46	37.3	2	3.45	3.82	4.3
1 250	1 251	12	46	37.3	3	4.24	4.79	6.5
1 250	1 251	12	46	37.3	4	5.02	5.75	8.7
1 250	1 251	12	46	37.3	5	5.80	6.72	10.8
1 250	1 251	12	46	37.3	6	6.58	7.68	13.0
1 250	1 251	12	46	37.3	7	7.37	8.65	15.1
1 250	1 251	12	46	37.3	8	8.15	9.61	17.3
1 250	1 251	12	46	37.3	9	8.93	10.58	19.5
1 250	1 251	12	46	37.3	10	9.71	11.54	21.6

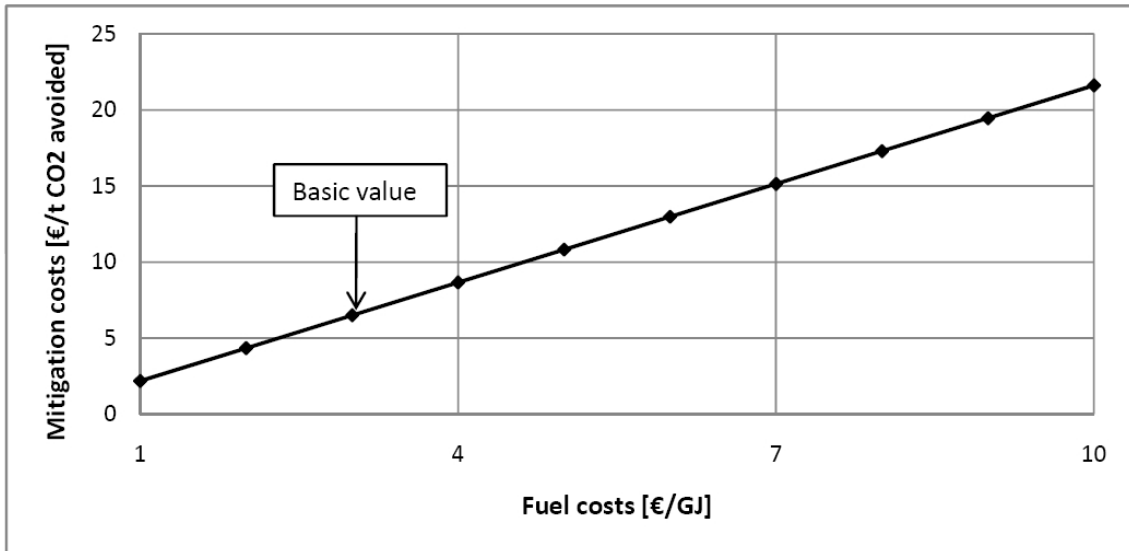


Figure 80: Influence of fuel costs on mitigation costs for Naki I

Table 61: Influence of capital costs on mitigation costs for Naki I

$C_{C(ref)}$ €/kW _{el}	$C_{C(Naki\ I)}$ €/kW _{el}	$C_{C(Naki\ I)} / C_{C(ref)}$ %	a %/yr	C_{fuel} €/GJ	COE_{ref} ct/kWh _{el}	$COE_{Naki\ I}$ ct/kWh _{el}	MC €/t CO ₂
1 250	1 250	100	12	3.0	4.24	4.78	6.5
1 250	1 500	120	12	3.0	4.24	5.16	10.9
1 250	1 750	140	12	3.0	4.24	5.54	15.4
1 250	2 000	160	12	3.0	4.24	5.92	19.9
1 250	2 250	180	12	3.0	4.24	6.29	24.3
1 250	2 500	200	12	3.0	4.24	6.67	28.8

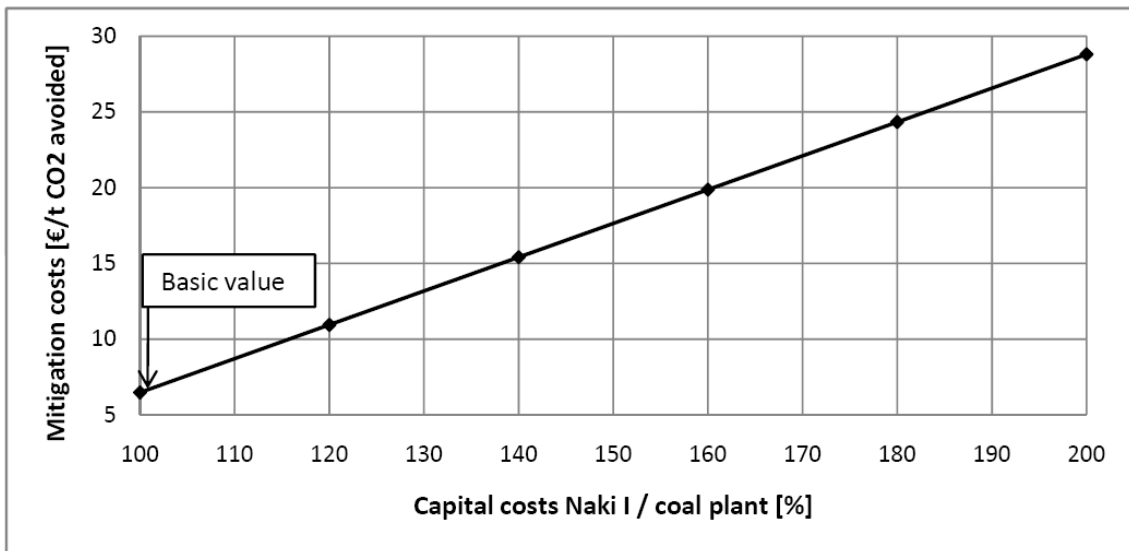


Figure 81: Influence of capital costs on mitigation costs for Naki I

Table 62: Influence of capital charge rate on mitigation costs for Naki I

$C_{C(\text{ref})}$	$C_{C(\text{Naki I})}$	a	η_{ref}	$\eta_{\text{Naki I}}$	C_{fuel}	COE_{ref}	$\text{COE}_{\text{Naki I}}$	MC
€/kW _{el}	€/kW _{el}	%/yr	%	%	€/GJ	ct/kWh _{el}	ct/kWh _{el}	€/t CO ₂
1 250	1 251	5	46	37.3	3.0	3.13	3.68	6.49
1 250	1 251	10	46	37.3	3.0	3.92	4.47	6.50
1 250	1 251	15	46	37.3	3.0	4.71	5.26	6.51
1 250	1 251	20	46	37.3	3.0	5.49	6.05	6.52
1 250	1 251	25	46	37.3	3.0	6.28	6.83	6.53

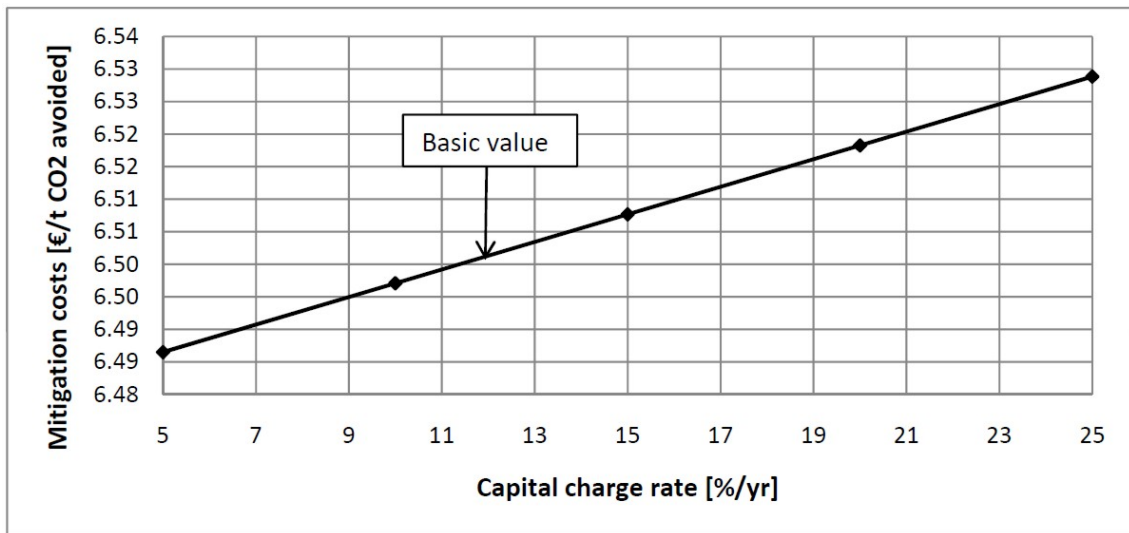


Figure 82: Influence of capital charge rate on mitigation costs for Naki I

Table 63: Influence of net efficiency of reference plant on mitigation costs for Naki I

$C_{C(\text{ref})}$	$C_{C(\text{Naki I})}$	a	η_{ref}	$\eta_{\text{Naki I}}$	C_{fuel}	COE_{ref}	$\text{COE}_{\text{Naki I}}$	MC
€/kW _{el}	€/kW _{el}	%/yr	%	%	€/GJ	ct/kWh _{el}	ct/kWh _{el}	€/t CO ₂
1 250	1 251	12	35	37.3	3.0	4.97	4.79	-1.7
1 250	1 251	12	40	37.3	3.0	4.59	4.79	2.0
1 250	1 251	12	45	37.3	3.0	4.29	4.79	5.8
1 250	1 251	12	50	37.3	3.0	4.05	4.79	9.5
1 250	1 251	12	55	37.3	3.0	3.85	4.79	13.2

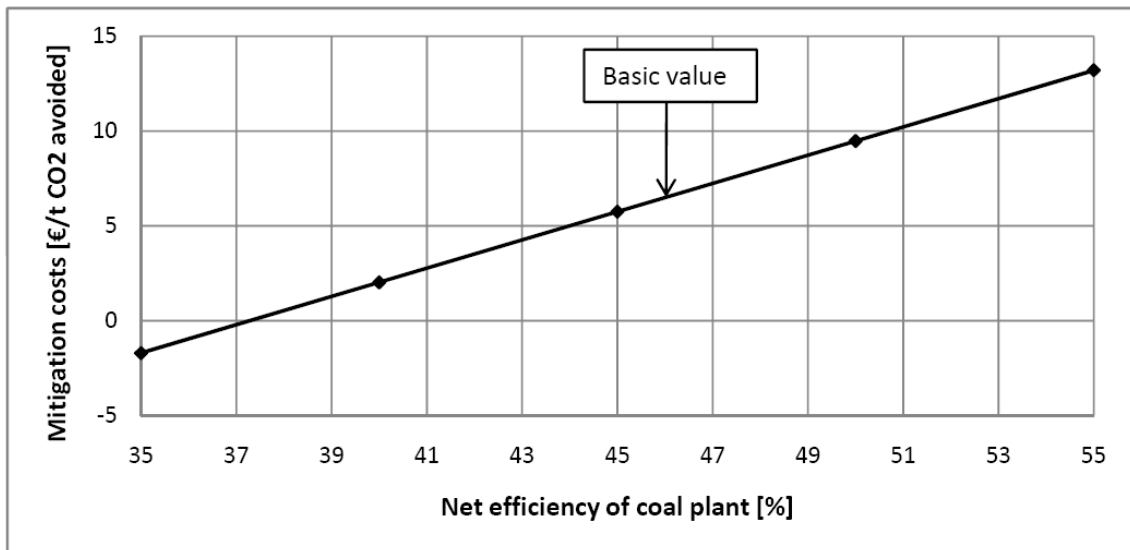


Figure 83: Influence of net efficiency of reference plant on mitigation costs for Naki I

Table 64: Influence of net efficiency of Naki I plant on mitigation costs

$C_{C(\text{ref})}$	$C_{C(\text{Naki I})}$	a	η_{ref}	$\eta_{\text{Naki I}}$	C_{fuel}	COE_{ref}	$\text{COE}_{\text{Naki I}}$	MC
€/kW _{el}	€/kW _{el}	%/yr	%	%	€/GJ	ct/kWh _{el}	ct/kWh _{el}	€/t CO ₂
1 250	1 251	12	46	25	3.0	4.24	6.21	23.3
1 250	1 251	12	46	30	3.0	4.24	5.49	14.8
1 250	1 251	12	46	35	3.0	4.24	4.98	8.8
1 250	1 251	12	46	40	3.0	4.24	4.59	4.2
1 250	1 251	12	46	45	3.0	4.24	4.29	0.6

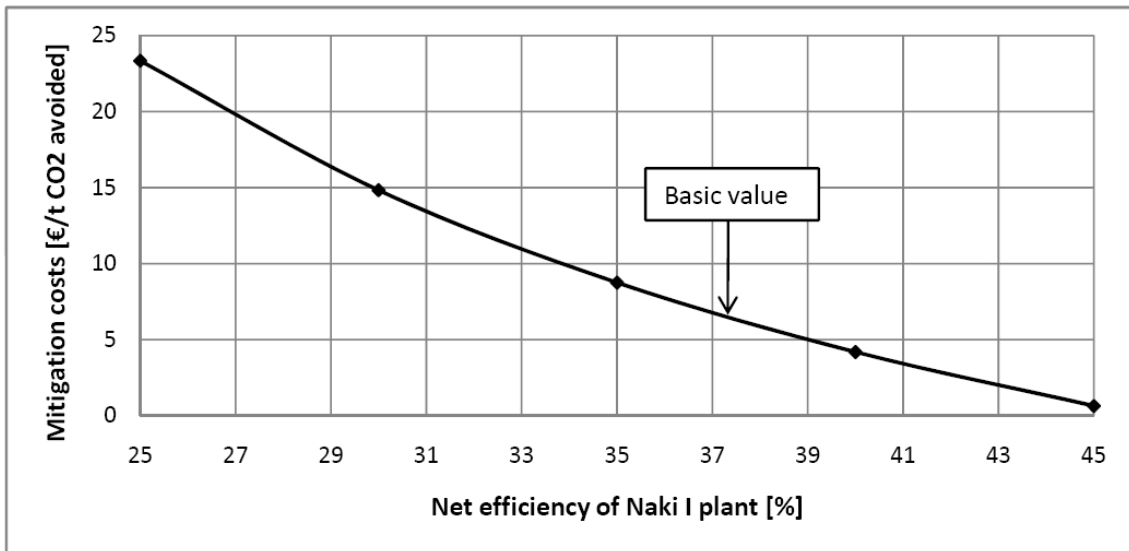


Figure 84: Influence of net efficiency of Naki I plant on mitigation costs

Cost sensitivity analysis for Naki II

Table 65: Influence of fuel costs on mitigation costs for Naki II

$C_{C(\text{ref})}$	$C_{C(\text{Naki II})}$	α	η_{ref}	$\eta_{\text{Naki II}}$	C_{fuel}	COE_{ref}	$\text{COE}_{\text{Naki II}}$	MC
€/kW _{el}	€/kW _{el}	%/yr	%	%	€/GJ	ct/kWh _{el}	ct/kWh _{el}	€/t CO ₂
570	962	12	59.2	51.3	1	1.47	2.16	20.5
570	962	12	59.2	51.3	2	2.08	2.86	23.3
570	962	12	59.2	51.3	3	2.69	3.56	26.1
570	962	12	59.2	51.3	4	3.29	4.26	28.9
570	962	12	59.2	51.3	5	3.90	4.96	31.7
570	962	12	59.2	51.3	6	4.51	5.66	34.5
570	962	12	59.2	51.3	7	5.12	6.37	37.2
570	962	12	59.2	51.3	8	5.73	7.07	40.0
570	962	12	59.2	51.3	9	6.33	7.77	42.8
570	962	12	59.2	51.3	10	6.94	8.47	45.6

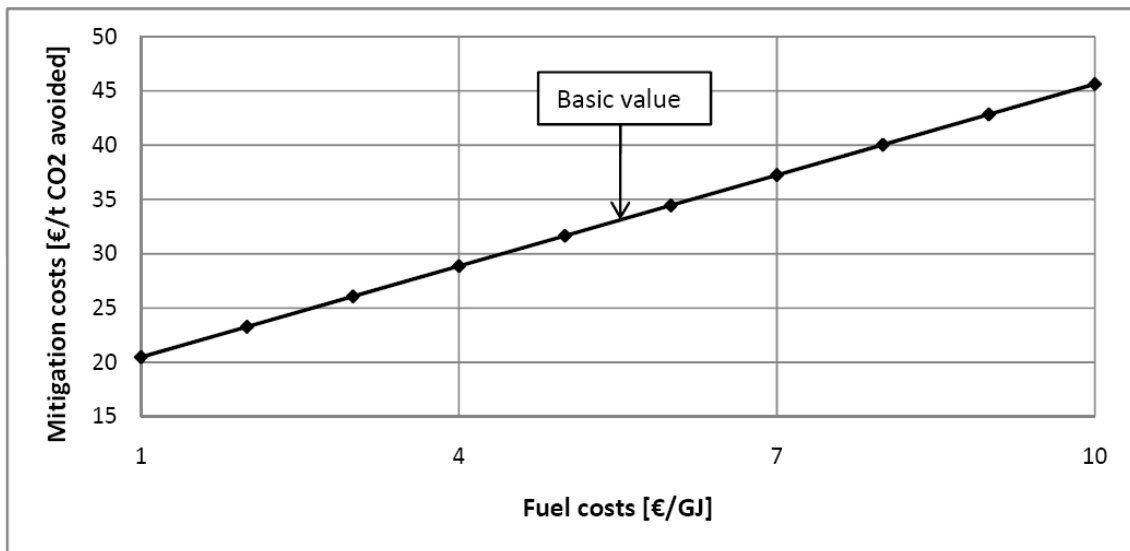


Figure 85: Influence of fuel costs on mitigation costs for Naki II

Table 66: Influence of capital costs on mitigation costs for Naki II

$C_{C(\text{ref})}$ €/kW _{el}	$C_{C(\text{Naki II})}$ €/kW _{el}	$C_{C(\text{Naki II})} / C_{C(\text{ref})}$ %	a %/yr	C_{fuel} €/GJ	COE_{ref} ct/kWh _{el}	$\text{COE}_{\text{Naki II}}$ ct/kWh _{el}	MC €/t CO ₂
570	570	100	12	5.5	4.21	4.72	15.4
570	684	120	12	5.5	4.21	4.89	20.5
570	799	140	12	5.5	4.21	5.07	25.7
570	913	160	12	5.5	4.21	5.24	30.8
570	1 027	180	12	5.5	4.21	5.41	36.0
570	1 141	200	12	5.5	4.21	5.58	41.1

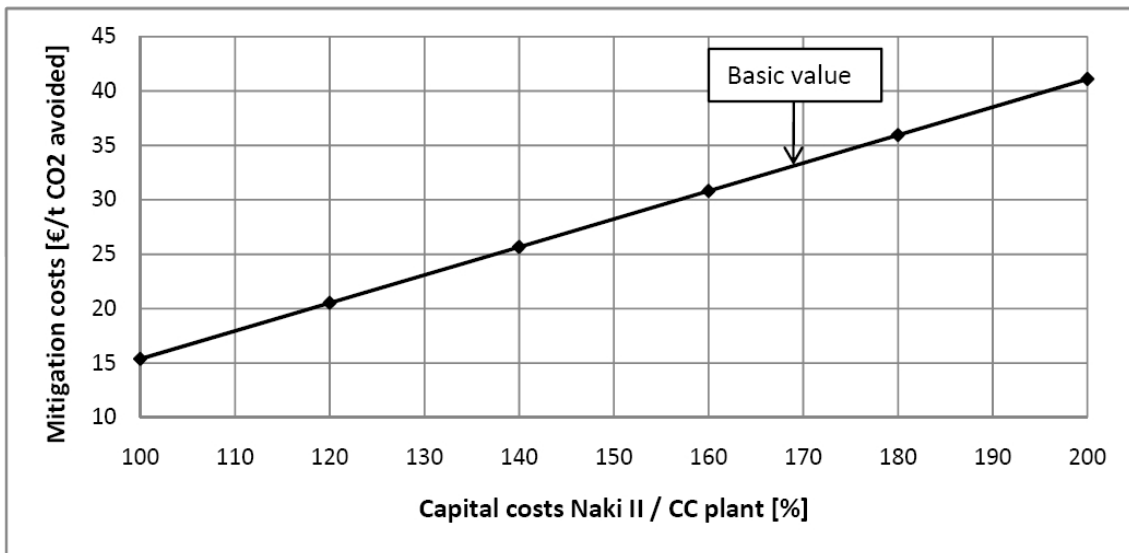


Figure 86: Influence of capital costs on mitigation costs for Naki II

Table 67: Influence of capital charge rate on mitigation costs for Naki II

$C_{C(\text{ref})}$	$C_{C(\text{Naki II})}$	a	η_{ref}	$\eta_{\text{Naki II}}$	C_{fuel}	COE_{ref}	$\text{COE}_{\text{Naki II}}$	MC
€/kW _{el}	€/kW _{el}	%/yr	%	%	€/GJ	ct/kWh _{el}	ct/kWh _{el}	€/t CO ₂
570	962	5	59.2	51.3	5.5	3.70	4.47	22.7
570	962	10	59.2	51.3	5.5	4.06	5.07	30.1
570	962	15	59.2	51.3	5.5	4.42	5.68	37.5
570	962	20	59.2	51.3	5.5	4.78	6.28	44.8
570	962	25	59.2	51.3	5.5	5.14	6.89	52.2

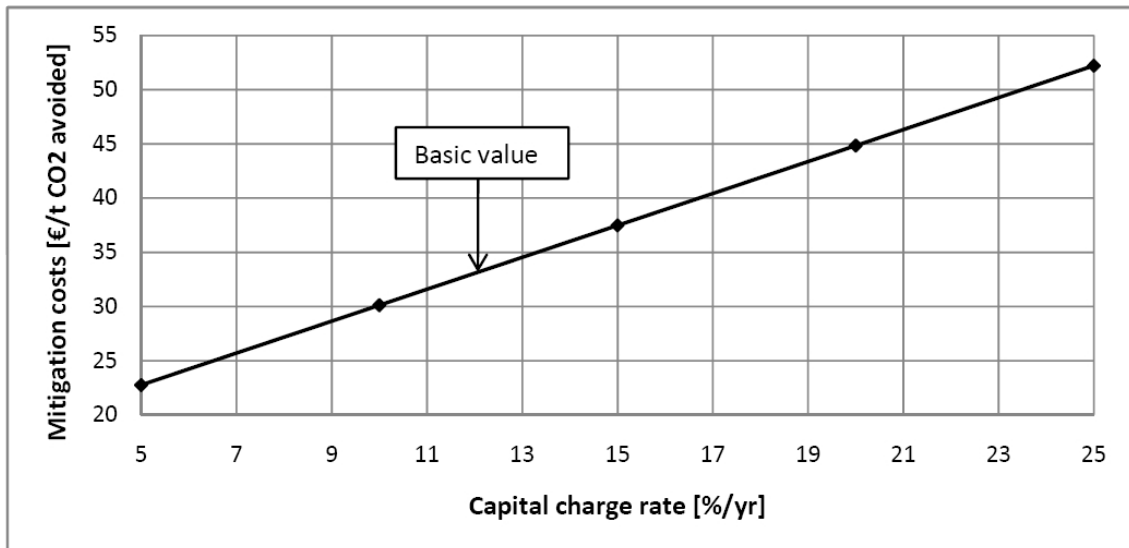


Figure 87: Influence of capital charge rate on mitigation costs for Naki II

Table 68: Influence of net efficiency of reference plant on mitigation costs for Naki II

$C_{C(\text{ref})}$	$C_{C(\text{Naki II})}$	a	η_{ref}	$\eta_{\text{Naki II}}$	C_{fuel}	COE_{ref}	$\text{COE}_{\text{Naki II}}$	MC
€/kW _{el}	€/kW _{el}	%/yr	%	%	€/GJ	ct/kWh _{el}	ct/kWh _{el}	€/t CO ₂
570	962	12	45	51.3	5.5	5.26	5.31	1.2
570	962	12	50	51.3	5.5	4.82	5.31	12.4
570	962	12	55	51.3	5.5	4.46	5.31	23.6
570	962	12	60	51.3	5.5	4.16	5.31	34.9
570	962	12	65	51.3	5.5	3.91	5.31	46.1

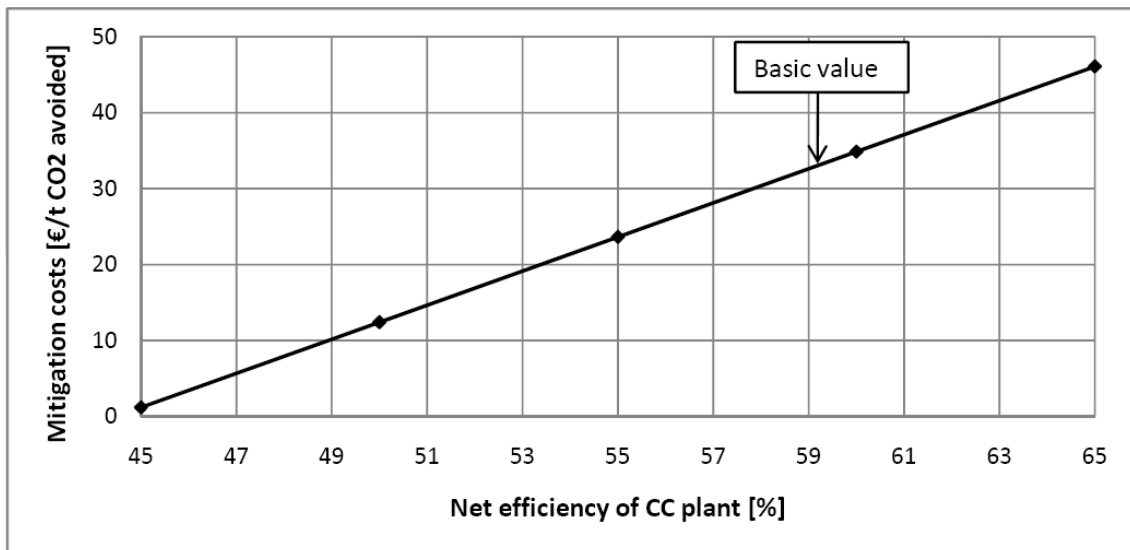


Figure 88: Influence of net efficiency of reference plant on mitigation costs for Naki II

Table 69: Influence of net efficiency of Naki II plant on mitigation costs

$C_{C(\text{ref})}$	$C_{C(\text{Naki II})}$	a	η_{ref}	$\eta_{\text{Naki II}}$	C_{fuel}	COE_{ref}	$\text{COE}_{\text{Naki II}}$	MC
€/kW _{el}	€/kW _{el}	%/yr	%	%	€/GJ	ct/kWh _{el}	ct/kWh _{el}	€/t CO ₂
570	962	12	59.2	40	5.5	4.21	6.40	65.6
570	962	12	59.2	45	5.5	4.21	5.85	49.2
570	962	12	59.2	50	5.5	4.21	5.41	36.1
570	962	12	59.2	55	5.5	4.21	5.05	25.3
570	962	12	59.2	60	5.5	4.21	4.75	16.4

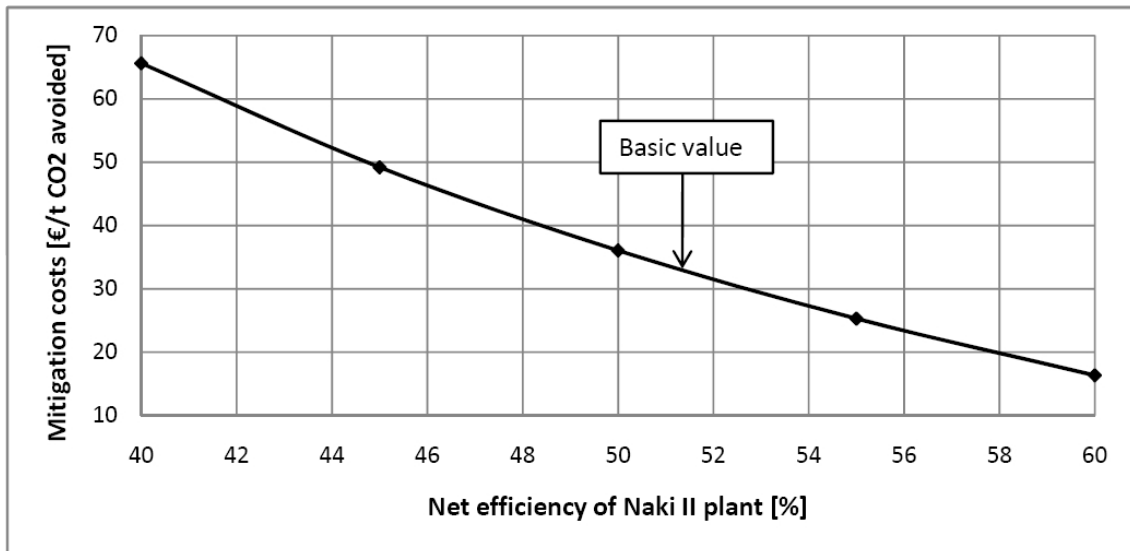


Figure 89: Influence of net efficiency of Naki II plant on mitigation costs

Cost sensitivity analysis for Naki III

Table 70: Influence of fuel costs on mitigation costs for Naki III

$C_{C(\text{ref})}$	$C_{C(\text{Naki III})}$	a	η_{ref}	$\eta_{\text{Naki III}}$	C_{fuel}	COE_{ref}	$\text{COE}_{\text{Naki III}}$	MC
€/kW _{el}	€/kW _{el}	%/yr	%	%	€/GJ	ct/kWh _{el}	ct/kWh _{el}	€/t CO ₂
570	1 133	12	59.2	50.5	1	1.47	2.42	28.5
570	1 133	12	59.2	50.5	2	2.08	3.14	31.6
570	1 133	12	59.2	50.5	3	2.69	3.85	34.7
570	1 133	12	59.2	50.5	4	3.29	4.56	37.9
570	1 133	12	59.2	50.5	5	3.90	5.28	41.0
570	1 133	12	59.2	50.5	6	4.51	5.99	44.1
570	1 133	12	59.2	50.5	7	5.12	6.70	47.3
570	1 133	12	59.2	50.5	8	5.73	7.41	50.4
570	1 133	12	59.2	50.5	9	6.33	8.13	53.5
570	1 133	12	59.2	50.5	10	6.94	8.84	56.6

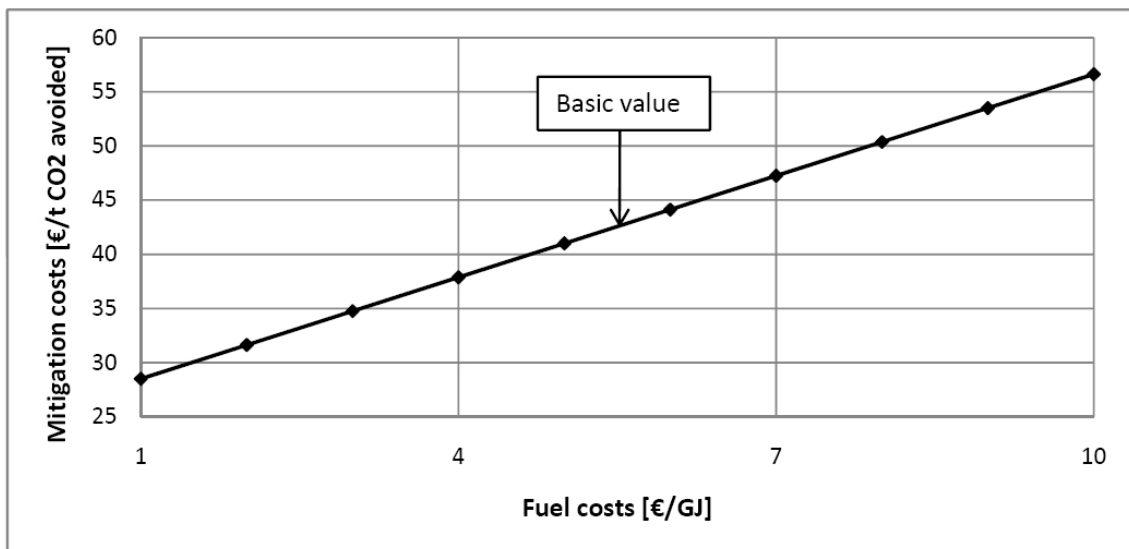


Figure 90: Influence of fuel costs on mitigation costs for Naki III

Table 71: Influence of capital costs on mitigation costs for Naki III

$C_{C(ref)}$ €/kW _{el}	$C_{C(Naki\ III)}$ €/kW _{el}	$C_{C(Naki\ III)} / C_{C(ref)}$ %	a %/yr	C_{fuel} €/GJ	COE_{ref} ct/kWh _{el}	$COE_{Naki\ III}$ ct/kWh _{el}	MC €/t CO ₂
570	570	100	12	5.5	4.21	4.78	17.2
570	684	120	12	5.5	4.21	4.95	22.3
570	799	140	12	5.5	4.21	5.13	27.5
570	913	160	12	5.5	4.21	5.30	32.6
570	1 027	180	12	5.5	4.21	5.47	37.8
570	1 141	200	12	5.5	4.21	5.64	42.9

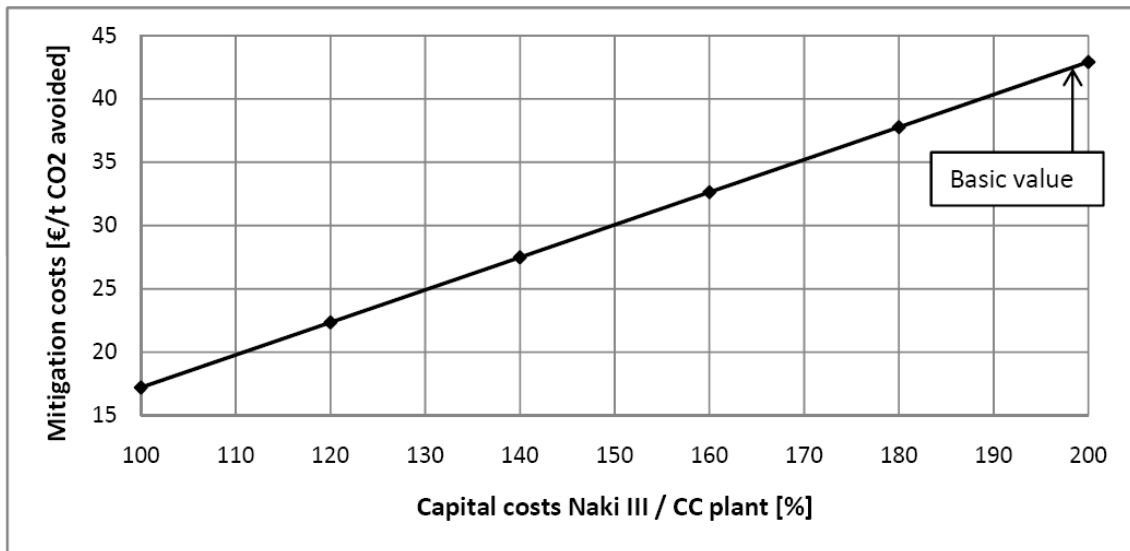


Figure 91: Influence of capital costs on mitigation costs for Naki III

Table 72: Influence of capital charge rate on mitigation costs for Naki III

$C_{C(\text{ref})}$	$C_{C(\text{Naki III})}$	a	η_{ref}	$\eta_{\text{Naki III}}$	C_{fuel}	COE_{ref}	$\text{COE}_{\text{Naki III}}$	MC
€/kW _{el}	€/kW _{el}	%/yr	%	%	€/GJ	ct/kWh _{el}	ct/kWh _{el}	€/t CO ₂
570	1 133	5	59.2	50.5	5.5	3.70	4.63	27.8
570	1 133	10	59.2	50.5	5.5	4.06	5.35	38.3
570	1 133	15	59.2	50.5	5.5	4.42	6.06	48.9
570	1 133	20	59.2	50.5	5.5	4.78	6.77	59.5
570	1 133	25	59.2	50.5	5.5	5.14	7.49	70.0

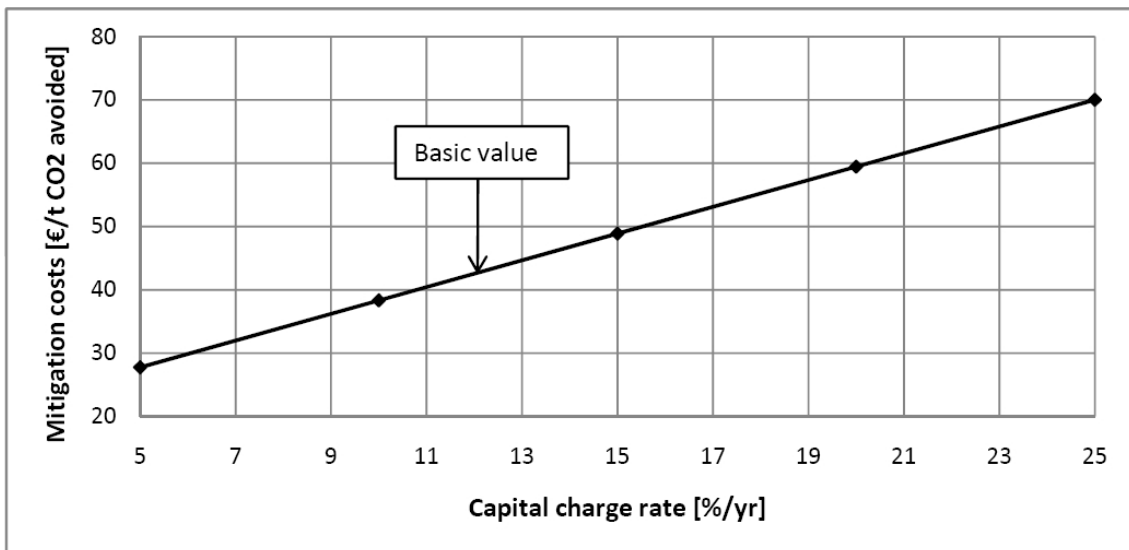


Figure 92: Influence of capital charge rate on mitigation costs for Naki III

Table 73: Influence of net efficiency of reference plant on mitigation costs for Naki III

$C_{C(\text{ref})}$	$C_{C(\text{Naki III})}$	a	η_{ref}	$\eta_{\text{Naki III}}$	C_{fuel}	COE_{ref}	$\text{COE}_{\text{Naki III}}$	MC
€/kW _{el}	€/kW _{el}	%/yr	%	%	€/GJ	ct/kWh _{el}	ct/kWh _{el}	€/t CO ₂
570	1 133	12	45	50.5	5.5	5.26	5.63	8.4
570	1 133	12	50	50.5	5.5	4.82	5.63	20.4
570	1 133	12	55	50.5	5.5	4.46	5.63	32.5
570	1 133	12	60	50.5	5.5	4.16	5.63	44.5
570	1 133	12	65	50.5	5.5	3.91	5.63	56.5

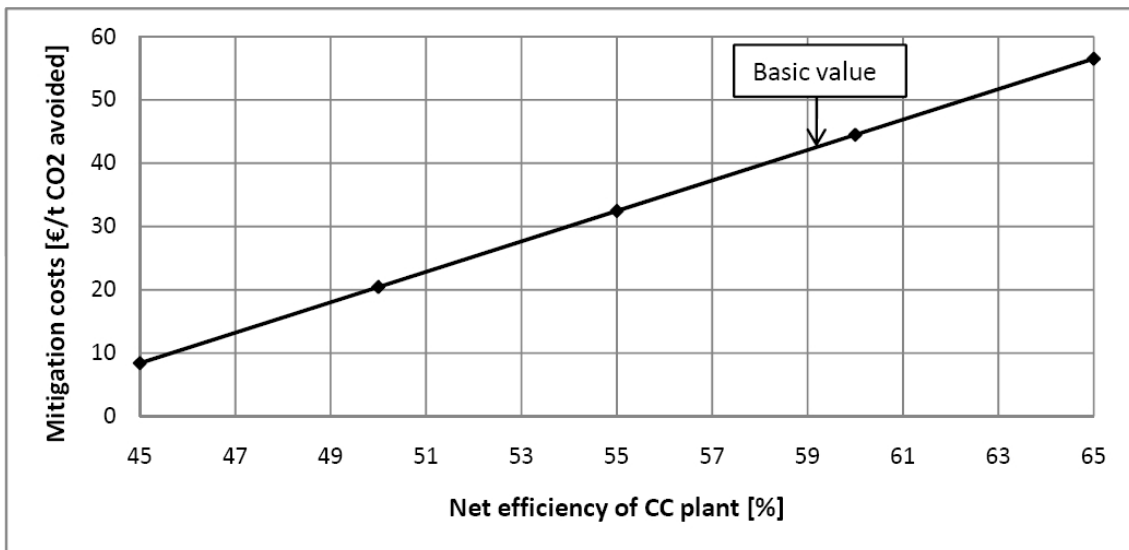


Figure 93: Influence of net efficiency of reference plant on mitigation costs for Naki III

Table 74: Influence of net efficiency of Naki III plant on mitigation costs

$C_{C(\text{ref})}$	$C_{C(\text{Naki III})}$	a	η_{ref}	$\eta_{\text{Naki III}}$	C_{fuel}	COE_{ref}	$\text{COE}_{\text{Naki III}}$	MC
€/kW _{el}	€/kW _{el}	%/yr	%	%	€/GJ	ct/kWh _{el}	ct/kWh _{el}	€/t CO ₂
570	1 133	12	59.2	40	5.5	4.21	6.66	73.3
570	1 133	12	59.2	45	5.5	4.21	6.11	56.9
570	1 133	12	59.2	50	5.5	4.21	5.67	43.7
570	1 133	12	59.2	55	5.5	4.21	5.31	33.0
570	1 133	12	59.2	60	5.5	4.21	5.01	24.0

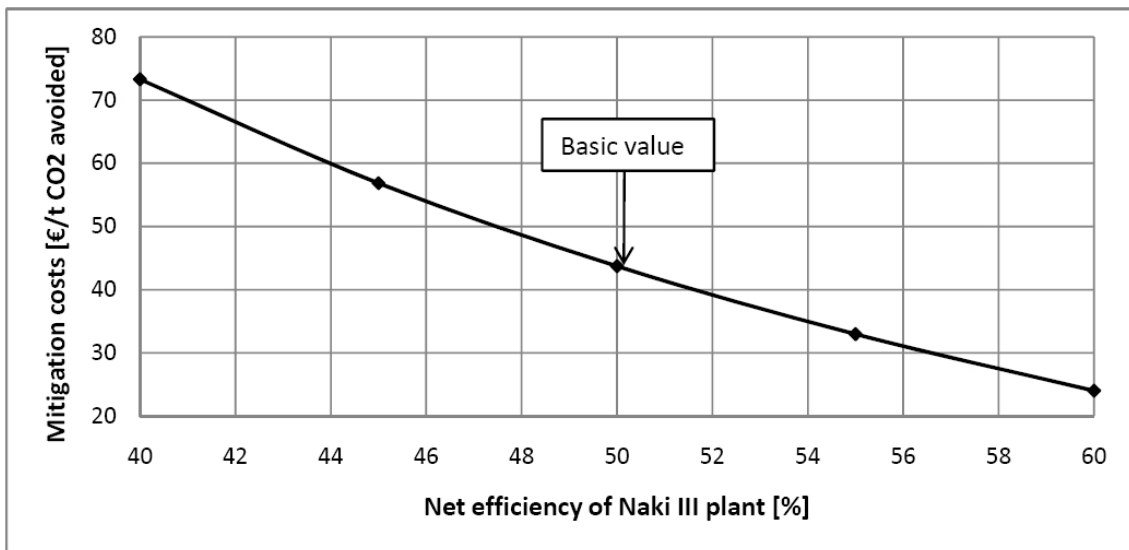


Figure 94: Influence of net efficiency of Naki III plant on mitigation costs

References

- [1] IEA Greenhouse Gas R&D Programme, Request March 2009, <http://www.ieagreen.org.uk/>
- [2] Nebojsa Nakicenovic, Arnulf Gröbler, Alan MCDonald: Global Energy Perspectives, Cambridge University Press, Cambridge, 1998
- [3] Kyoto Protocol to the United Nations Framework Convention on Climate Change, Request March 2009, <http://unfccc.int/resource/docs/convkp/kpeng.pdf>
- [4] Metz B., Davidson O., Heleen de Coninck, Loos M., Meyer L.: IPCC Special Report on Carbon Dioxide Capture and Storage, Cambridge University Press, Cambridge, 2005
- [5] Vattenfall, Request March 2009, <http://www.vattenfall.de/>
- [6] Yantovski E.I.: Energy and Exergy Currents: An Introduction to Exergonomics, Nova Science Publisher Inc., New York, 1994
- [7] Yantovski E.I., Zvagolsky K.N., Gavrilenko V.A.: The COOPERATE-Demo Power Cycle, Energy Convers. Mgmt Vol. 36, No. 6-9, 1995
- [8] Yantovski E., Gorski J., Shokotov M.: Zero Emissions Power Cycles, CRC Press Taylor&Francis Group, New York, 2009
- [9] Naqvi R., Bolland O., Brandvoll O., Helle K.: Chemical Looping Combustion - Analysis of Natural Gas Fired Power Cycles With Inherent CO₂ Capture, ASME Turbo Expo 2004, GT2004-53359, Vienna, Austria
- [10] Mathieu P., Nihart R.: Sensivity analysis of the MATIANT cycle, Energy Conversion and Managenemt 40 (1999) 1687-1700
- [11] SimTech Simulation Technology, Request February 2009 <http://www.simtechnology.com/english/SimTech.php>
- [12] Moser M.: Thermodynamische und wirtschaftliche Optimierung des Graz Cycle. Diplomarbeit am Institut für Thermische Turbomaschinen und Maschinendynamik, TU Graz, 2003
- [13] Sanz W., Jericha H., Bauer B., Göttlich E.: Qualitative and Quantitative Comparison of Two Promising Oxy-Fuel Power Cycles For CO₂ Capture. ASME Turbo Expo 2007, GT2007-27375, Montreal, Canada
- [14] Lukasser A.: Graz Cycle, eine Innovation zur CO₂-Rückhaltung. Diplomarbeit am Institut für Thermische Turbomaschinen und Maschinendynamik, TU Graz, 1997
- [15] NIST Chemistry WebBook, Request October 2008, <http://webbook.nist.gov/chemistry/>

- [16] Sanz W., Jericha H., Luckel F., Göttlich E., Heitmeir F.: A Further Step Towards a Graz Cycle Power Plant For CO₂ Capture. ASME Turbo Expo 2005, GT2005-68456, Nevada, USA
- [17] Jericha H.: Skriptum zur Vorlesung: Thermische Turbomaschinen, 3.erweiterte Auflage 1994, Herausgegeben vom Skriptenreferat der TU Graz
- [18] Jericha H., Göttlich E.: Optimierung der Gasturbinen für einen geschlossenen Prozess mit CO₂-Rückhaltung. VDI-Berichte Nr. 1721, 2002
- [19] Jericha H., Göttlich E., Sanz W., Heitmeir F.: Design Optimisation of the Graz Cycle Prototype Plant. ASME Turbo Expo 2003, GT2003-38120, Atlanta, USA
- [20] Jericha H., Göttlich E.: Conceptual Design for an Industrial Prototype Graz Cycle Power Plant. ASME Turbo Expo 2002, GT2002-30118, Amsterdam, Netherlands
- [21] Jericha H., Sanz W., Paßrucker H.: Analytische Beschreibung und Optimierung dreidimensionaler verwundener Schaufelprofile, VDI Berichte 1109, März 1994
- [22] Schulze G., Blaha C., Hennecke D., Henne J.: The Performance of a New Axial Single Stage Transonic Compressor, 12th International Symposium on Airbreathing Engines in September 1995, Melbourne
- [23] Hacker V., Jericha H., Fesharaki M., Friedrich K., Lukasser A.: Graz Cycle Enhancement by Medium and High Temperature Fuel Cells; ICOPE 1997
- [24] Böhler Edelstahl GmbH & Co KG, Request April 2009, http://www.bohleredelstahl.com/english/3864_ENG_HTML.php
- [25] Private communication with Prof. Jericha, April 2009
- [26] Jericha H., Sanz W., Pieringer P., Göttlich E., Erroi P.: Konstruktion der ersten Stufe der HTT-Gasturbine für den Graz Cycle Prototyp, 2004, VDI Conference Leverkusen, Germany
- [27] Jericha H., Sanz W., Göttlich E., Neumayer F.: Design Details of a 600MW Graz Cycle Thermal Power Plant for CO₂ Capture. ASME Turbo Expo 2008, GT2008-50515, Berlin, Germany
- [28] Göttlicher G.: Energetik der Kohlendioxidrückhaltung in Kraftwerken, Fortschritt - Berichte VDI, Reihe 6 Energietechnik, Nr.421, Düsseldorf: VDI Verlag 1999
- [29] Heegemann H.: Variantenvergleich von erdgasbefeuerten Kraftwerken mit CO₂-Abtrennung, Diplomarbeit am Institut für Wärmetechnik, TU Graz, 2008
- [30] Energie für die Zukunft, Das neue Kraftwerk Westfalen, RWE Power AG, Request March 2009, <http://www.rwe.com/web/cms/mediablob/de/12130/data/4387/zweiter-download.pdf>

- [31] GuD Lingen, RWE Power AG, Request May 2009, <http://www.rwe.com/web/cms/mediablob/de/77404/data/7252/kraftwerke-lingen-pdf.pdf>

- [32] Energiewirtschaftliches Gesamtkonzept 2030, Szenariendokumentation, Studie vom Energiewirtschaftlichen Institut an der Universität zu Köln, 2007, Request March 2009, http://www.ewi.uni-koeln.de/fileadmin/user/Gutachten/Energiewirtschaftliches_Gesamtkonzept_2030.pdf